Nonlinear arm responses to continuous and pulse-shaped force perturbations

by
Bart van Vliet*

Master of Science Thesis

For the degree Master of Science in BioMedical Engineering
at Delft University of Technology

Supervisors:

Dr. Ir. R. Happee
Dr. Ir. E. de Vlugt
Prof. Dr F.C.T. van der Helm

April 19, 2012

*E-mail adress:
b.vanvliet-3@student.tudelft.nl
vanvlietbvv@gmail.com

Abstract

This study quantifies and explores the nonlinearities of human arm responses to large force perturbations while subjects (n=10) performed either a position or relax task. Continuous perturbations with large variations of amplitude levels (RMS values of 2.5, 7.5, 22.5 mm displacements) and pulse perturbations with large amplitudes (average of 16 cm displacements) were applied at the hand by a 2-DOF robotic manipulator. Linear multivariable identification techniques were used to estimate the endpoint mechanical admittance from the continuous perturbations. The admittance is the relationship between force input and displacement output. Reflexive and intrinsic parameters of a 2-DOF linear arm model were fitted onto the estimated endpoint admittance. This model was used to predict the pulse perturbations. In particular, we determined to what extent human arm displacements in response to large amplitude force pulses can be predicted from identification of continuous perturbations with small amplitudes.
Results showed that the estimated admittance for the relax task is a factor 18 larger compared to the estimated admittance for the position task. For the position and relax task, the estimated admittance respectively decreased with a factor 1.5 and increased with a factor 3.8 at the largest perturbation amplitude compared to the lowest amplitude. For the position task, this effect probably resulted from adaptation to the perturbation. The nonlinearity observed for the relax task might be well explained by nonlinear muscle properties such as the short range stiffness. On average, model predictions underestimated the peak displacements in response to the pulse stimulus by a factor 1.7. This shows the need to include nonlinearities in models for pulse shaped loading conditions.

Contents

CHAPTER 1

Introduction

Road traffic accidents are a major cause of death and injuries. In the European Union, there were 35 000 fatal accidents in 2009 because of road traffic collisions and many more people were seriously injured (ETSC, 2011). Advanced safety systems are currently developed that prevent or mitigate traffic accidents by active interventions e.g. pre-crash activated seat belts, autonomous braking systems and lane change manoeuvres. These systems can induce low and high velocity impacts to occupants. To optimally design such systems, realistic human body models (mathematical models and car crash dummies) are required. However, we do not know whether the current human body models react in a realistic manner to impact-like disturbances since neuromuscular stabilization properties in impact situations are to date largely unknown.
Human joint dynamics may be separated into an intrinsic and a reflexive part, both contributing to posture maintenance. Intrinsic properties are represented by visco-elasticity of contractile and passive tissues. The reflexive feedback mechanism consists of sensory organs such as muscle spindles. The existing literature shows that the intrinsic and reflexive system are highly nonlinear (de Vlugt et al., 2011; Stein and Kearney, 1995; Kearney and Hunter, 1982). Hill-type muscle models and Huxley models are commonly used nonlinear models in current whole-body simulation software packages such as MADYMO (Rooij et al., 2011; van der Horst, 2002). However, few included nonlinear sensors as, for example, proposed by Mileusnic et al. (2006). Only limited data is available to validate these complex models (Östh et al., 2010; Nemirovsky and van Rooij, 2010).
Human experiments are necessary to increase knowledge about mechanisms involved in human stabilization responses to large forces. The main problem is that it is not possible to estimate an unique set of intrinsic and reflexive parameters for the very complex human models used in the automotive industry. Even for a simple linear model, Happee and van Drunen (2009) were not able to accurately estimate reflexive feedback parameters using impact perturbation experiments.
The Laboratory for Neuromuscular Control at Delft University of Technology has shown that intrinsic and reflexive components can be estimated successfully by linear frequency domain identification techniques (Van der Helm et al., 2002; de Vlugt et al., 2002; Schouten et al., 2008; Mugge et al., 2009; Forbes et al., 2011). They derived the mechanical admittance (relationship between force input and displacement output) by using continuous force perturbations applied by robotic manipulators and parameters of simple linear body segment models with lumped agonist and antagonist muscles were estimated. Typically, experiments were performed with small perturbation amplitudes justifying linear analysis. No literature was found of these type of perturbation experiments with a large variation of perturbation amplitude levels. Consequently, we do not know whether these type of experiments are sensitive to large variations of perturbation amplitude.
Thus, limited data is available of force perturbation experiments with large amplitude levels. Our research objective is therefore to:

> *explore and quantify nonlinearities of human arm responses to large force perturbations.*

Continuous and pulse perturbations were applied to the human arm by a 2-DOF robotic manipulator to analyze multi-joint nonlinearities. In this paper we examined the following four questions: what is the effect of 1) task instruction, 2) stimulus amplitude, 3) continuous versus pulse perturbations, and 4) nonlinearities of inertial properties.
The effect of task instruction was investigated by participants performing a position (posture

maintenance) and relax task to imitate attentive and inattentive subjects. The effect of amplitude was investigated by 1) continuous perturbations with large variations of amplitude levels, 2) pulse perturbations with large amplitudes and 3) comparing responses to continuous and pulse perturbations by fitting a linear model to the response to continuous perturbations, and using this to predict the pulse response. This showed to what extent human arm displacements in response to large amplitude force pulses can be predicted from identification of continuous perturbations with small amplitudes. Several studies found that neuromuscular nonlinearity of the human motor system is characterized as a less than proportional increase in force or electromyography (EMG) activity with larger perturbation amplitudes and velocities (de Vlugt et al., 2011; Kearney et al., 1997; Stein and Kearney, 1995; Kearney and Hunter, 1982). However, these experiments were primarily position perturbations with a force task. For force perturbations with a position task, amplitude effects are hardly investigated. We hypothesize that the model predictions will show a lower admittance to force pulse perturbations than the experimental human arm response. Finally, the effect of nonlinearities from inertial properties was evaluated by developing a nonlinear skeletal model. The model was geometrically nonlinear and contained nonlinear velocity terms (centripetal and Coriolis).

CHAPTER 2

Methods

2.1 Subjects

Ten right-handed healthy male subjects with a mean (standard deviation, SD) age of 26.2 (3.2) years participated in the experiment. The research was approved by the institution Human Research Ethics Committee and all participants provided written informed consent.

2.2 Experimental setup

To analyze the intrinsic and reflexive components of the human arm, force disturbances were applied in a horizontal plane by a two-joint robotic manipulator (de Vlugt et al., 2003). The experimental setup is schematically presented in figure 2.1. Seated subjects were strapped by a four-point seatbelt in order to minimize movements of the trunk and translation of the shoulder. During the experiments, subjects were asked to hold the handle of the manipulator (with the forearm 90° in pronation) which was free to move in a horizontal plane. The seat height was adjusted such that the upper arm was around 90° in abduction. The initial joint angles were calculated with the acromion position and initial hand position in the manipulator coordinate frame and the arm segment lengths measured with a caliper. Average (SD, over subjects) values for the arm posture were 22.5° (0.7°) of shoulder anteflexion (θ_s) and the elbow angle (θ_e) was 82.3° (0.68°). This was a safe posture with the manipulator not able to reach the thorax. The weight of the arm was supported by a rope of about two meters which was attached to the ceiling. Movements of the wrist joint were constrained by a cuff resulting only in shoulder-elbow motion. This multi-joint setup is used for several reasons. Not only nonlinearities of mono- but also bi-articular muscles can be analyzed. Secondly, nonlinear effects from inertial properties (geometrical, centripetal and Coriolis) can be assessed. The large range of motion of the shoulder and elbow joint makes the arm appropriate to investigate amplitude effects. Moreover, the arm is able to sustain high forces without causing injuries or discomfort.
The manipulator acted as a linear mechanical system with virtual mass-spring-damper properties, henceforth called the environment. The mass was set at 3 kg and the damping at 0 N s/m being minimal values realized with this setup. The stiffness was set at 20 N/m to counteract drift from the equilibrium position.
A closed-loop block scheme of the experimental setup is presented in figure 2.2 which shows the interaction between the nonlinear human arm and the linear environment. External force disturbances $\mathbf{d}(t)$ together with the reaction forces $\mathbf{f}(t)$ are applied at the virtual environment resulting in the displacement of the handle $\mathbf{x}(t)$.

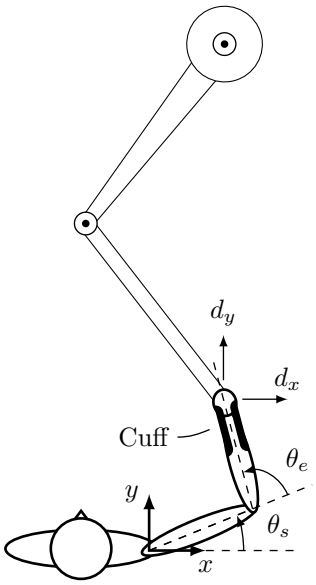

Figure 2.1 – Schematic drawing of the experimental setup (top view). The subject is holding the handle of the manipulator. Force perturbations were applied in two directions (d_x and d_y). Only shoulder and elbow rotations were possible, because the wrist movement was constrained by a cuff and the trunk was strapped by a four-point seatbelt.

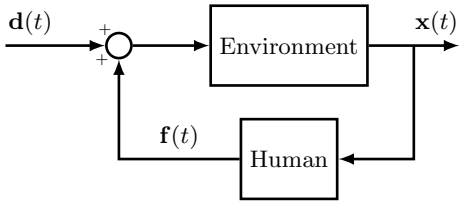

Figure 2.2 – Closed-loop block scheme of the experimental setup where the human arm is linked to the manipulator (environment). The external force disturbance $\mathbf{d}(t) = [d_x(t)\ d_y(t)]^T$ together with the reaction force between the hand and the handle $\mathbf{f}(t) = [f_x(t)\ f_y(t)]^T$ is applied at the environment. This results to handle displacement $\mathbf{x}(t) = [x_x(t)\ x_y(t)]^T$.

2.3 Instrumentation

Two orthogonal horizontal components of the reaction forces applied by the subjects were recorded by strain gauges mounted between the handle and the robot arm. Two optical angular encoders (17 bits per 360°) recorded the angles of the two manipulator joints by which the handle displacements were obtained. The reaction forces and manipulator joint angles were recorded with a sampling frequency of 200 Hz.
Surface Electromyography (EMG) (Delsys Bagnoli-8, Boston, USA, inter-electrode distance 10 mm) of eight arm muscles was recorded with a sampling frequency of 2000 Hz after 20-1000 Hz bandpass filtering. The measured muscles were: m. pectoralis major clavicular part, m. lattisimus dorsi, m. deltoideus anterior and posterior, m. biceps short head, m. brachioradialis and the m. triceps lateralis and longum.
Top view movies were made of each trial to quantify the shoulder translation during the perturbations.

2.4 Perturbation signals

The force perturbation signals consisted of transient (pulses) and continuous (multisines) perturbations. At each trial, subjects received either a single pulse or a multisine perturbation directly followed by a single pulse.

Pulse perturbation

The transient perturbation was a pulse signal consisting of a half sine wave with a duration of 80 ms (figure 2.3). The onset of the pulse was randomized between 5 and 20 seconds from the start of the trial. As can be seen in figure 2.4, two pulse directions were applied at an angle of 20° and 200° with respect to the fronto-parallel axis. These directions primarily induced flexion and extension of the elbow joint. The pulse amplitudes were varied as described in section 2.5.

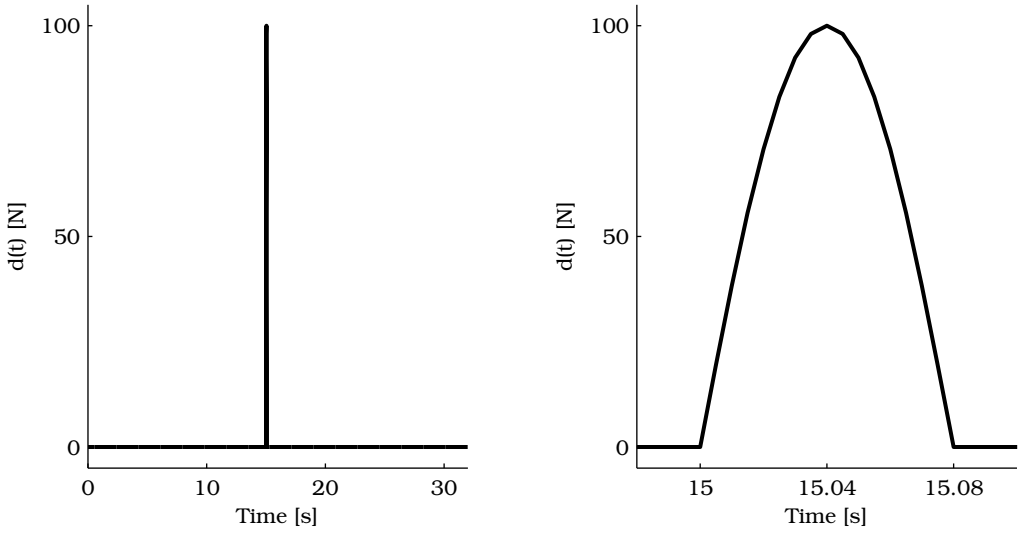

Figure 2.3 – Left: An example of a total perturbation signal consisting of a single pulse with an amplitude of 100 N. Right: time segment showing the characteristics of the pulse. The pulse signal consisted of a half sine wave with a duration of 80 ms.

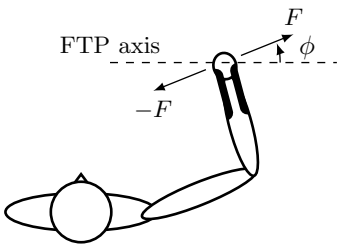

Figure 2.4 – Schematic drawing of the force pulse direction. The pulse was either applied at an angle of 20° or 200° with respect to the fronto-parallel (FTP) axis.

Multisine followed by a pulse perturbation

Pulse perturbations were applied with pre-perturbations. Random continuous force perturbations were applied x- and y-direction (d_x and d_y, figure 2.1) which enabled identification in the frequency domain (see section 2.6). Multisine signals of 20.48 sec (2^{12} samples) were generated off-line in the frequency domain with equal powerspectra as shown in figure 2.5. The multisine was extended by a copy of itself and the first 32 sec were used for the experiment. The multisines consisted of 72 superimposed sinusoids of different frequencies ranging from 0.2-40 Hz. These frequencies were arranged in 18 clusters of four adjacent frequencies. This improved the signal-to-noise ratio compared to full bandwidth perturbation signal with power at every frequency. To obtain a even higher signal-to-noise ratio, the multisine signal was designed with an optimal crest factor. An additional advantage was that the cresting removed undesirable outliers in the force signal.
The reduced power method was used to adequately excite the system at frequencies necessary for modeling, but to evoke low frequency control behavior (Mugge et al., 2007). The full power part ranged from 0.2-1.5 Hz and was linearly spaced resulting in four clusters of power. A reduced power with a relative amplitude of 15% was applied for frequencies ranged from 1.8-40 Hz. This reduced power part was logarithmically spaced resulting in ten clusters of power. Additionally, 4 clusters were added in the range of 1.8-7 Hz to capture the dynamics of the arm around the eigenfrequency in more detail.

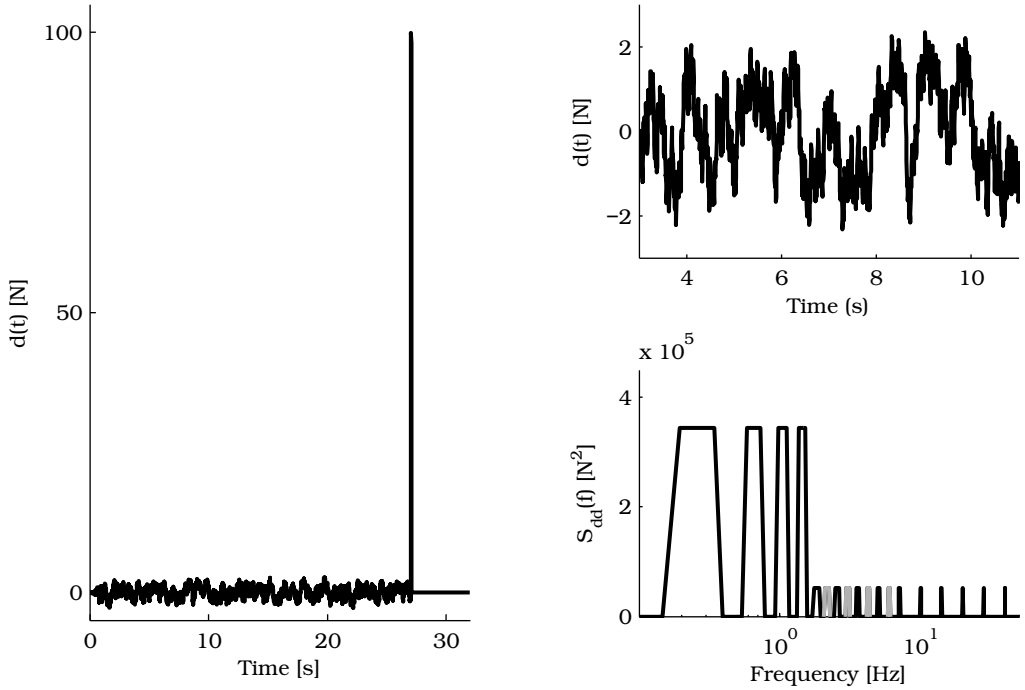

Figure 2.5 – Left: an example of a multisine perturbation followed by a pulse perturbation. A pulse with the same characteristics as the pulse in figure 2.3 was superimposed to the multisine which was faded to zero within 40 ms. Upper right: time segment of the multisine. Lower right: autospectral density of the multisine signals. The full power part was linearly spaced from 0.2 to 1.5 Hz. Subsequent frequencies were logarithmic distributed and contained 15% reduced power up to 40 Hz. In order to capture dynamics around the eigenfrequency, four extra reduced power clusters (shown in grey) were added which were also logarithmically spaced.

2.5 Experimental procedure

Task instruction

To investigate the influence of the task instruction, subjects were asked to perform two tasks:

1. Position task (PT). The instruction was 'keep the position of the manipulator handle at the target by minimizing the displacements'. The handle position and the target was visualized on a computer screen in front of the subject.

2. Relax task (RT). The instruction was 'relax the arm and shoulder completely and do not react to the disturbances'.

Experimental conditions

The experimental conditions are given in table 2.1. As already described, subjects were asked to perform either a position or relax tasks and either single pulse perturbations or continuous perturbations followed by a single pulse perturbation were applied. To examine nonlinearities of the neuromusculoskeletal (NMS) system different amplitudes of the perturbation signals were applied; three levels for the multisines and two levels for the pulses. The three intended hand displacements for the multisine perturbations were 2.5, 7.5 and 22.5 mm root mean square (RMS). The required forces for the multisine perturbations were determined prior to the experiment in a practicing session. The applied RMS force of the continuous perturbations was adjusted for each subject to achieve the intended displacements. All force pulses were scaled with the applied RMS force from the multisine perturbation with intended RMS displacement 7.5 mm (condition $PT_{7.5}$). The conditions with intended RMS displacements 0 and 7.5 mm were repeated twice to investigate reproducibility. The remaining conditions were performed once to minimize the influence of fatigue. This resulted in a total of 32 trials which were carried out in randomized order.

Table 2.1 – Experimental conditions including the task, RMS values of the multisine perturbations, amplitude values of the pulse perturbations and the number of repetitions. The position and relax task are respectively abbreviated by PT and RT.

Condition	Task	Multisine perturbations (RMS[a])			Pulse perturbations (peak amp.)		Nr. of repetitions
		Intended displ. (mm)	Mean (SD[b]) applied force (N)	Mean (SD) displ. (mm)	Mean (SD) applied force (N)	Mean (SD) displ. (cm)	
PT_0	PT	0	0	-	53.9[c] (13.0) · [±1, ±2][d]	6.20[e] (1.88), 13.85 (3.72)	2
$PT_{2.5}$	PT	2.5	1.2 (0.2)	2.5 (0.3)	53.9 (13.0) · ±2	10.40 (1.69)	1
$PT_{7.5}$	PT	7.5	5.4 (1.3)	7.9 (0.7)	53.9 (13.0) · [±1, ±2]	4.78 (0.81), 9.14 (1.18)	2
$PT_{22.5}$	PT	22.5	16.6 (4.8)	21.4 (1.9)	53.9 (13.0) · ±2	9.70 (2.29)	1
RT_0	RT	0	0	-	53.9 (13.0) · ±1	19.38 (4.51)	2
$RT_{2.5}$	RT	2.5	0.6 (0.1)	4.3 (1.5)	53.9 (13.0) · ±1	19.84 (4.64)	1
$RT_{7.5}$	RT	7.5	0.9 (0.2)	9.3 (2.7)	53.9 (13.0) · ±1	20.76 (4.98)	2
$RT_{22.5}$	RT	22.5	1.8 (0.3)	30.0 (9.9)	53.9 (13.0) · ±1	25.01 (6.27)	1

[a] root mean square (RMS)
[b] standard deviation (SD)
[c] 53.9 is ten times the applied RMS force of the multisine with intended displacement 7.5 mm ($PT_{7.5}$)
[d] negative and positive values are respectively 20° and 200° with the FTP axis as depicted in figure 2.4. The minimum and maximum pulse amplitude is represented by the multiplication of respectively 1 and 2.
[e] this value is the averaged displacements over the left and right pulse direction and over subjects for the minimum pulse amplitude level. The same holds for the maximum pulse amplitude.

2.6 Spectral analysis

The multisine responses were analyzed using linear identification techniques.

Matrix frequency response functions

The measured manipulator displacements and forces were analyzed in a 2D cartesian coordinate system with directions x = right, and y = forward (see figure 2.1). Matrix frequency response functions (MFRFs) describing the admittance of the human arm were estimated by a multivariable closed-loop identification technique (de Vlugt et al., 2003). This technique will briefly be summarized in this section and the full derivation is given in appendix A.
Figure 2.6 shows the closed loop system of the human arm impedance $\mathbf{H_{xf}}^{-1}$ and the environment $\mathbf{E_{xz}}$ in the frequency domain. The summation of the external disturbance signal $\mathbf{D}(f)$ and the hand reaction force $\mathbf{F}(f)$ is the input to the environment. The output of the total system is the handle displacement $\mathbf{X}(f)$. Unknown noise signals $\mathbf{N}(f)$ and $\mathbf{M}(f)$ are included in the figure. Signal $\mathbf{N}(f)$ describes the part of the hand reaction force which was uncorrelated with the disturbance signal. Signal $\mathbf{M}(f)$ is also uncorrelated with the disturbance signal and describes the measurement noise together with the excluded dynamics due to linearization. The purpose of the multivariable closed-loop identification is to minimize effects of both noise signals and obtain estimated MFRF of the human arm admittance $\mathbf{H_{xf}}(f)$. The effects of noise can be minimized by the use of spectral estimators.

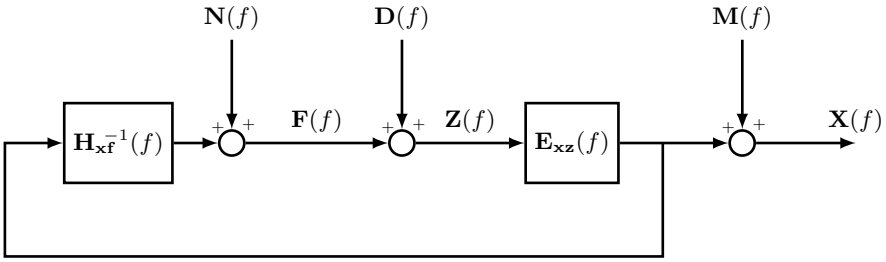

Figure 2.6 – Linear closed-loop block scheme of the human arm impedance $\mathbf{H_{xf}}^{-1}(f)$ combined with the admittance of the environment $\mathbf{E_{xz}}(f)$. The input to the environment is the summation of the external force disturbance $\mathbf{D}(f)$ and the hand reaction force $\mathbf{F}(f)$. The system output is the handle displacement $\mathbf{X}(f)$. Noise $\mathbf{N}(f)$ describes the part of the hand reaction force which was uncorrelated with the disturbance signal. Signal $\mathbf{M}(f)$ is also uncorrelated with the disturbance signal and describes the measurement noise together with the excluded dynamics due to linearization.

The estimated spectral densities in matrix notation are given as

$$\begin{aligned} \hat{\mathbf{\Phi}}_{\mathbf{dx}}(n\Delta_f) &= \begin{bmatrix} \hat{\Phi}_{d_x x_x}(n\Delta_f) & \hat{\Phi}_{d_x x_y}(n\Delta_f) \\ \hat{\Phi}_{d_y x_x}(n\Delta_f) & \hat{\Phi}_{d_y x_y}(n\Delta_f) \end{bmatrix} \\ \hat{\mathbf{\Phi}}_{\mathbf{df}}(n\Delta_f) &= \begin{bmatrix} \hat{\Phi}_{d_x f_x}(n\Delta_f) & \hat{\Phi}_{d_x f_y}(n\Delta_f) \\ \hat{\Phi}_{d_y f_x}(n\Delta_f) & \hat{\Phi}_{d_y f_y}(n\Delta_f) \end{bmatrix} \end{aligned} \qquad n = 0, 1 \ldots, N/2 \tag{2.1}$$

where N denotes the number of samples of the time domain signals and Δ_f the sampling increment in frequency domain.
The closed-loop estimated MFRF of the human arm admittance can be calculated by multiplication of the following spectral densities

$$\hat{\mathbf{H}}_{\mathbf{xf}}(n\Delta_f) = \hat{\mathbf{\Phi}}^T_{\mathbf{dx}}(n\Delta_f) \cdot (\hat{\mathbf{\Phi}}^{-1}_{\mathbf{df}})^T(n\Delta_f), \tag{2.2}$$

with the two-by-two matrix given as

$$\hat{\mathbf{H}}_{\mathbf{xf}}(n\Delta_f) = \begin{bmatrix} \hat{H}_{x_x f_x}(n\Delta_f) & \hat{H}_{x_x f_y}(n\Delta_f) \\ \hat{H}_{x_y f_x}(n\Delta_f) & \hat{H}_{x_y f_y}(n\Delta_f) \end{bmatrix} \tag{2.3}$$

Frequency averaging was applied on the spectral estimators over four adjacent frequencies for the estimation of the MFRFs. MFRFs were obtained by taking the gain and phase of $\hat{\mathbf{H}}_{\mathbf{xf}}$ for each element and frequency point.

Multiple coherence

Multiple coherence functions are a measure for linearity between the disturbance input and the resulting displacements, which are defined as.

$$\hat{\gamma}^2_{x_i d_{xy}} = \frac{\hat{P}_{x_i d_x}\hat{\Phi}_{d_x x_i} + \hat{P}_{x_i d_y}\hat{\Phi}_{d_y x_i}}{\hat{\Phi}_{x_i x_i}} \qquad i \in [x, y], \tag{2.4}$$

where $\hat{\gamma}^2_{x_x d_{xy}}$ and $\hat{\gamma}^2_{x_y d_{xy}}$ are respectively the multiple coherence functions from both input signals (D_x and D_y) to the output in x-direction (X_x) and from both input signals (D_x and D_y) to the output in y-direction (X_y). The term $\hat{P}_{x_i d_y}$ refers to elements of the estimated admittance of the total system from input $\mathbf{D}$ tot output $\mathbf{X}$ (equation A.22). The multiple coherence functions equals one for a linear system without noise and decrease by noise entering the system.

2.7 Parametric modeling

A simplified version of the linear state-space arm-environment model from De Vlugt et al. (2006) was used to estimate physical interpretable parameters (section 2.7). The model consisted of the environment, grip dynamics and the NMS system (figure 2.7). The latter includes the intrinsic musculoskeleton, sensors, neural time delay and activation dynamics. To investigate nonlinearities from inertial properties, a nonlinear skeletal model was developed in Simulink. A brief description of the linear and non-linear skeletal model is given below (see appendix B for the full model derivation).

Linear model

The geometrical representation of the 2 degrees of freedom (DOF) arm model is presented in figure 2.8. The humerus and forearm including the hand, cuff and handle mass were modeled as two segments with point masses (m_h and m_f). The point masses are located in the middle of the segments. The vector of generalized coordinates was chosen to be

$$\mathbf{q} = \begin{bmatrix} \theta_s \\ \theta_e \end{bmatrix} \tag{2.5}$$

with s and e respectively the shoulder and elbow joint.

The linear equations of motion for the human arm dynamics are given as

$$\ddot{\mathbf{q}} = (\mathbf{T}_\mathbf{q}^T \mathbf{M} \mathbf{T}_\mathbf{q})^{-1} \{-\mathbf{B}\dot{\mathbf{q}} - \mathbf{K}\mathbf{q} + \boldsymbol{\tau_e} - \boldsymbol{\tau_r}\}, \tag{2.6}$$

with $\mathbf{M}$, $\mathbf{B}$ and $\mathbf{K}$ the mass, intrinsic joint stiffness and intrinsic joint damping matrix, $\mathbf{T}_\mathbf{q} = \frac{\partial \mathbf{T}(\mathbf{q})}{\partial \mathbf{q}}$ is the mapping from generalized coordinates to cartesian coordinates and $\boldsymbol{\tau_e}$ the joint torque from the external force, given as

$$\boldsymbol{\tau_e} = \mathbf{J}^T \mathbf{f} \tag{2.7}$$

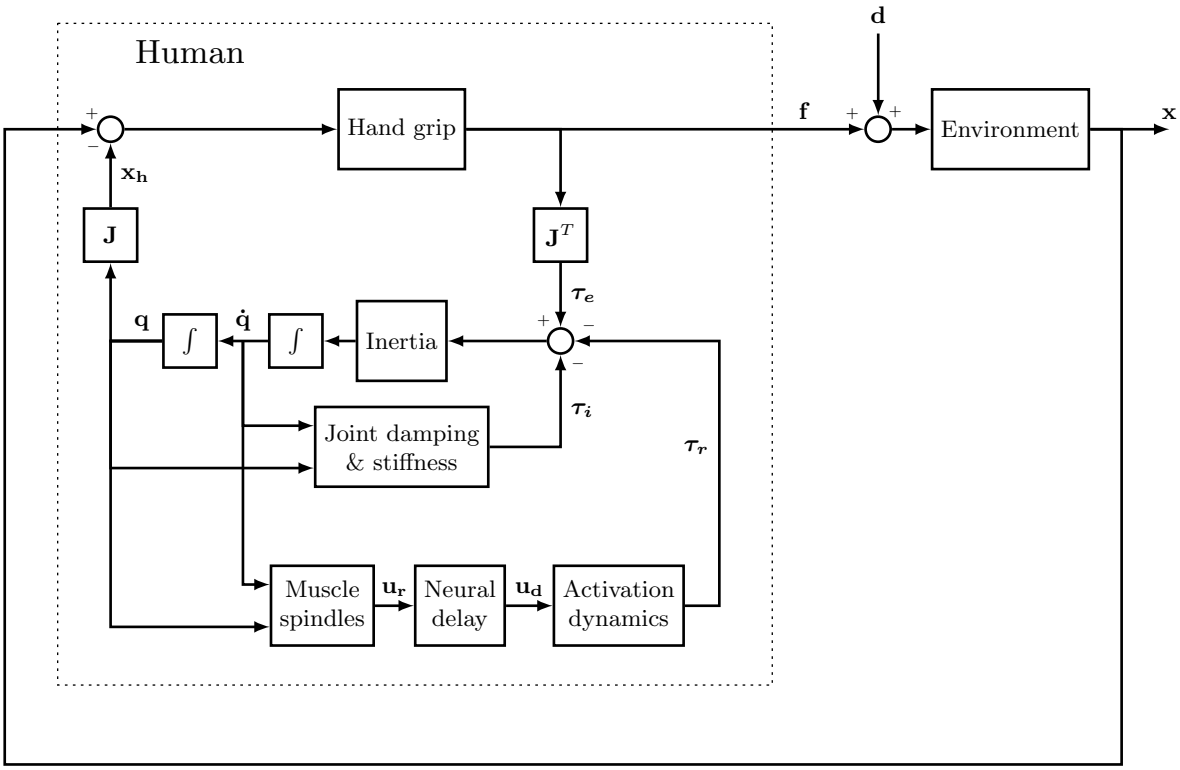

Figure 2.7 – Block scheme of the human arm model linked to the environment. The arm model consisted of the grip dynamics and the NMS system.

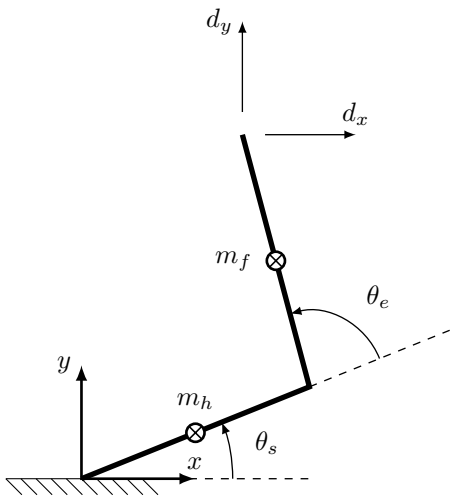

Figure 2.8 – Geometrical representation of the 2 dof arm model. The generalized coordinates θ_s and θ_e represents the shoulder and elbow angle, respectively. The parameter m_h denotes the mass of the humerus. The mass of the forearm, the hand, the cuff and the handle is captured in one parameter m_f.

where $\mathbf{J}$ is the jacobian and $\mathbf{f}$ the hand reaction force. The model was linearized by taking $\mathbf{T_q}$ and $\mathbf{J}$ constant at the mean joint angles during the multisine perturbations. The joint torque, $\boldsymbol{\tau_r}$, results from reflexive feedback force generated by the sensors accompanying with neural transport delay and activation dynamics. The sensors are the muscle spindles which has known to have an excitatory effect on the alpha motorneurons. The sensor dynamics are written as

$$\mathbf{u_r} = \mathbf{K_v}\dot{\mathbf{q}} + \mathbf{K_p}\mathbf{q} \tag{2.8}$$

with $\mathbf{K_v}$ and $\mathbf{K_p}$ respectively the velocity and position feedback gains, and $\mathbf{u_r}$ the input to the neural transport delay. The arm model was simplified by taken all muscle moment arms equal. This is done by choosing equal off-diagonal parameters for the matrices $\mathbf{M}$, $\mathbf{B}$, $\mathbf{K}$, $\mathbf{K_v}$ and $\mathbf{K_p}$. For the stiffness matrix this will looks like

$$\mathbf{K} = \begin{bmatrix} k_s & k_{se} \\ k_{es} & k_e \end{bmatrix}, \tag{2.9}$$

where single joint stiffness parameter are k_s and k_e, and the bi-articular joint parameter $k_{se} = k_{es}$. The diagonal parameters represents stiffness due to simultaneous synergistic single and two joint muscle activation (Hogan, 1985). The corresponding joint muscle parameters contributed by muscle groups are given by the following matrix

$$\mathbf{K} = \begin{bmatrix} k_s^* & k_{se} \\ k_{es} & k_e^* \end{bmatrix}, \tag{2.10}$$

with single-joint muscle stiffness parameters on the diagonal $k_s^* = k_s - k_{se}$ and $k_e^* = k_e - k_{es}$. Other matrices on joint level were converted to matrices on joint muscle level.

The neural delay is modeled by two third order Padé approximations. The muscles of the shoulder and the bi-articular shoulder-elbow muscles were modeled with the same time delay (T_{ds}). Likewise, one delay parameter T_{de} was taken for the muscles of the elbow and the bi-articular elbow-shoulder muscles. The activation dynamics was described by a critically damped second order Butterworth filter consisting of two cut-off frequency parameters for the shoulder the elbow and the bi-articular joint similar as the above described delay parameters, ($f_{act,s}$ and $f_{act,e}$).

The environment and grip dynamics are expressed in a two DOF cartesian coordinate frame $\mathbf{x} = [x_x\ x_y]^T$. The equations of motion for the environment are

$$\ddot{\mathbf{x}} = \mathbf{M_e^{-1}} \left(-\mathbf{B_e}\dot{\mathbf{x}} - \mathbf{K_e}\mathbf{x} + \mathbf{d} - \mathbf{f}\right), \tag{2.11}$$

with $\mathbf{x}$ the manipulator endpoint displacements and $\mathbf{d}$ the perturbation force $\mathbf{M_e}$, $\mathbf{B_e}$ and $\mathbf{K_e}$ the mass, stiffness and damping matrix of the environment dynamics.

The human arm and the environment are linked by the grip dynamics, which is given as

$$\mathbf{f} = \mathbf{B_h}(\dot{\mathbf{x}} - \dot{\mathbf{x}}_\mathbf{h}) + \mathbf{K_h}(\mathbf{x} - \mathbf{x_h}),$$

where B_h and K_h are the handgrip damping and stiffness matrix, and x_h the hand displacements. The hand displacements can be expressed in terms of the generalized coordinates

$$\mathbf{x_h} = \mathbf{qJ} \tag{2.12}$$

The matrices $\mathbf{M_e}$, $\mathbf{B_e}$, $\mathbf{K_e}$, $\mathbf{B_h}$ and $\mathbf{K_h}$ are chosen with equal diagonal terms and the off-diagonal terms zero. For $\mathbf{K_h}$ this is given by

$$\mathbf{K_h} = \begin{bmatrix} k_h & 0 \\ 0 & k_h \end{bmatrix}, \tag{2.13}$$

The model was simplified for the parameter estimation as motivated in appendix E. The mass parameters were taken together in one parameter according to $m_{tot} = m_h + m_f$ with

$$m_h = 0.49 \cdot m_{tot} \tag{2.14}$$
$$m_f = 0.51 \cdot m_{tot} \tag{2.15}$$
$$\tag{2.16}$$

The proportions of m_{tot} were determined by average mass values from De Vlugt et al. (2006) where the cuff and handle mass were taken into account. Neural delay and cut-off frequency parameters were fixed with equal values for each single and bi-articular joint respectively at 30 ms and 3.5 Hz. The handgrip parameters for the position task were fixed at $b_h = 57$ Ns/m and $k_h = 22.4$ kN/m, and for the relax task at $b_h = 32.8$ Ns/m and $k_h = 8.4$ kN/m. This are averaged parameter values obtained from the optimization described in appendix C and D. Finally, there are thirteen model parameters to be estimated (table 2.2).

Table 2.2 – Intrinsic and reflexive model parameters to be estimated.

Nr.	Parameter	Unit	Nr.	Parameter	Unit
Segmental mass			*Velocity feedback*		
1	m_{tot}	kg	11	k_{v_s}	Nms/rad
Joint damping			12	$k_{v_{se}}$	Nms/rad
3	b_s	Nms/rad	13	k_{v_e}	Nms/rad
4	b_{se}	Nms/rad	*Position feedback*		
5	b_e	Nms/rad	14	k_{p_s}	Nm/rad
Joint stiffness			15	$k_{p_{se}}$	Nm/rad
6	k_s	Nm/rad	16	k_{p_e}	Nm/rad
7	k_{se}	Nm/rad			
8	k_e	Nm/rad			
Environmental mass, damping and stiffness					
	m_{env}	N s^2 /m			
	b_{env}	N s /m			
	k_{env}	N /m			

Non-linear skeletal model

The above described linear model is extended with nonlinearities from inertial properties (geometrical, centripetal and Coriolis). The nonlinear model has an additional term in the equations of motion for the human arm dynamics. Now, the equations of motion becomes

$$\ddot{\mathbf{q}} = (\mathbf{T}_\mathbf{q}^T \mathbf{M} \mathbf{T}_\mathbf{q})^{-1} \left\{ -\mathbf{B}\dot{\mathbf{q}} - \mathbf{K}\mathbf{q} - \mathbf{T}_\mathbf{q}^T \mathbf{M}\mathbf{g} + \boldsymbol{\tau_e} - \boldsymbol{\tau_r} \right\}, \tag{2.17}$$

with $\mathbf{g} = \frac{\partial \mathbf{T}_\mathbf{q}(\mathbf{q})}{\partial \mathbf{q}} \dot{\mathbf{q}}^2$. The matrices $\mathbf{T}_\mathbf{q}$ and $\mathbf{J}$ were not taken constant, but updated for every time step during the simulation.

Parameter estimation

The linear model parameters described in the previous section were estimated by optimization in frequency domain. The optimization sometimes resulted in an unstable system for the position task. As described in appendix C this was resolved using a penalty function. The used criterion function is described below.

The MFRF of the linear model was fitted onto the estimated MFRF by using the following error function

$$\begin{aligned} \epsilon_{xi}(f_k) &= \gamma_{xd_{xy}}(f_k) \left| \ln \left(\frac{\hat{\hat{H}}_{x_x f_i}(f_k)}{\hat{H}_{x_x f_i}(f_k)} \right) \right| \\ \epsilon_{yi}(f_k) &= \gamma_{yd_{xy}}(f_k) \left| \ln \left(\frac{\hat{\hat{H}}_{x_y f_i}(f_k)}{\hat{H}_{x_y f_i}(f_k)} \right) \right| \end{aligned} \qquad i \in [x, y],\ k = 1 \ldots n_f, \tag{2.18}$$

where $\hat{H}_{xf}$ denotes the four elements of the estimated MFRF, $\hat{\hat{H}}_{xf}$ the four elements of the MFRF of the model, n_f the number of frequency points of the frequency vector f_k. The error function was weighted by the square root of the multiple coherence functions (equation 2.4). The quadratic criterion function that was minimized is given as

$$V = \frac{1}{N} \sum_{k=1}^{N} \left(\boldsymbol{\epsilon}(k) \cdot p(\mathrm{Re}[\sigma_{max}]) \right)^2 \qquad N = 4 \cdot n_f \tag{2.19}$$

with n_f the number of frequency points and the error vector contains four error vectors for each element of the MFRF, given as

$$\boldsymbol{\epsilon} = [\boldsymbol{\epsilon_{xx}}\ \boldsymbol{\epsilon_{xy}}\ \boldsymbol{\epsilon_{yx}}\ \boldsymbol{\epsilon_{yy}}]^T \tag{2.20}$$

The penalty function yields

$$p(\mathrm{Re}[\sigma_{max}]) = 10 \cdot (1e10^{\mathrm{Re}[\sigma_{max}]+0.5}) + 1, \tag{2.21}$$

where $\mathrm{Re}[\sigma_{max}]$ denotes the maximum eigenvalue (real part) of the state-space matrix A of the total system (arm + environment).

The accuracy of the estimated model parameters was validated by the standard error of the mean (SEM), which is given as

$$\mathrm{SEM} = \sqrt{\mathrm{diag}\left(\frac{1}{N}(\mathbf{J}^T \cdot \mathbf{J})^{-1}\boldsymbol{\epsilon} \cdot \boldsymbol{\epsilon}^T\right)} \tag{2.22}$$

where the jacobian is the partial derivative of the criterion function with respect to the parameters.

The estimated model parameters were validated by the variance accounted for (VAF), given as

$$\mathrm{VAF}_i = \left(1 - \frac{\sum_{k=1}^{n} |x_i(t_k) - \hat{x}_i(t_k)|^2}{\sum_{k=1}^{n} |x_i(t_k)|^2}\right) \cdot 100\%, \qquad i \in [x,\ y] \tag{2.23}$$

with $x_i(t)$ the recorded handle displacement and $\hat{x}_i(t)$ the handle displacements predicted by the parametric model in either x- or y-direction. The recorded and predicted displacements for the continuous perturbations were high pass filtered (0.40 Hz, 3th order Butterworth filter) to remove voluntary interventions. The VAF describes the goodness of the model fit in time domain.

2.8 Pulse response analysis

To quantify the admittance in response to pulse perturbations the following simple metric was derived

$$\text{Pulse admittance} = \frac{||x||_{max}}{||f||_{max}}, \tag{2.24}$$

where $||x||_{max}$ and $||f||_{max}$ denote the recorded peak (maximum vector 2-norm) hand displacements and recorded peak hand reaction force. For the position task, the peak displacements and peak hand reaction forces were determined for a time span of 300 ms after onset of the pulse perturbation. For the relax task, the time span was chosen 1 sec. In these time spans, the vector 2-norm of the displacements showed a parabolic curve.

Figure 2.9 shows the outline of this study. Parameters of the linear model were estimated using continuous perturbations. The pulse response was predicted by the linear and nonlinear skeletal model. The state of the system at the onset of the pulse was taken into account by simulating the total disturbance signal response (i.e. the multisine with the pulse) of the linear model. In order to investigate only the effect of nonlinearities from inertial properties to the pulse prediction, we want the linear and nonlinear skeletal model to have the same state at the onset of the pulse. Therefore, the state of the linear model at the onset of the pulse was used as the initial state for the nonlinear skeletal model where only the pulse disturbance response was simulated.

The accuracy of the pulse prediction was quantified by the following ratio

$$\text{Pulse prediction} = \frac{||\hat{x}||_{max}}{||x||_{max}} \cdot 100\%, \tag{2.25}$$

where $||\hat{x}||_{max}$ and $||x||_{max}$ denote the maximum vector 2-norm of the simulated and recorded displacements in response to the pulse. The same time spans were used as for the pulse gain.

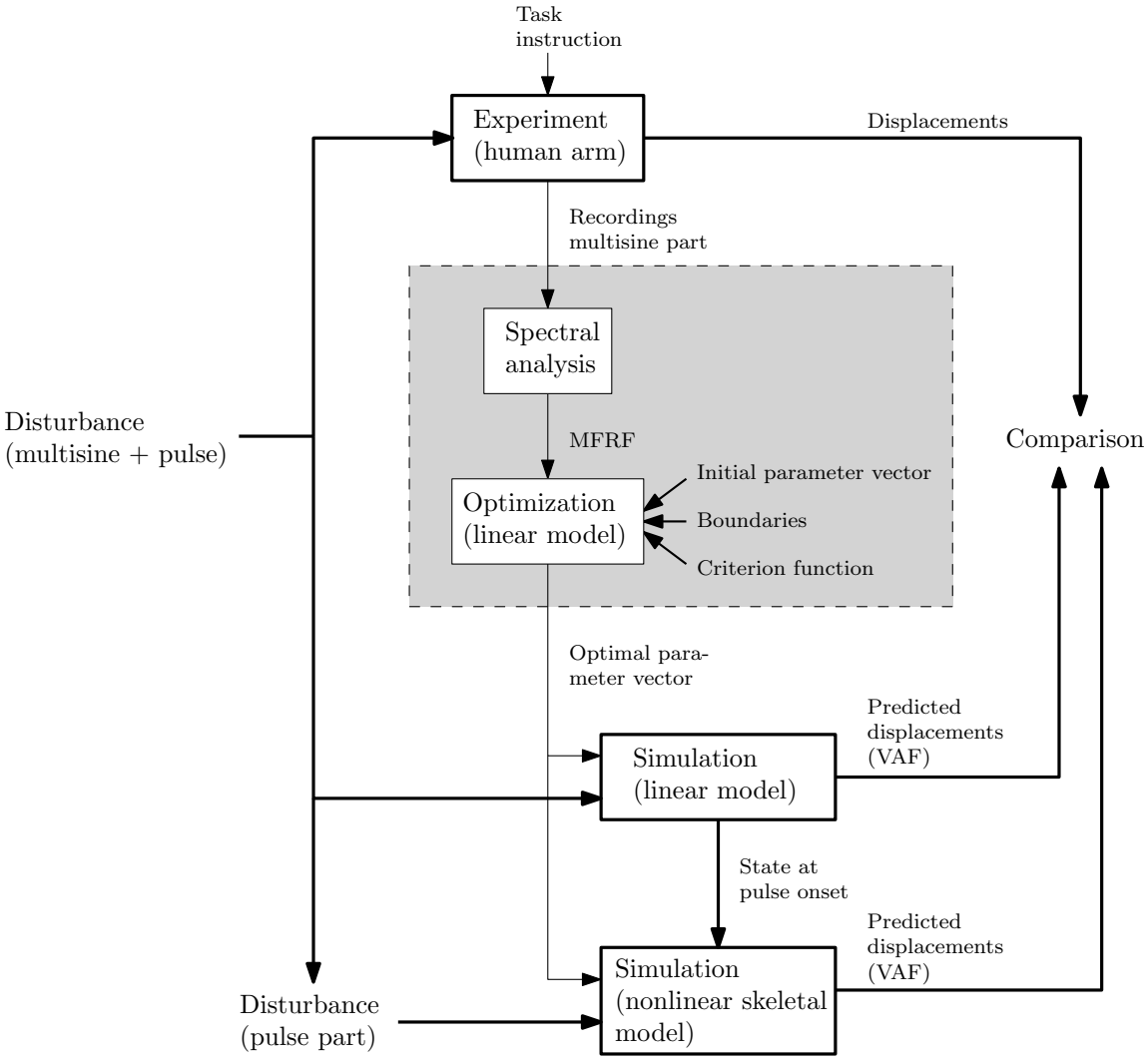

Figure 2.9 – Flow chart of the study. The total disturbance signal applied at the human arm (experiment) was the input to the linear model. The pulse response of the nonlinear skeletal model was simulated with the initial state at the pulse onset obtained from the linear model simulation. The handle displacements were compared to the predicted displacements of the linear and nonlinear skeletal model. The grey area denotes the procedure to obtain the estimated linear model parameters. The estimated linear model parameters were used for both the linear and nonlinear skeletal model simulations.

2.9 Statistical analysis

Statistical analysis was performed to investigate the effect of amplitude and pre-perturbations. Tests were done on the estimated admittance, parameters, peak displacements, pulse gain and pulse prediction. A one way repeated measures ANOVA was carried out to determine effects between the different amplitude levels of the continuous perturbations (RMS values of 0, 2.5, 7.5 and 22.5 mm). Post-hoc tests using the Bonferroni correction were used to determine between which groups the significant differences occurred. The assumption of sphericity was tested for every repeated measures ANOVA. When the assumption of sphericity was violated, the Greenhouse-Geisser adjustment was applied. Each condition was tested for normality (Shapiro-Wilk test). Friedman's one-way ANOVA by ranks was used instead of a repeated measures ANOVA when a group was not normally distributed. Friedman's test ranks the values of the three conditions from 1 to 3 for each subject. The effect of amplitude for the minimum and maximum pulse level

was tested by a dependent t-test.
The analysis of the estimated admittance needs further explanation. The repeated measures ANOVA was used to determine wether the averaged gain over subjects at each frequency point differed significantly between three conditions (for the position task $PT_{2.5}$, $PT_{7.5}$ and $PT_{22.5}$, and for the relax task $RT_{2.5}$, $RT_{7.5}$ and $RT_{22.5}$). Effects were considered significant when at least four adjacent frequency points showed a significant difference for each individual frequency point.

CHAPTER 3

Results

Results of the spectral analysis are shown in section 3.1. Subsequently, results of the parametric modeling are shown in section 3.2. Finally, results of the pulse response analysis are described in section 3.3.

3.1 Spectral analysis

This section describes the results of the spectral analysis of the continuous perturbation signals. First, the variability of the estimated admittances of one condition is shown. Then the position and relax task are compared for one condition. Subsequently, amplitude effects (RMS values of 2.5, 7.5 and 7.5 mm) on the admittance will be described for the position and relax task. Finally, the averaged multiple coherences will be described.

For one typical subject, the gain and phase of the estimated admittance for eight trials of the condition $PT_{7.5}$ are presented in figure 3.1. As can be seen from the individual trials, the gain and phase characteristics of the diagonal elements of the admittance ($\mathbf{H_{xx}}$ and $\mathbf{H_{yy}}$) are estimated rather consistent for the lower and higher frequencies, but irregular peaks are present around 3-7 Hz. This justifies the choice of adding extra frequencies to the disturbance signal around these frequencies (figure 2.5). The off-diagonal elements of the estimated admittance ($\mathbf{H_{xy}}$ and $\mathbf{H_{yx}}$) show even more more variance indicating that the off-diagonal elements are more sensitive to noise. Furthermore, this figure shows the averaged estimated MFRFs over the trials. This averaged estimated admittance is not the mean of the gain and phase, because averaging occurred on the spectral estimators.

The position and relax task are compared for the conditions $PT_{7.5}$ and $RT_{7.5}$ in figure 3.2. The effect of task instruction is clearly visible at the lower frequencies. The large difference between the two task instructions is indicated by calculating the relative difference in gain averaged over the first two frequency points for the diagonal elements. Here, the gain for the relax task appears to be a factor 18 larger than the gain for the position task. The low admittance for the position task indicates stiffening whereas the high admittance for the relax task indicates a yielding effect. Remarkably, the admittance for the position task is higher around 5-10 Hz which is possibly primarily the result of high intrinsic stiffness, because it is well known that oscillation peaks shift to higher frequencies with increasing stiffness.

The averaged estimated admittance over subjects for the three different amplitude levels are presented in figure 3.3 for the position task and in figure 3.4 for the relax task. For both tasks, most of the lower frequencies show statistically significant different gains. It is difficult to see the differences in gain from figures 3.3 and 3.4 because of the logarithmic scale. Therefore, the gain characteristics are shown on a linear scale in figure 3.5 for both the position and relax task. It is clear from this figure that the difference between the three amplitude levels at the lower frequencies has an opposite effect for the relax and position task. For the position task, the higher the amplitude level, the lower the admittance. Higher admittances at higher amplitude levels are observed for the relax task. To get an indication of the physical meaning of the differences, the relative difference in gain between the minimum and maximum amplitude level of the first two frequency points for the diagonal terms is calculated. This relative difference appears to be a factor 1.5 for the position task and a factor 3.8 for the relax task.

Figure 3.6 shows the multiple coherence functions $\gamma^2_{xd_{xy}}$ (from both disturbance inputs to the displacement in x-direction) and $\gamma^2_{yd_{xy}}$ (from both disturbance inputs to the displacement in y-

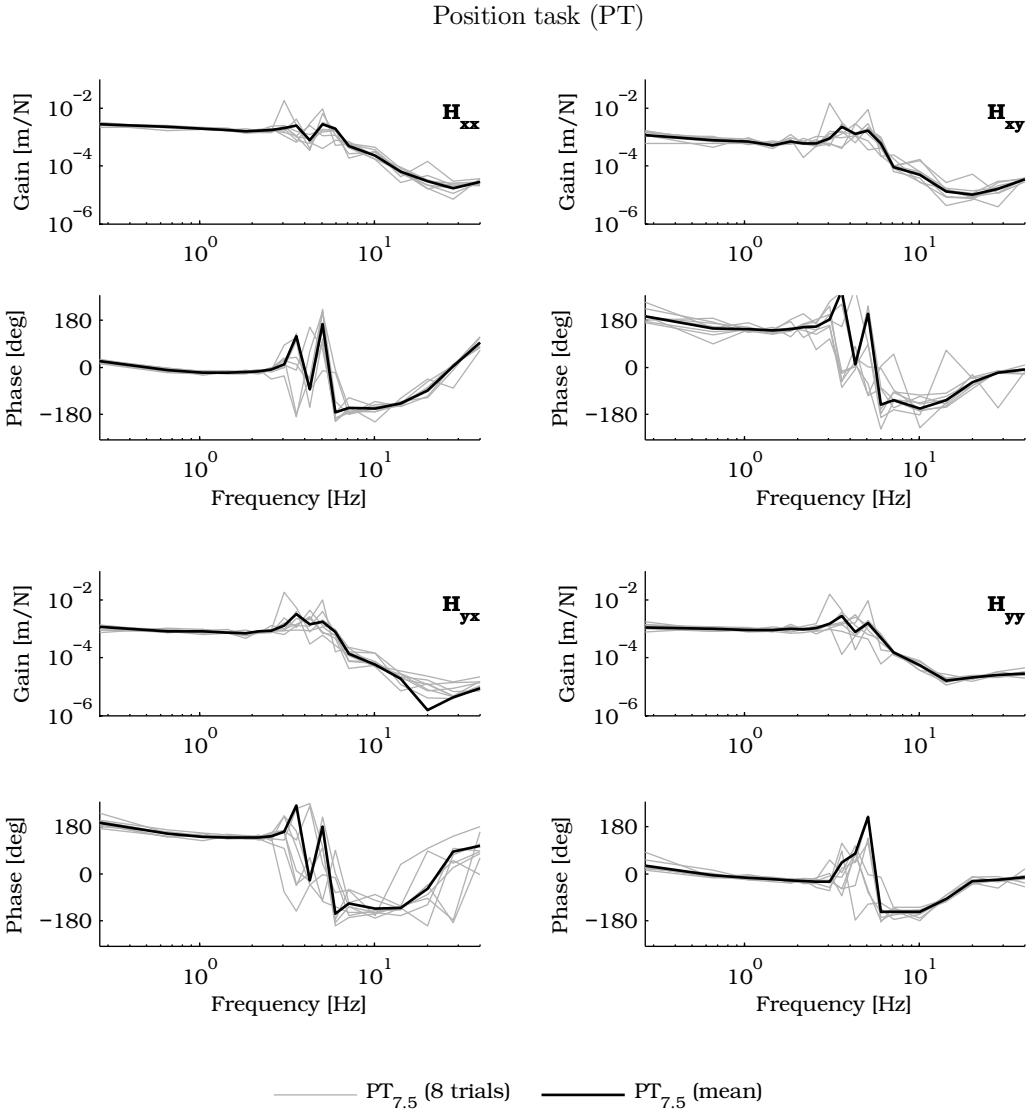

Figure 3.1 – Estimated matrix frequency response (MFRF) functions of one typical subject for the position task (PT). Grey lines: eight trials of condition $PT_{7.5}$. Black lines: averaged estimated MFRFs of these 8 trials.

direction). The left figures show the multiple coherence functions for the PT and the right figures for the RT. Overall, the multiple coherence for the position task is high over the full frequency range whereas the multiple coherence for the relax task drops frequencies >1.5 Hz. This is probably caused by the low signal to noise ratio at the frequency points where the reduced power method was applied. Compared to the two higher amplitude levels in the position task, a lower multiple coherence is observed for $PT_{2.5}$ also probably due to a low signal-to-noise-ratio.

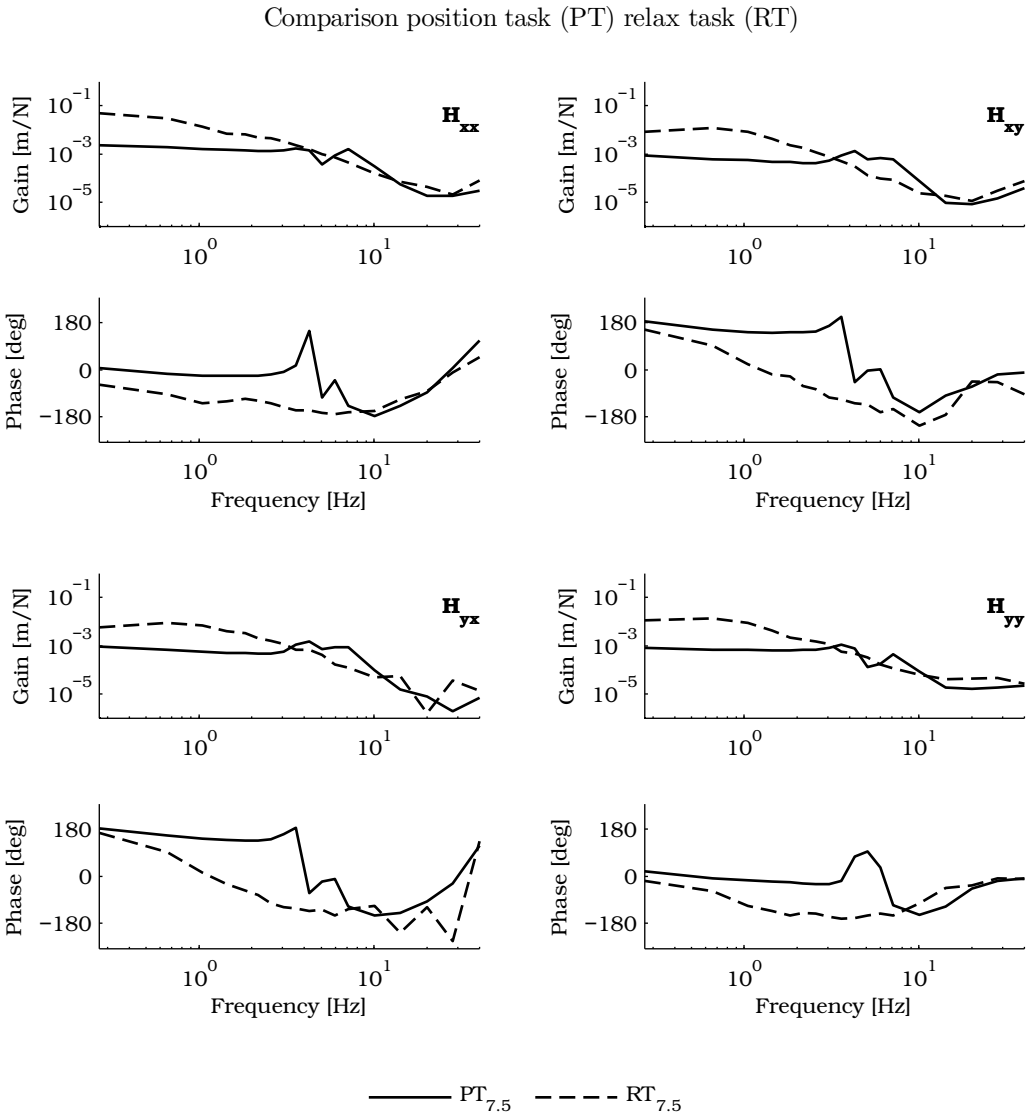

Figure 3.2 – Estimated matrix frequency response (MFRF) functions averaged over all subjects for two different conditions ($PT_{7.5}$, $RT_{7.5}$) showing the difference between the position and relax task.

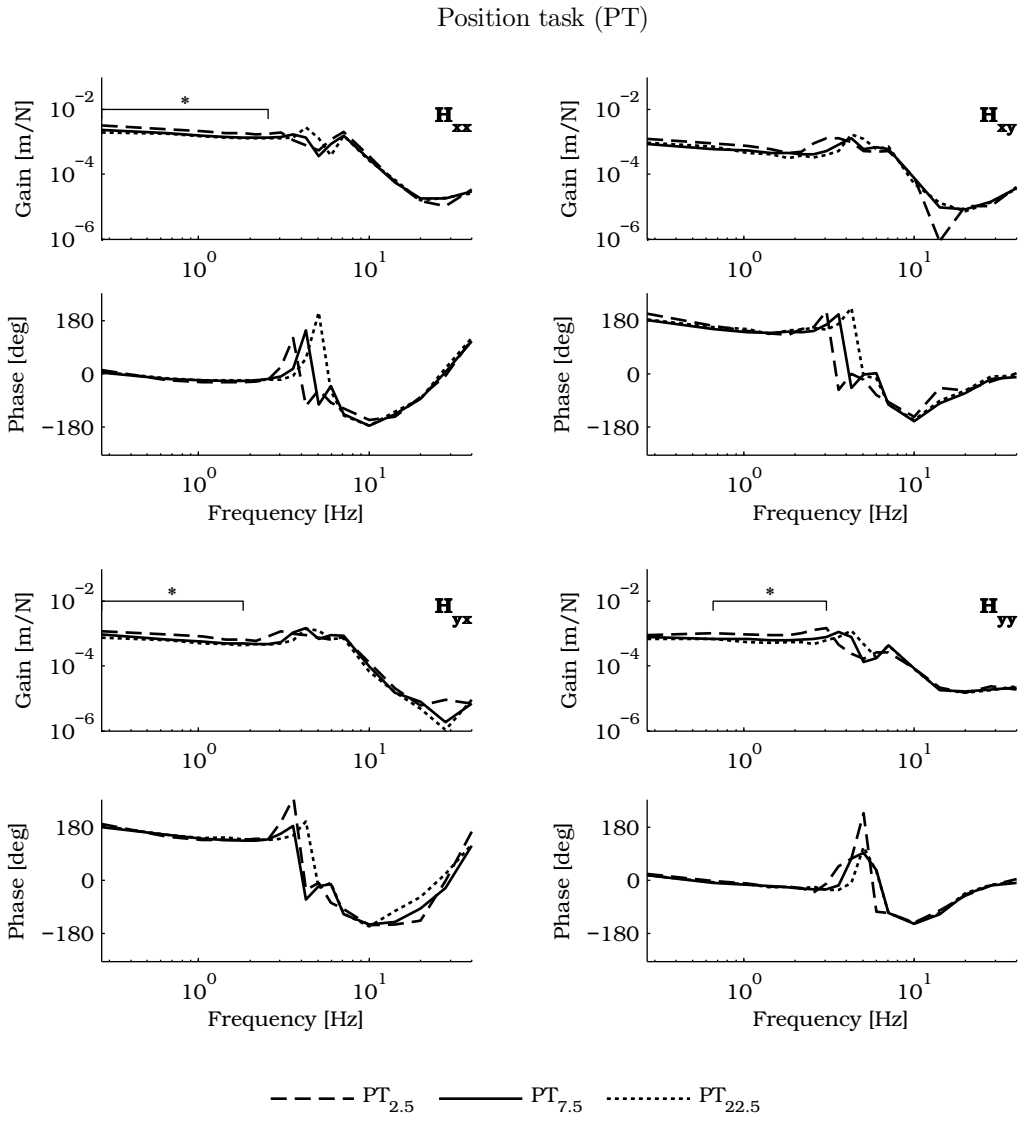

Figure 3.3 – Estimated matrix frequency response (MFRF) functions averaged over all subjects for the three conditions $PT_{2.5}$, $PT_{7.5}$ and $PT_{22.5}$. The symbol $*$ means significant differences between the three conditions at $p < 0.05$.

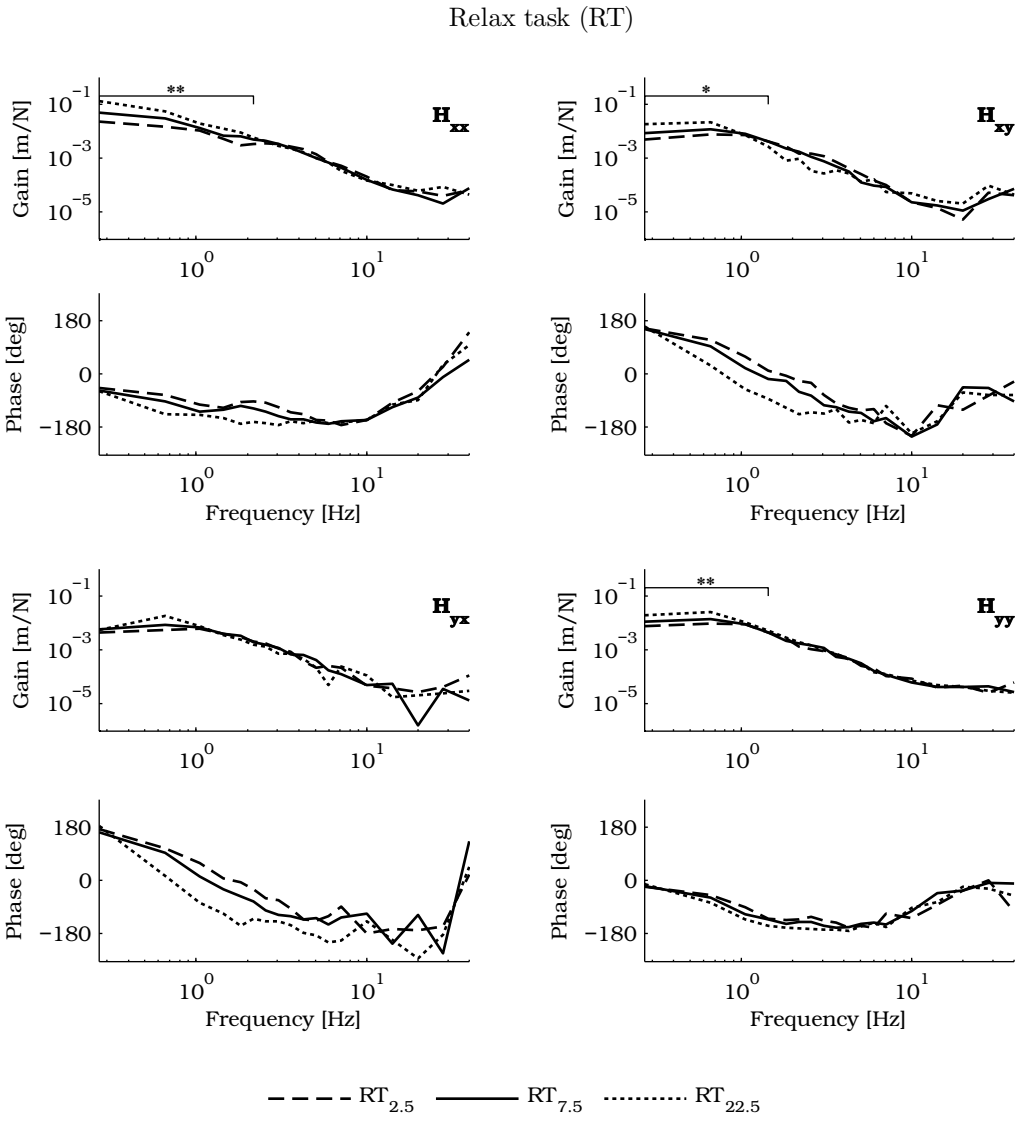

Figure 3.4 – Estimated matrix frequency response (MFRF) functions averaged over all subjects for the three conditions $RT_{2.5}$, $RT_{7.5}$ and $RT_{22.5}$. The symbol $*$ means significant differences between conditions at $p < 0.05$ and $**$ at $p < 0.01$.

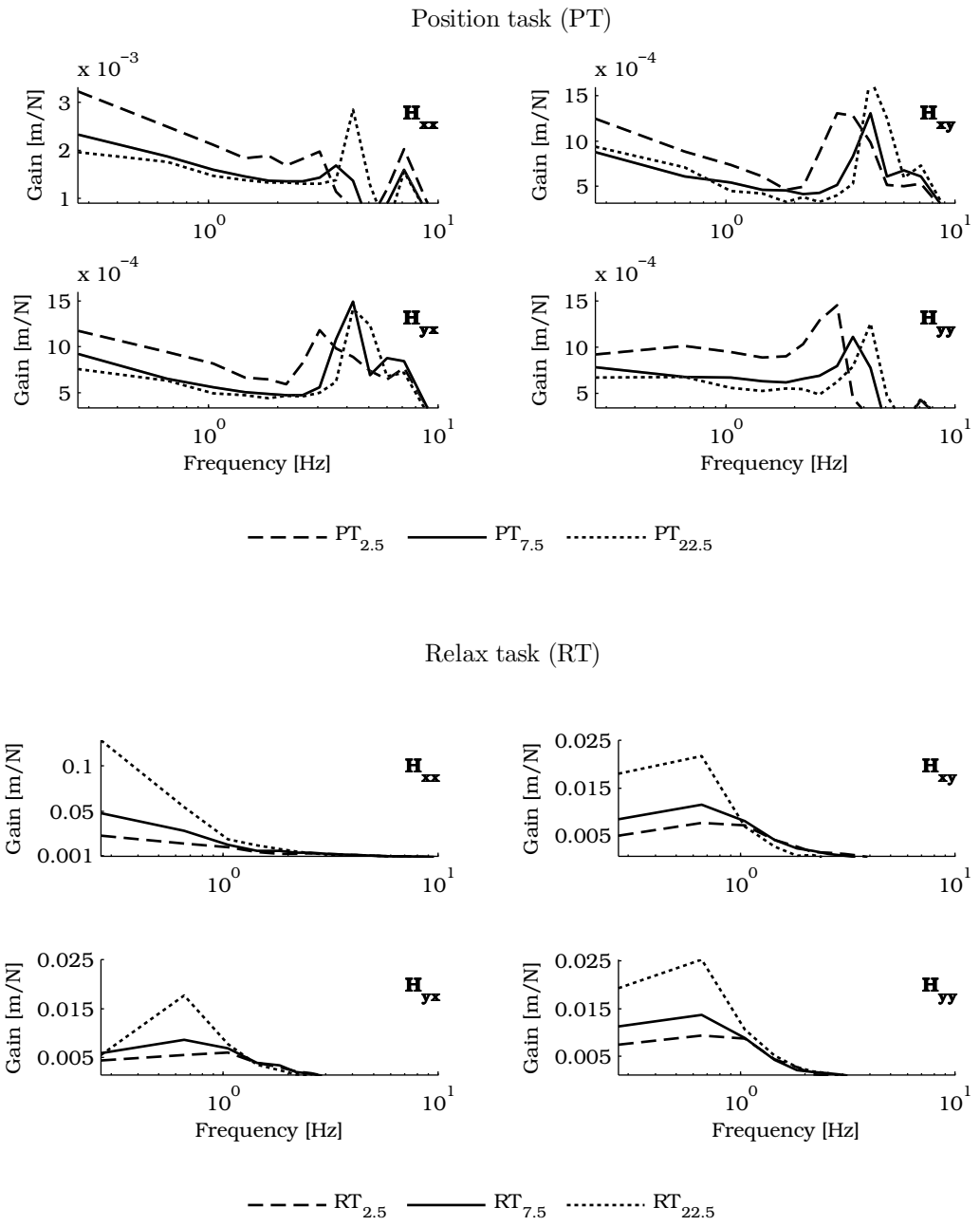

Figure 3.5 – Gain characteristics of figures 3.3 and 3.4 on a linear scale at the lower frequencies ($\leq$ 10 Hz) for both the position (upper figures) and relax (lower figures) task. The gain is zoomed in on the parts where the significant effects between the three conditions (indicated by the subscripts 2.5, 7.5 and 22.5) are clearly visible.

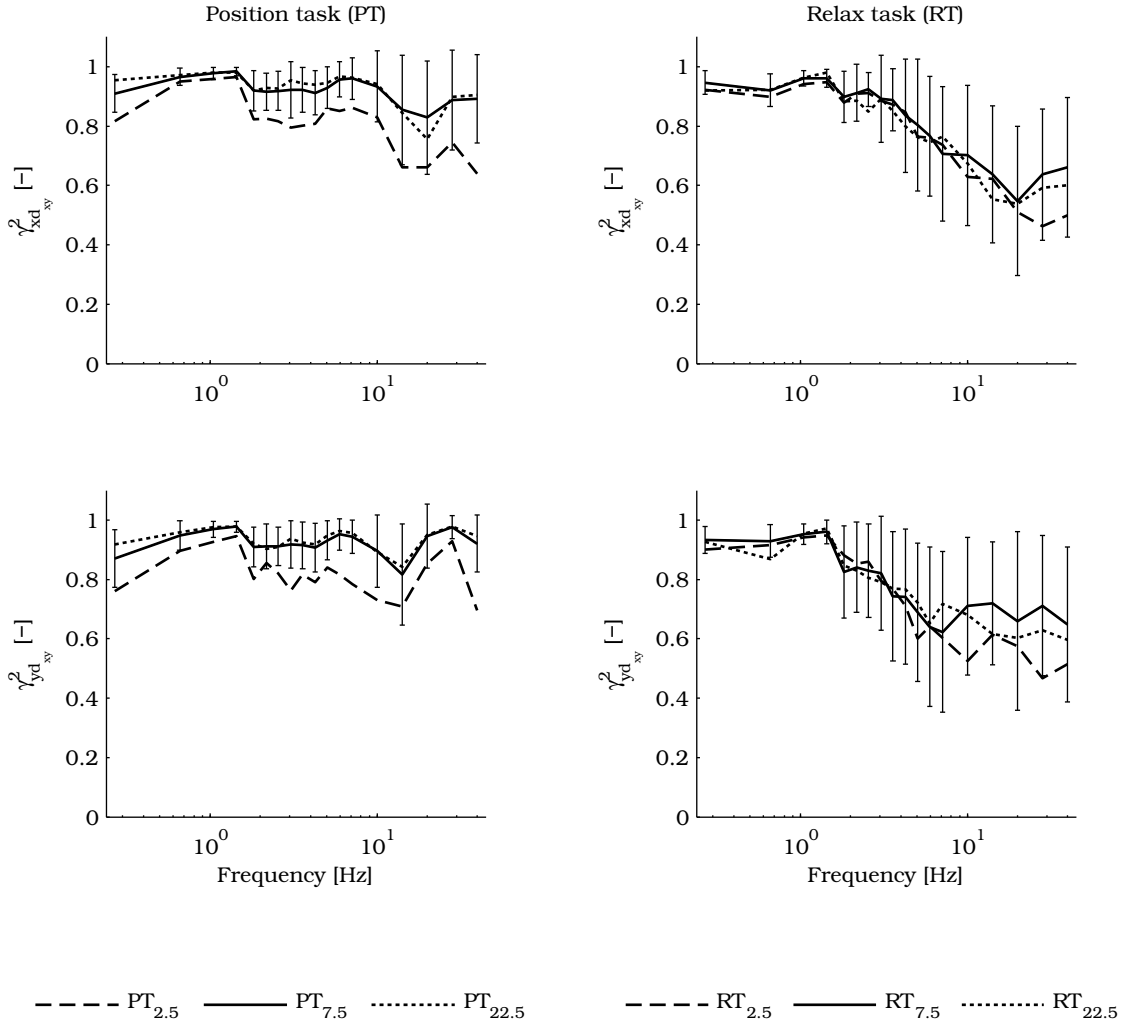

Figure 3.6 – Multiple coherence functions averaged over all subjects for the three different RMS levels of displacements. The upper figures show $\gamma^2_{xd_{xy}}$ which is the multiple coherence function from both disturbance inputs to the displacement in x-direction. The lower figures show $\gamma^2_{yd_{xy}}$ which is the multiple coherence function from both disturbance inputs to the displacement in y-direction. Left figures: position task ($PT_{2.5}$, $PT_{7.5}$ and $PT_{22.5}$). Right figures: relax task ($RT_{2.5}$, $RT_{7.5}$ and $RT_{22.5}$). The errorbars represent the standard deviation of the condition 7.5 mm RMS displacements ($PT_{7.5}$ and $RT_{7.5}$).

3.2 Parametric modeling

This section describes the accuracy of the estimated model parameters in frequency and time domain are shown. After that, amplitude effects will be described for the estimated parameters on joint level and for the converted parameters to muscle groups.

Figures 3.7 and 3.8 show examples of the model fit in frequency domain for the position and relax task, respectively. For the position task, the model has difficulties describing the gain and phase at frequencies higher than 4 Hz. The model describes a first oscillation peak well, but a second smaller peak is not captured by the model. A good fit of the second smaller peak was obtained by extending the model structure with force or velocity feedback. However, we choose to exclude force and acceleration feedback due to the presence of local minima in the optimization. The limitations of the parameter estimation are described in appendices C-E. The fit for the relax task is rather good as can be seen in figure 3.8. The estimated admittance shows some irregularities at higher frequencies which is consistent with the drop seen in the multiple coherence functions (figure 3.6).

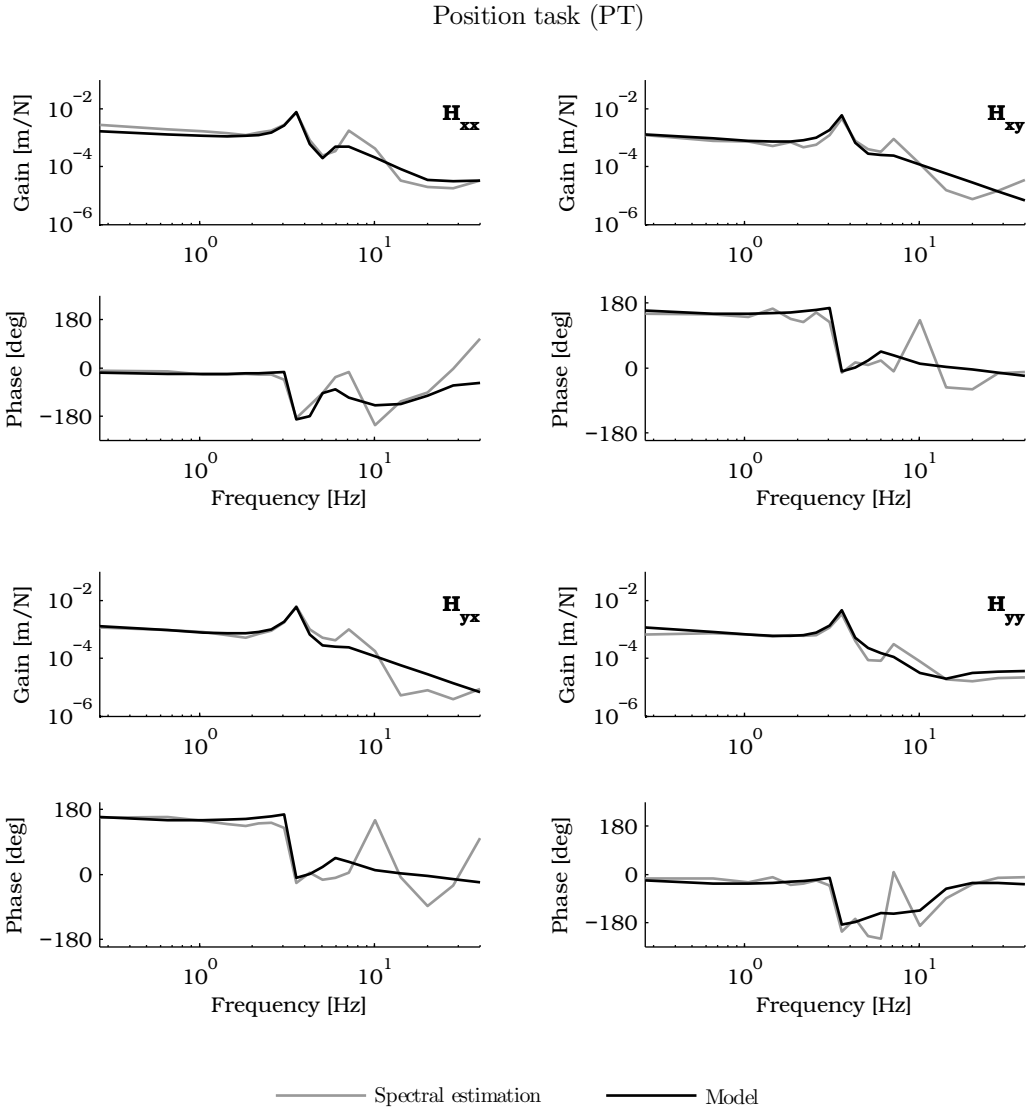

Figure 3.7 – Fit of the admittance of the arm model (black lines) onto the estimated admittance of the human arm (grey lines) for one specific trial of the condition $PT_{7.5}$.

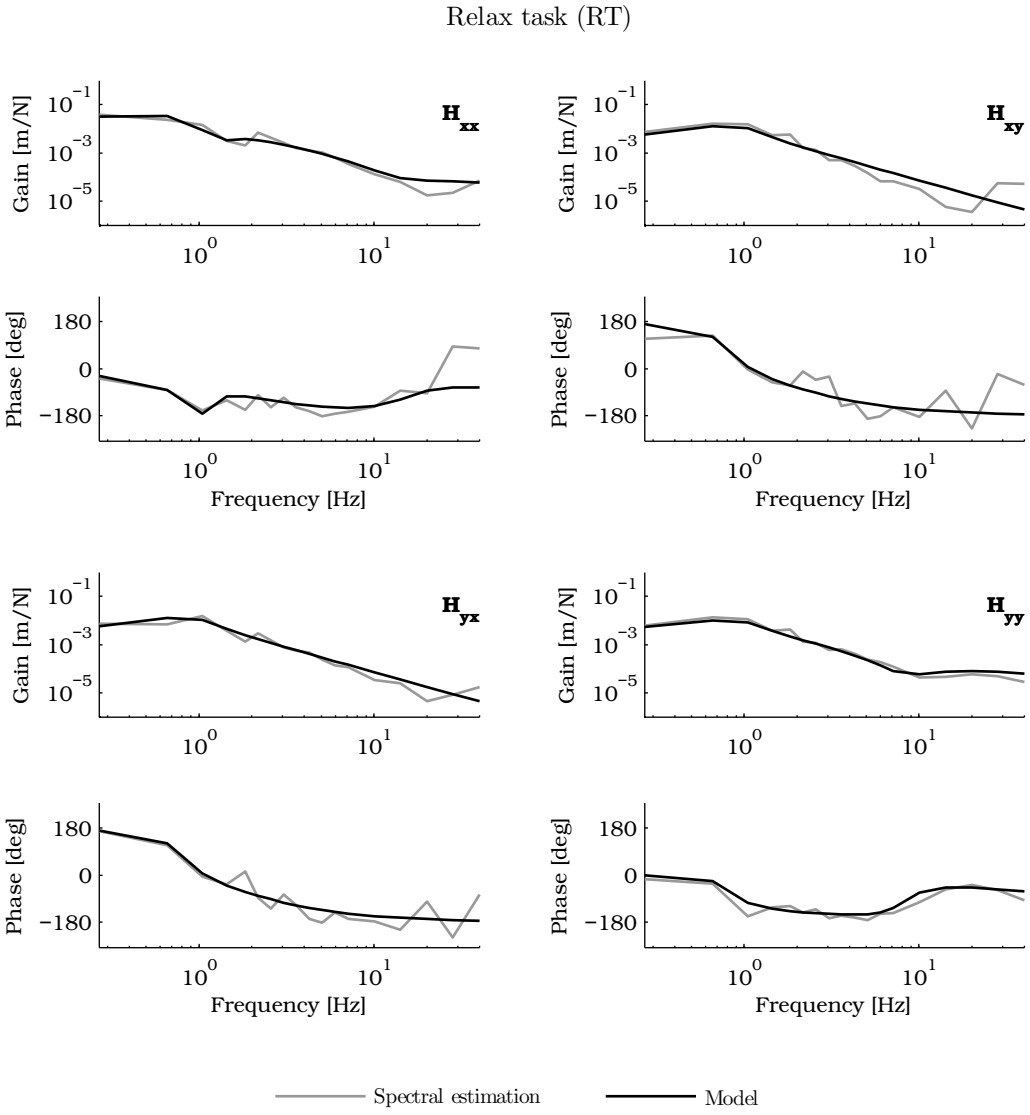

Figure 3.8 – Fit of the admittance of the arm model (black lines) onto the estimated admittance of the human arm (grey lines) for one specific trial of the condition $RT_{7.5}$.

The linear model obtained by optimization in the frequency domain was used to simulate the time response. An example of the model fit in time domain for the position and relax task are respectively given in figures 3.9 and 3.10. The accuracy of the time domain fits is determined by the VAF. Figure 3.11 shows the average VAF values over subjects of the linear model and nonlinear skeletal model simulations for the three levels of continuous perturbations. Clearly, the nonlinear skeletal model simulation with optimized linear model parameters do not lead to relevant changes in the time domain predictions. The average VAFs for the lowest level (2.5 mm) is lower than the other two conditions. The averaged VAF for $RT_{22.5}$ is higher than the condition $RT_{7.5}$. For the other conditions, almost equal VAFs are observed between the largest two perturbation levels.

The estimated linear model parameters together with the corresponding SEMs for all joint combinations and different amplitude levels are shown in figure 3.12 and 3.13 respectively for the position and the relax task. Compared to the position task, much lower intrinsic parameter values are found for the relax task. This result is in agreement with the differences in admittance for both tasks shown in the previous section.
Most of the SEMs exceed the corresponding parameter value for the position task. Overall, it can

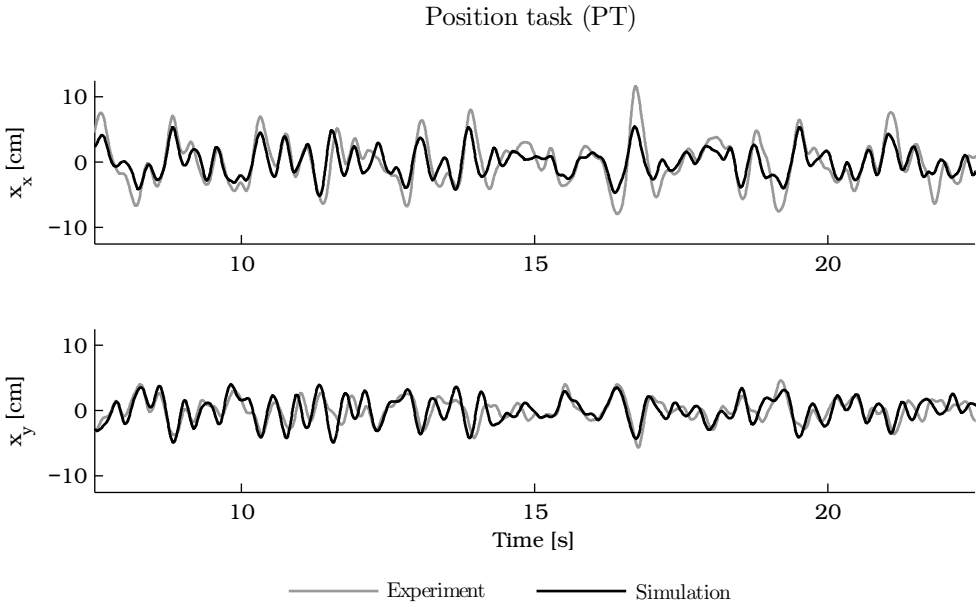

Figure 3.9 – Time sample of the linear model fit of one trial for the condition $PT_{7.5}$. The recorded displacements (grey lines) and the simulated displacements (black lines) in x-direction and y-direction are respectively shown in the upper and lower figure.

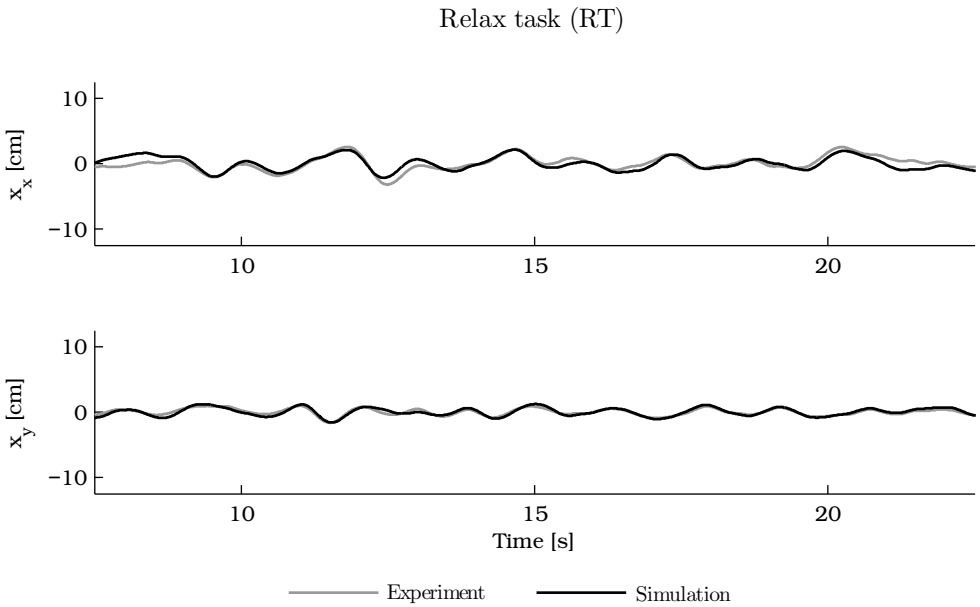

Figure 3.10 – Time sample of the linear model fit of one trial for the condition $RT_{7.5}$. The recorded displacements (grey lines) and the simulated displacements (black lines) in x-direction and y-direction are respectively shown in the upper and lower figure.

be concluded that the parameters of the position task are not estimated accurately in spite of the explorations and simplifications in appendices C-E. The relax task show better SEMs compared to the position task. Most of the SEMs are lower than the corresponding parameter value and some parameters exceed the corresponding parameter value slightly. For the relax task, figure 3.13 shows highly significant effects of stimulus amplitude for all estimated parameters being lower for larger amplitudes. For the position task the nonlinear behavior was less clear. Only 3 out of 12 parameters show significant effects of amplitude. The effect was not consistent; the shoulder position feedback parameter decreases and the shoulder stiffness and velocity feedback

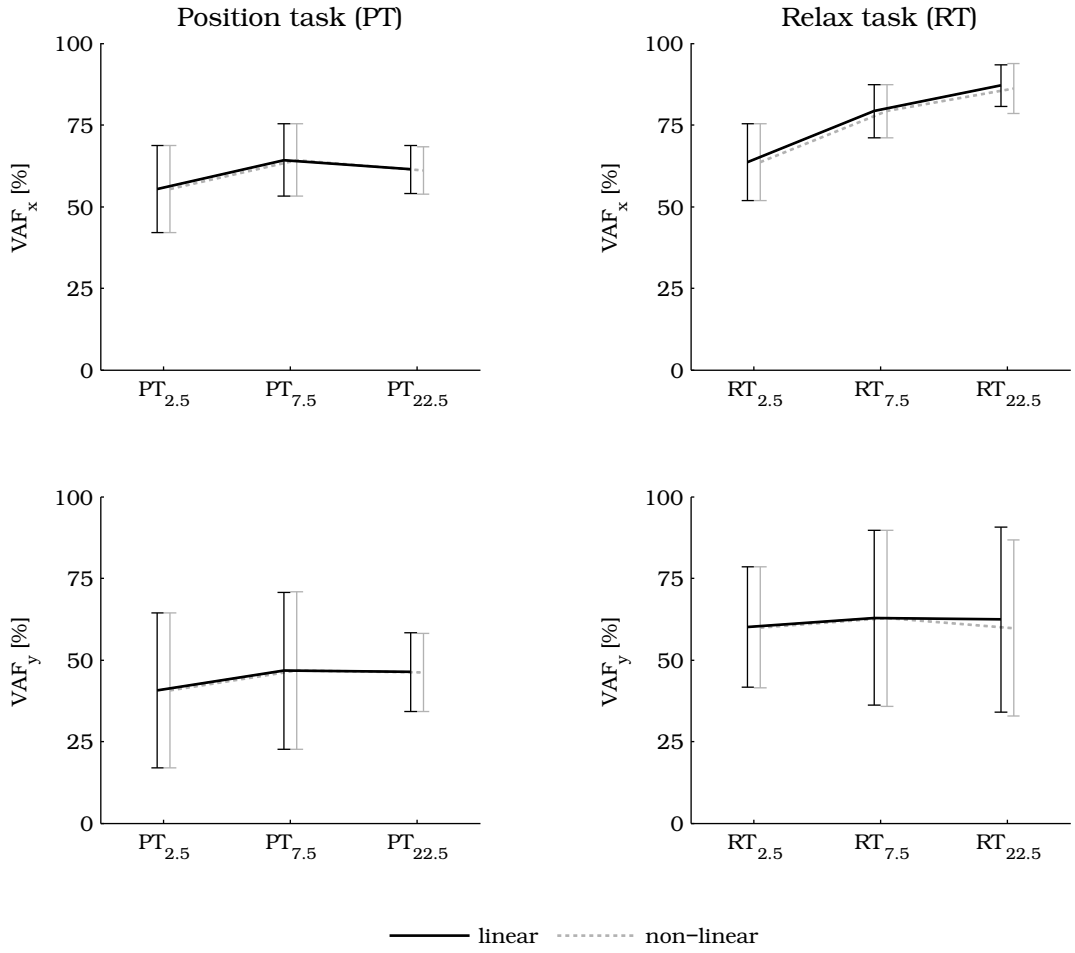

Figure 3.11 – The VAFs in x-direction (upper pictures) and y-direction (lower pictures) calculated with the linear (grey lines) and nonlinear (black lines) skeletal model for the position task (left pictures) and the relax tasks (right pictures). The errorbars denote the standard deviation over all trials.

increase with larger stimulus amplitudes.
For the position task, parameter values increase from the shoulder to elbow joint except for the intrinsic stiffness parameters. The intrinsic stiffness parameter shows a significant difference between conditions (p=0.002) for the shoulder joint. The stiffness is higher for the highest amplitude level. The velocity feedback shows higher feedback gains for the largest amplitude level of the multi-joint and elbow joint parameters. This effect is only significant for the multi-joint velocity feedback gain (p=0.003). The position feedback of the shoulder joint shows an opposite effect; a significantly higher gain for the decreasing amplitude level (p=0.045). The estimated parameters for the muscle groups are shown in figure 3.14 for the position task (left figures). These parameters are converted from the estimated parameters on joint level (figure 3.12). For the shoulder muscles, the stiffness, position and velocity feedback parameter change significantly between conditions. The reflexes decrease whereas the stiffness increases with larger amplitude levels. The effect of the multi-joint velocity feedback parameter is already described for figure 3.12. In general, the shoulder muscle parameters are low compared to the multi-joint shoulder-elbow and elbow parameters.
For the relax task, all parameters are significantly different between the three different amplitude levels at p=0.000 and show the same effect: a higher damping and stiffness for lower amplitude levels. The damping parameter values are very low with small differences between conditions. On the other hand, a very large amplitude effect can be seen for the stiffness parameters. The converted estimated parameters for the muscle groups are shown in figure 3.14 for the relax task

(right figures). It is apparent from this figure that the stiffness decrease is present in both the single and multi-joint muscles. However, the multi-joint shoulder-elbow muscle stiffness parameter shows the largest stiffness drop.

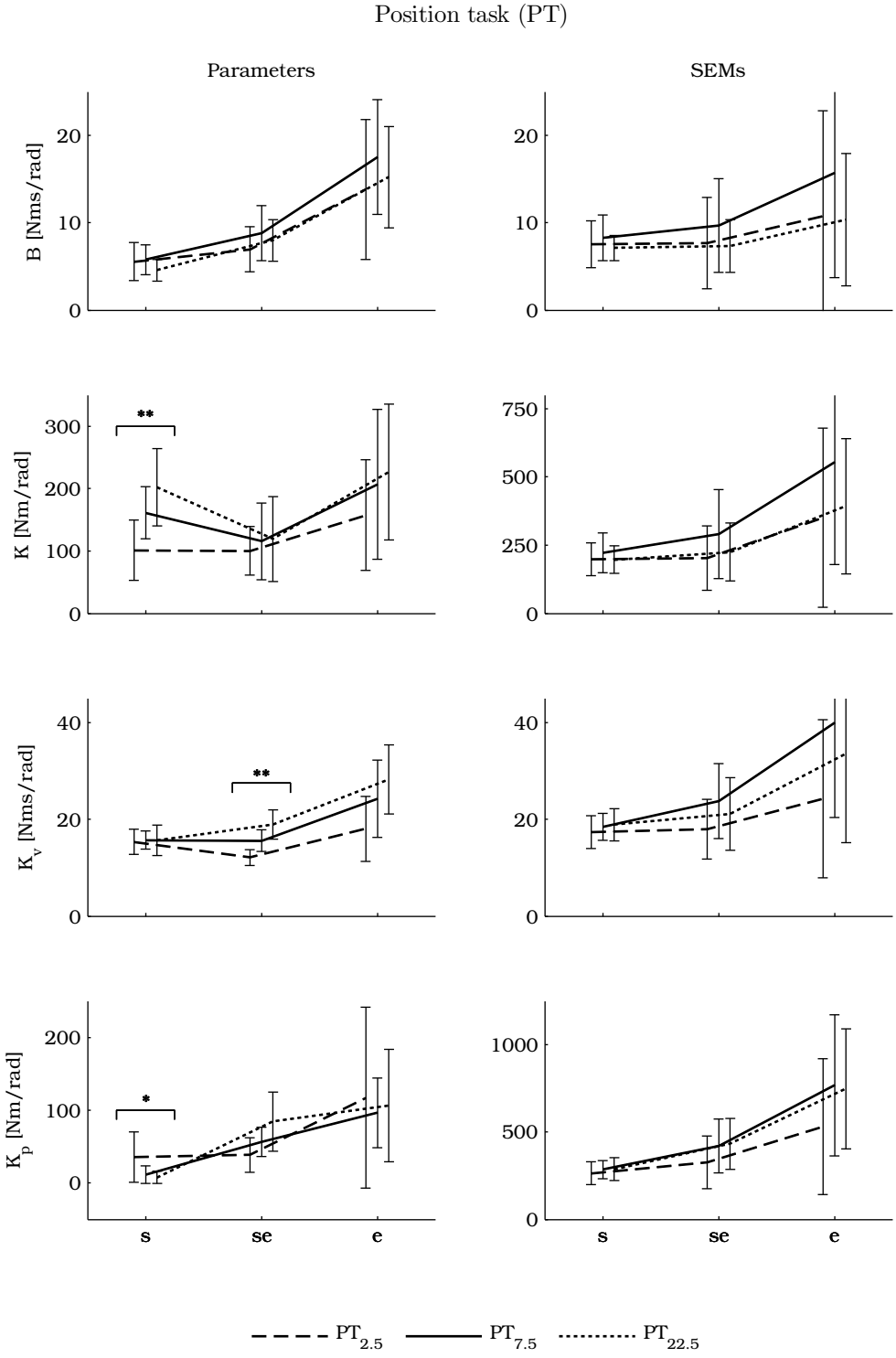

Figure 3.12 – Mean estimated *joint* parameter and corresponding SEM values for all joint combinations (s: shoulder, se: shoulder-elbow and e: elbow) respectively in the left and right figures. Each value is presented for the conditions $PT_{2.5}$, $PT_{7.5}$ and $PT_{22.5}$. The errorbars represents the standard deviation over subjects. The symbol $*$ means a significant difference between conditions at $p < 0.05$ and $**$ at $p < 0.01$.

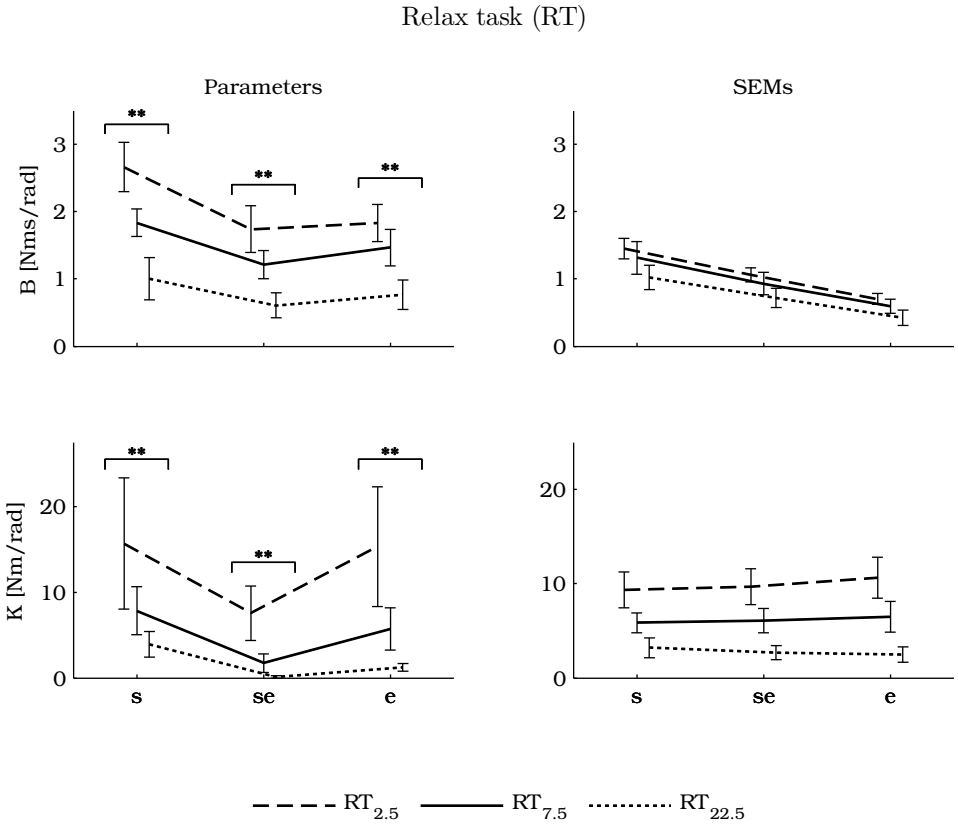

Figure 3.13 – Mean estimated *joint* parameter and corresponding SEM values for all joint combinations (s: shoulder, se: shoulder-elbow and e: elbow) respectively in the left and right figures. Each value is presented for the conditions $RT_{2.5}$, $RT_{7.5}$ and $RT_{22.5}$. The errorbars represents the standard deviation over subjects. For all joint combinations, all parameters show significant differences between conditions at $p < 0.01$, indicated by the symbol $**$.

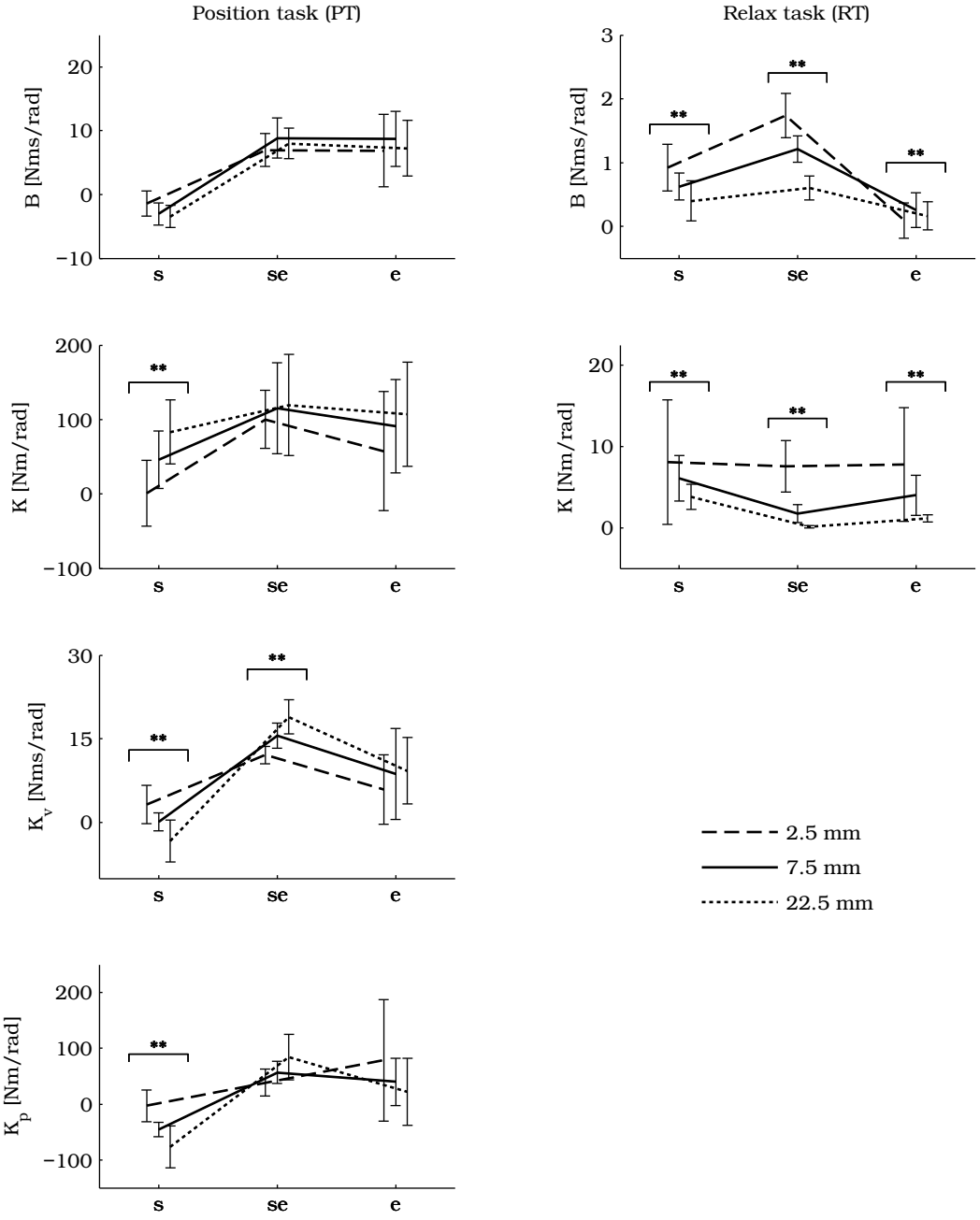

Figure 3.14 – Mean estimated joint *muscle* parameters for all muscle groups (*s*: shoulder, *se*: shoulder-elbow and *e*: elbow) for the position task (left figures) and relax task (right figures). These values are converted from the parameters on *joint* level of figure 3.13 (position task) and 3.13 (relax task), see equation 2.10. Each value is presented for the conditions 2.5, 7.5 and 22.5 mm of the continuous perturbation amplitude levels. The errorbars represents the standard deviation over subjects. The symbol ** means a significant difference between conditions at $p < 0.01$.

3.3 Pulse response

This section describes the results of the pulse perturbations. First the peak displacements and pulse admittance are presented, after which the pulse trajectories and pulse prediction are shown.

Figure 3.15 shows the recorded peak displacements of the pulse response for the minimum and maximum pulse level. The effect of task instruction is clearly visible. For the minimum pulse level, the peak displacement for the relax task is about a factor 3.5 larger than for the position task.

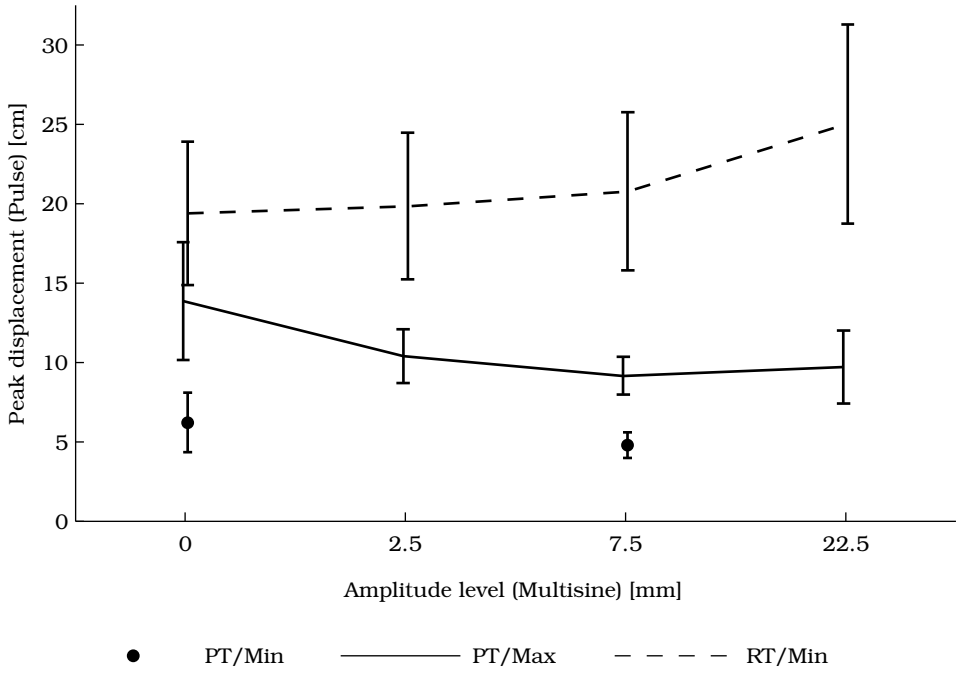

Figure 3.15 – Mean recorded peak displacements ($||\mathbf{x}||_{max}$) of the pulse response for the minimum (Min) and maximum (Max) pulse amplitude. The peak displacements are presented for different amplitude levels of the pre-perturbations (multisines). The maximum pulse amplitude was only applied during the position task (PT). The minimum pulse amplitude was applied during condition $PT_{7.5}$ and all the conditions of the relax task (RT). The errorbars denote the standard deviation over subjects.

Figure 3.15 is not appropriate to determine nonlinear behavior because the peak hand reaction force should be taken into consideration. Therefore the peak displacement divided by the peak hand reaction force (pulse admittance) is calculated, see figure 3.16. For the position task, we can evaluate the effect of pulse amplitude and the effect of pre-perturbations. The lower picture of figure 3.16 shows the pulse admittances for the minimum and maximum pulse amplitude (conditions PT_0 and $PT_{7.5}$). The pulse admittance for the maximum pulse amplitude is a factor 1.3 and 1.5 larger than for the minimum pulse amplitude respectively for the conditions PT_0 and $PT_{7.5}$. A dependent t-test revealed a significant difference for the condition PT_0 at p= 0.009 and $PT_{7.5}$ at p= 0.001. Secondly, the pulse admittance is larger without pre-perturbations compared to the pulse admittances with pre-perturbations. A repeated measures ANOVA showed a significant difference (p=0.001) between the four amplitude levels of the continuous perturbations. A post hoc analysis showed no significant difference between PT_0 and $PT_{2.5}$. Significant difference are found between the conditions PT_0 and $PT_{7.5}$ (p=0.021), between PT_0 and $PT_{22.5}$ (p=0.012), and between $PT_{2.5}$ and $PT_{22.5}$ (p=0.046).
An opposite effect is observed for the relax task; pre-perturbations lead to higher pulse admittances (figure 3.16). In addition, the higher the amplitude level of the pre-perturbations, the higher the pulse admittances. A repeated measures ANOVA showed a significant difference (p=0.000) between the four amplitude levels of the continuous perturbations. A post hoc analysis

revealed that there is no significant difference between RT_0 and $RT_{2.5}$. However, there is a significant effect between condition RT_0 and $RT_{7.5}$ (p=0.001), and between RT_0 and $RT_{22.5}$ (p=0.002). Besides that, there is a significant effect between condition $RT_{2.5}$ and $RT_{7.5}$ (p=0.049), and between $RT_{7.5}$ and $RT_{22.5}$ (p=0.009).

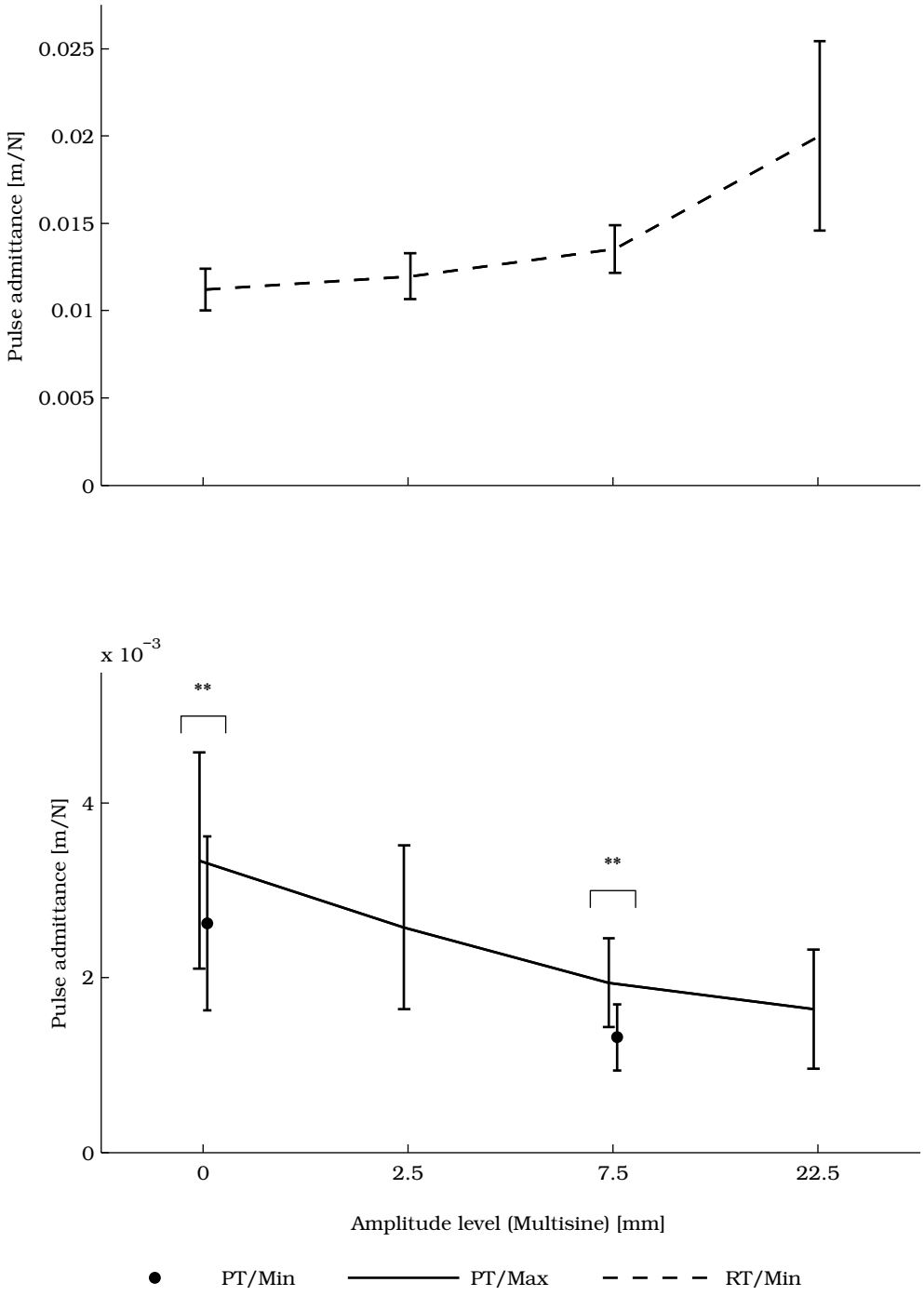

Figure 3.16 – Average pulse admittance for the maximum and minimum pulse level for the position task. The pulse admittance is the peak displacements divided by the peak hand reaction force. The errorbars denote the standard deviation over all trials of the corresponding condition. The symbol ** means significant differences between the two averaged pulse admittances at $p < 0.01$.

Figures 3.17 and 3.18 show examples of the recorded pulse response trajectories and the linear model prediction for the position and relax task, respectively. The recorded trajectory (grey dotted lines) show typical characteristics. The initial response matches quite good with the direction of the pulse perturbation (grey arrows). Subsequently, there is a systematic curl in upward and downward direction respectively for the left and right pulse direction. Our very simple linear model predicts these characteristics rather well. The predictions also show a matching initial direction with the same systematic curl. However, it can be seen that the model underestimates the recorded displacements. This is indicated by the black arrows, showing the peak displacements. Furthermore, the predicted trajectories for the relax task corresponds more with the recordings compared to the position task trajectories.

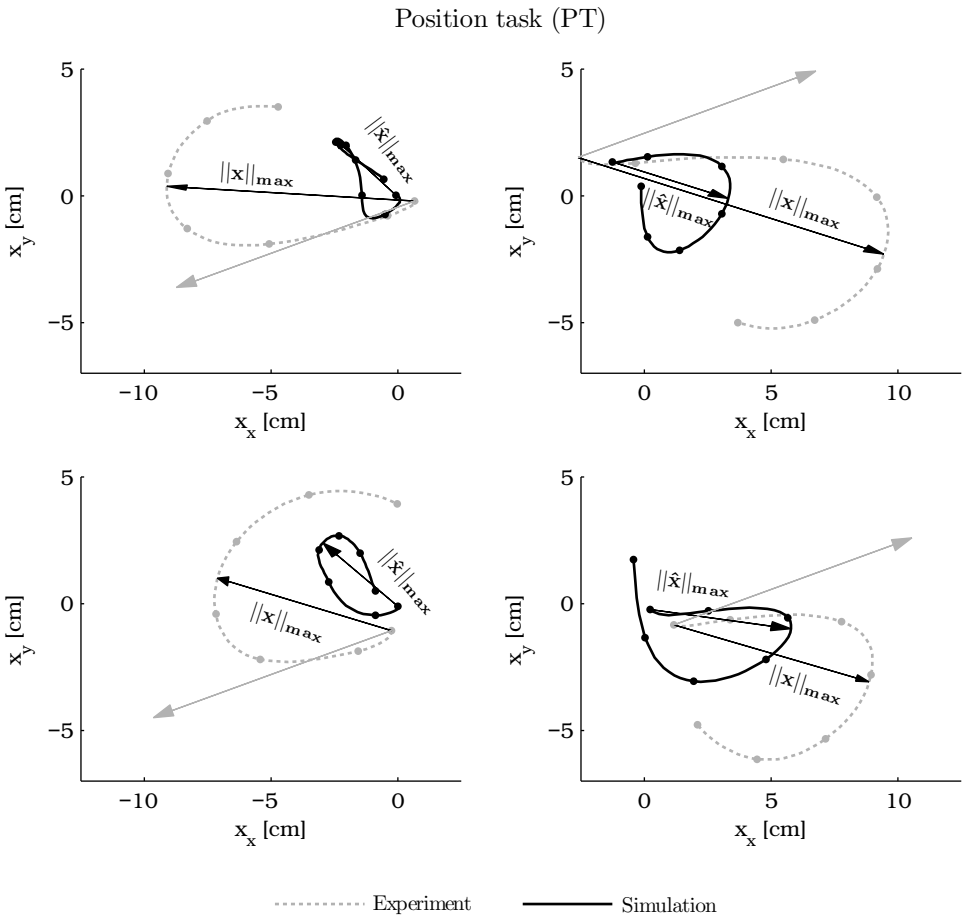

Figure 3.17 – Examples of the recorded (grey line) and linear model simulated (black line) handle trajectories in x- and y-direction of a typical subject performing a position task ($PT_{7.5}$) were the maximum pulse amplitude was applied. The black arrows indicate the recorded ($||\mathbf{x}||_{max}$) and simulated ($||\hat{\mathbf{x}}||_{max}$) peak displacements. The grey arrow indicate the direction of the pulse perturbation. This figure shows a time sample of 300 ms from the onset of the pulse disturbance. The dots indicate time steps of 50 ms.

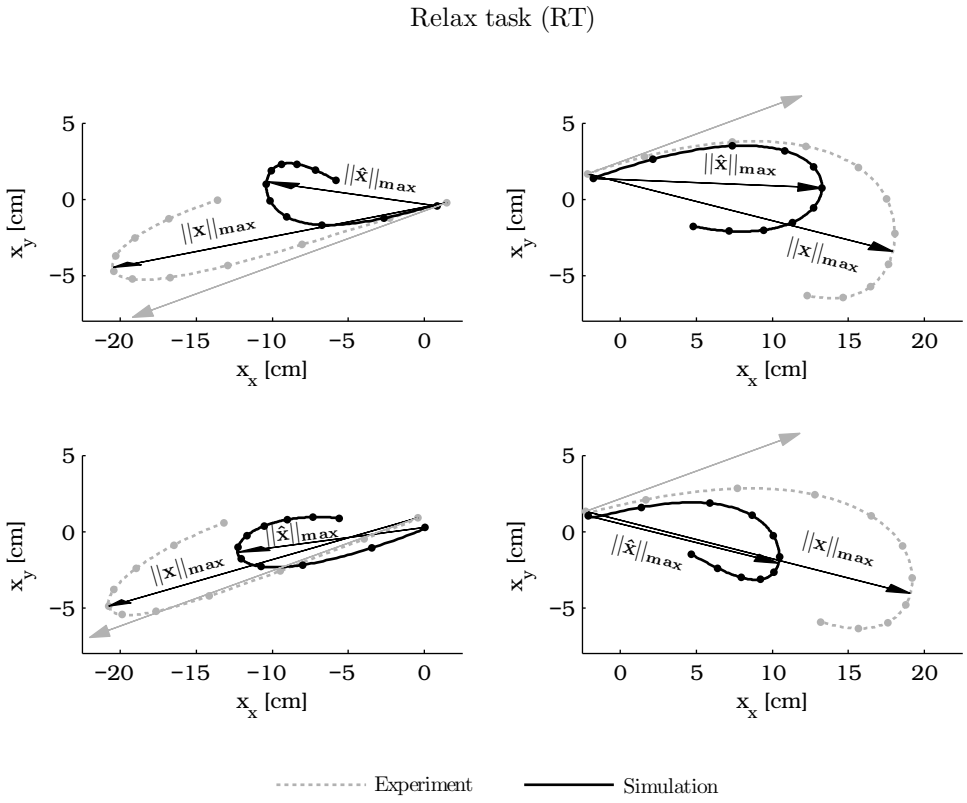

Figure 3.18 – Examples of the recorded (grey line) and linear model simulated (black line) handle trajectories in x- and y-direction of a typical subject performing a relax task ($RT_{7.5}$). The black arrows indicate the recorded ($||\mathbf{x}||_{max}$) and simulated ($||\hat{\mathbf{x}}||_{max}$) peak displacements. The grey arrow indicate the direction of the pulse perturbation. This figure shows a time sample of 1 sec from the onset of the pulse disturbance. The dots indicate time steps of 100 ms.

The averaged pulse predictions in percentages are shown in figure 3.19 for the linear and nonlinear skeletal model. The peak displacements predicted by the model are only 40-80% of the recorded peak displacements. This shows that displacements in response to force pulses are up to 2.5 times higher than what is predicted based on a model fitted to the continuous perturbations.
The relax task and resist task show a similar trend; the prediction increases for the higher amplitudes of the pre-perturbations. The pulse prediction of the linear model for the position task increases 11.9% between condition $PT_{2.5}$/Max and $PT_{22.5}$/Max. The pulse response of condition $PT_{7.5}$/Min predicts the pulse response only 5% higher than $PT_{7.5}$/Max. For the relax task, a 38.5% higher prediction is observed between condition $RT_{2.5}$/Min and $RT_{22.5}$/Min. Only the linear model predictions were tested for significance by a repeated measures ANOVA. There are no significant different pulse predictions between different conditions for the position task. The relax task shows that there is a significant difference between conditions (p=0.000). A post hoc test revealed that the differences are significant between all combinations of the three conditions (p=0.000). There are no relevant differences observed between the linear and non-linear skeletal model predictions (see figure 3.19).

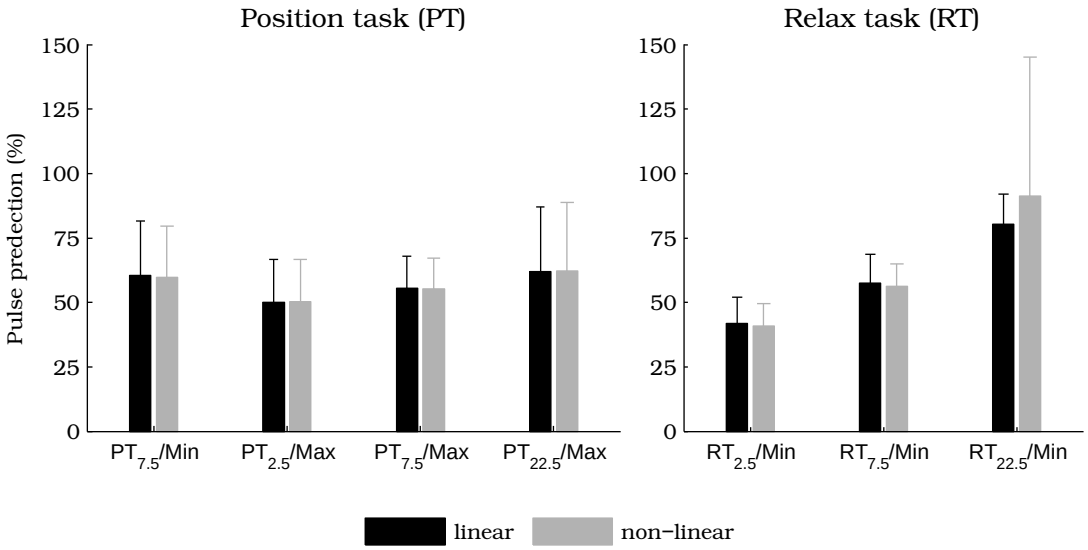

Figure 3.19 – Bar plots of the pulse prediction of the recorded peak displacements in percentages. The pulse prediction is defined as the ratio between the simulated peak displacement and the recorded peak displacement in percentages. Results are shown for the linear (black bars) and nonlinear (grey bars) skeletal model simulation for the position tasks (left figures) and the relax tasks (right figure). The pulse predictions are presented for different amplitude levels of the pre-perturbations (multisines). The maximum pulse amplitude (Max) was only applied during the position task (PT). The minimum pulse amplitude (Min) was applied during condition $PT_{7.5}$ and all the conditions of the relax task (RT). The errorbars denote the standard deviation over all trials of the corresponding condition.

CHAPTER 4

Discussion

In this study we quantified and explored the nonlinearities of human arm responses to large force perturbations. In particular, we investigated wether the pulse response of the human arm can be predicted using a linear model of which the parameters were identified using continuous perturbations. Results showed that the measured peak displacements are on average a factor 1.7 larger than the linear model prediction. This shows a enlarged admittance during pulse perturbations. The effect of nonlinearities from inertial properties (geometrical, centripetal and Coriolis) appeared to be small. Most likely, nonlinearities from intrinsic and reflexive properties contributes substantially to the pulse response. We strongly recommend to incorporate these nonlinear properties in human body models for predicting pulse responses.

Methodology

Perturbation experiments of the human arm were carried out successfully. Subjects felt comfortable throughout the whole experiment, but experienced the condition $PT_{22.5}$ as being rather heavy. The RMS force amplitude of the continuous perturbations was adjusted for each subject to achieve three target displacements (RMS values of 2.5, 7.5 and 22.5 mm). These target displacements were achieved quite well for the position task (table 2.1). For the relax task, the recorded displacements were larger than intended and showed a larger variability between subjects compared to the position task. Apparently, the displacements were very sensitive to small variations of the perturbation force and the extent subjects were able to relax. Large variability between subjects for the relax task is already reported at ankle joint experiments (Abbink et al., 2004). The pulse amplitudes were scaled with the applied force for the continuous perturbations (condition $PT_{7.5}$). The scaling and pulse directions appeared to be very effective, because large joint rotations were achieved in both the elbow and the shoulder joint (appendix F). Moreover, all applied pulse perturbations were within the limits of the safety system of the manipulator.
Parameters of a linear arm model were estimated by model optimization onto the estimated admittance. We concluded that the parameters for the position task are not estimated accurately despite the explorations and simplifications in appendices C-E. Three main problems were observed: 1) the SEMs were higher than the corresponding parameter value, 2) a penalty function was necessary to obtain stable systems and 3) the optimal parameter set depended on the initial parameter vector. Several suggestions can be made to improve the parameter estimation. The time domain signals of repeated trials can be averaged to increase the signal-to-noise ratio. This averaging technique requires equal disturbance signals in repeated trials. However, the current data does not allow averaging in time domain since we choose to generate different disturbance signals for each trial to minimize predictability. Secondly, some parameters such as limb mass can be jointly estimated over different conditions. Third, signals can be separated from noise by subspace modeling. This probably results in estimated admittances with less variance compared to the admittances we calculated (figure 3.1). However, this technique is currently used for linear identification. A more straightforward approach continuing our work would be nonlinear time domain identification. This enables to estimate the parameters of a model with nonlinearities from inertial, intrinsic and reflexive properties. In addition, one parameter set can be estimated using multiple trials with parameter estimation in the time domain.
It is important to mention that the movies made during the experiments showed larger translation of the shoulder for larger perturbation amplitudes of subjects performing a position task. Consequently, the joint rotations were underestimated, because we considered the acromion in a fixed position during the whole experiment. Subsequent research should measure the kinematics

by a motion capture system. This data can be used as an extra input to the model.

Effects of task instruction

Large differences between the position and relax task were shown for the admittances (figure 3.2), estimated intrinsic parameters (figures 3.12 and 3.13) and peak displacements (figure 3.15). We observed a stiffening effect for the position task and a yielding effect for the relax task in agreement with previous studies (Mugge et al., 2010; Venrooij et al., 2010; Schouten et al., 2008; Abbink, 2007; Schouten et al., 2003; Van der Helm et al., 2002). During the position task, subjects resisted the force perturbations by high levels of co-contraction and reflex gains. This strategy resulted in very low admittances at low frequencies compared to the relax task. Results of the relax task showed high admittance and low estimated intrinsic damping and stiffness. This indicates that muscular activity was minimal during the relax task.

Effects of amplitude

Result showed that the estimated admittance and parameters depended in a nonlinear manner on perturbation amplitude in both the relax and position task.
For the relax task, the effects of amplitude were highly significant; a higher admittance was observed for larger amplitudes (figure 3.4). This effect could be explained by nonlinearities of intrinsic and reflexive properties. First of all, short range stiffness has previously been demonstrated in the relaxed human muscle (van Eesbeek et al., 2010; Loram et al., 2007; Axelson and Hagbarth, 2001; MacKay et al., 1986; Lakie et al., 1984). The elastic limit for the shoulder and elbow joint might be between 0.7-1.8 degrees as was estimated in appendix F. This appendix also showed that the elastic limit probably was exceeded in condition $RT_{7.5}$. And indeed, the parameter estimation showed a very high intrinsic stiffness drop between conditions $RT_{2.5}$ and $RT_{7.5}$ (figure 3.13). A second possible explanation for the higher admittance with larger amplitudes is that subjects were more relaxed during larger perturbations but this should be investigated by EMG analysis. We were not able to estimate the reflexive parameters for the relax task accurately. Yet one study found highly nonlinear behavior of Ia afferent activity measured by microneurography in subjects performing a relax task during continuous perturbation experiments (Kakuda, 2000). Nonlinear reflexes are also demonstrated in transient perturbation experiments in the relaxed muscle. (de Vlugt et al., 2010). As a next step, the recorded EMG data should be analyzed to investigate reflexive activity and determine if subjects were able to fully relax during the perturbations.
Surprisingly, opposite effects in the admittance and parameters were shown for the position task; there was a lower admittance for larger amplitude levels (figure 3.3). It is reasonable to think that subjects made more effort (higher co-contraction) for larger amplitude levels. This corresponds to the increased shoulder muscle stiffness parameters found for higher amplitude levels (figure 3.14). It is interesting that the velocity feedback parameter for the shoulder muscle was larger for smaller amplitudes (figure 3.14). Smaller amplitudes also means a lower velocity. Literature has shown velocity feedback nonlinearity in the active human muscle (Kearney et al., 1997; Stein and Kearney, 1995; Kearney and Hunter, 1984, 1983). This might suggests that during the larger continuous perturbation, shoulder joint muscles increase co-contraction levels, but do not change the velocity feedback gains. On the contrary, the velocity feedback gains of the multi-joint shoulder elbow muscle showed an increased gain for larger perturbation amplitudes. Analysis of EMG data will provide more insight in the level of co-contraction during the position task.
Only for the position task, the effect of two different pulse amplitudes was investigated. As expected, the admittance was significantly higher for larger pulse amplitudes (PT_0 and $PT_{7.5}$ in figure 3.16). This could be attributed to nonlinearities of intrinsic and reflexive properties. Nonlinearities of intrinsic and reflexive properties showing an increased admittance at higher amplitudes in the active human muscle was previously demonstrated in numerous studies (de Vlugt et al., 2011; van Eesbeek et al., 2010; Cathers et al., 1999; Kearney et al., 1997; Gollhofer et al., 1997; Diener et al., 1984; Kearney and Hunter, 1984, 1983; Neilson and McCaughey, 1981).

Effects of pre-perturbations

The effect of the continuous pre-perturbations on the pulse response was investigated by comparing pulses without pre-perturbations and pulses with 3 different levels of pre-perturbations (RMS values of 2.5, 7.5 and 22.5 mm). Significant but opposite effects were observed for the relax and position task.
Results of the relax task showed significantly higher pulse admittances when pre-perturbations were applied compared to no pre-perturbations (figure 3.16). This effect was significant between the conditions RT_0 & $RT_{7.5}$ and $RT_{2.5}$ & $RT_{7.5}$, but not between condition RT_0 & $RT_{2.5}$. We can explain this result by nonlinearities from intrinsic properties. We showed that pre-perturbations of the lowest amplitude level ($RT_{2.5}$) probably did not exceed the elastic limit (appendix F). This might imply that the stiffness did not differ during the conditions RT_0 & $RT_{2.5}$, and therefore showed no significant change in pulse admittance. These effects of pre-perturbations have already been reported in the relaxed muscle and are called the thixotropic behavior of muscles (Loram et al., 2007; Axelson and Hagbarth, 2001; Lakie et al., 1984). Thixotropic behavior of the muscle means that the intrinsic stiffness of a muscle depends on immediate preceding history of movements. It is believed that the short range stiffness is responsible for this behavior. Secondly, reflexive properties might also contribute to this nonlinear behavior. A nonlinear effect of pre-perturbations on the reflexive response was reported by Stein and Kearney (1995). They showed a decrease in the amplitude of the reflex response with increasing velocity of the pre-perturbations. In our experiment we increased the amplitude, thus the velocity of the perturbation. It is possible that this nonlinearity is also responsible for the higher pulse admittances observed for the conditions with pre-perturbations.
In contrast to the relax task, the position task showed that pulse admittances decreased when pre-perturbations were applied (figure 3.16). Subjects probably adapted to the perturbation as already mentioned in the previous section. Hence, the lower admittance observed during the higher amplitude levels of the pre-perturbation resulted in more resistance against the pulse perturbations. de Vlugt et al. (2011) showed an increased stiffness drop beyond the elastic limit with larger voluntary torques. From this point of view, the nonlinear effects of the two different pulse amplitudes for the condition $PT_{7.5}$ will be larger assuming subjects increased their muscle activation compared to condition PT_0. As expected, a larger nonlinearity was observed for the pulse admittance with pre-perturbations.

Pulse response prediction

We tried to predict force pulse responses of a 2-DOF human arm in the horizontal plane by a simple linear model estimated from continuous perturbations. The experimental recordings showed trajectories with curl. Curl is already described at the human arm by Hogan (1985). Although the curl is predicted rather well by the linear model, the peak displacements of the predictions were only 40-80% of the experimental recordings (figure 3.19). By linear identification techniques, we linearized around an equilibrium point. The model only captures the behavior within the range of the applied continuous perturbations. The joint rotations for the pulse perturbations were much larger compared to the continuous perturbations and as already described previously, larger amplitudes resulted in a larger admittance. Thus, the estimated parameters were estimated onto continuous perturbation responses having a lower admittance than the pulse response. We can extend this idea to the result showing a higher percentage pulse prediction for models optimized onto larger continuous perturbations. The models were optimized onto a large range of displacements probably capturing a higher admittance. Evidently, the pulse prediction was higher. We failed to prove significant higher pulse predictions for the position task, probably because of the large standard deviations. Identification with a better noise reduction will probably reduced the standard deviations.

Comparison with previous work

De Vlugt et al. (2006) investigated amplitude effects with the same robotic manipulator. There are several differences between the methodology of their study compared to our work. First of all, they investigated position tasks, but did not test the relax task. Secondly, they used a 3-dof human arm model including the wrist joint, whereas we a used cuff to immobilize the wrist joint. By excluding the wrist joint, the number of parameters were reduced from 41 to 26 from the original model. Another important difference is that De Vlugt et al. (2006) obtained the estimated admittance from ARX models. ARX models resulted in low variance admittances. Due to time limitations in this thesis project, we did not obtain ARX models from our data.
De Vlugt et al. (2006) applied continuous perturbations of different amplitude levels (RMS values of 4, 5.5 and 7 mm displacements). Their study has been unable to demonstrate any significant parameter change with varying amplitudes. A possible explanation for this might be the small ranges between the amplitude levels. In contrast, we were able to show significant amplitude effects by applying a much wider range of amplitudes (RMS values of 2.5, 7.5 and 22.5 mm displacements).
Different results were also found for the estimated parameters. De Vlugt et al. (2006) found the largest reflexive feedback in the shoulder joint. In contrast, our results showed the largest reflexive feedback in the elbow joint. There are several explanations for this discrepancy. Previous studies have shown that the contribution of reflexive feedback depends on perturbation bandwidth (Van der Helm et al., 2002; Stein and Kearney, 1995). We used the reduced power method to evoke low frequent behavior, whereas De Vlugt et al. (2006) applied full-band disturbances. Secondly, it has been shown that the admittance is strongly dependent on position (Mirbagheri et al., 2000). The averaged elbow and shoulder joint angles were about 5 degrees higher in the study of De Vlugt et al. (2006). Although the differences were small, this might account for some variation in the estimated admittances. Last, we should keep in mind that we encountered problems during parameter estimation.

Implications

Our results showed that the linear model predictions seriously underestimated the pulse response of the human arm. For the automotive industry, this is an indication for interpreting model simulation results carefully. For example, occupants might come in contact with restraints (hit the side-window) during lane change manoeuvres which was not predicted by modeling. Further research is necessary to determined if the trunk and head neck system also show larger admittances with larger amplitudes. Generally, occupants experience impact-like disturbances without pre-perturbations during road traffic accidents. Our results showed no significant different peak displacements between the conditions PT_0 and $PT_{2.5}$, and between RT_0 and $RT_{2.5}$. Although the signal to noise ratio was low, the lowest continuous perturbation level thus seems adequate to predict the pulse response without pre-perturbations. The methodological challenge will be to improve the signal-to-noise ratio, but keep the pulse response close to the condition without pre-perturbations. As already mentioned, this might be achieved by ARX or subspace modeling techniques. However, nonlinear identification will be needed to capture both behavior of the lowest continuous perturbation amplitude and the following pulse perturbation.
The Laboratory of Neuromuscular Control (TU Delft) aims to understand neuromuscular control in both healthy subjects and patients with neurological dysfunction. We demonstrated that the human arm admittance is significantly amplitude dependent. Joint excursion depends on the perturbation and neuromuscular behavior. This research emphasizes the importance of subject specific adjustment of the force signal. Otherwise, a comparison between patients (e.g. having rigidity) and controls might be hard to make. Another interesting result was that subject probably adapted to the perturbation signal. A possible explanation might be the visual feedback of the hand displacements provided on a screen during the experiment. Subjects might considered the small displacements shown on the screen as a good performance and thereby reducing their effort to minimize displacements. A possible solution for reducing the effects of the adaptation might be scaling the hand displacement shown on the screen, such that all conditions show the

same deviations on the screen. This is something to consider for clinical application, because often there are large differences between patients and controls. A very nice research question for a next experiment is: 'what is the effect of scaling the displacements of the visual feedback on the admittance?'.

CHAPTER 5

Conclusion

Our results showed highly nonlinear amplitude-dependent behavior of the human arm. Significant effects of amplitude were demonstrated in the estimated admittances and parameters. For the position and relax task, respectively lower and larger admittances were observed for larger continuous perturbation amplitudes. For the position task, this effect probably resulted from adaptation to the perturbation stimulus. The nonlinearity observed for the relax task might be well explained by nonlinear muscle properties such as short range stiffness. On average, model predictions underestimated the peak displacements in response to the pulse stimulus by a factor 1.7. This shows the need to include nonlinearities in models for pulse shaped loading conditions.

Appendices

APPENDIX A

Spectral Analysis

This appendix shows the derivation of the estimated arm, environment and total (arm + environment) admittance. The method is not developed during my master thesis project, but is a summary of the method proposed by de Vlugt et al. (2003). Nevertheless, the derivations are included in my report for completeness.

The discrete Fourier Transform (DFT) of the applied disturbance signal $\mathbf{d}(t) = [d_x(t)\ d_y(t)]^T$ is given as

$$D_i(k\Delta_f) = \sum_{t=1}^{N} d_i(t) e^{-j2\pi k\Delta_f t/N} \qquad i \in [x, y],\ k = 0, 1 \ldots, N-1 \tag{A.1}$$

where the number of samples $N = 2^{12}$ and the increment in frequency domain after Fourier transformation

$$\Delta_f = \frac{1}{N\Delta_t}, \tag{A.2}$$

with Δ_t the sampling increment of the time signal. In a similar way, DFTs are obtained from the hand reaction force $\mathbf{f}(t)$, the recorded handle position $\mathbf{x}(t)$, the force applied at the environment $\mathbf{z}(t)$ and the noise signals $\mathbf{n}(t)$ and $\mathbf{m}(t)$. The Fourier transforms are symmetric with the first sample the DC component (sum of the time signal). This first sample is removed and only half of the DFTs are used in the spectral analysis. The resulting vector notations for the x- and y-component of the DFTs can be written as

$$\begin{aligned}
\mathbf{D}(n\Delta_f) &= [D_x(n\Delta_f)\ D_y(n\Delta_f)]^T \\
\mathbf{F}(n\Delta_f) &= [F_x(n\Delta_f)\ F_y(n\Delta_f)]^T \\
\mathbf{X}(n\Delta_f) &= [X_x(n\Delta_f)\ X_y(n\Delta_f)]^T \\
\mathbf{Z}(n\Delta_f) &= [Z_x(n\Delta_f)\ Z_y(n\Delta_f)]^T \\
\mathbf{N}(n\Delta_f) &= [N_x(n\Delta_f)\ N_y(n\Delta_f)]^T \\
\mathbf{M}(n\Delta_f) &= [M_x(n\Delta_f)\ M_y(n\Delta_f)]^T
\end{aligned} \qquad n = 0, 1 \ldots, N/2 \tag{A.3}$$

where the superscript T represents the vector transposed.

Figure 2.6 shows a block scheme of the human arm combined with the environment. The discrete human arm and the environment matrices are given as

$$\mathbf{H_{xf}}(n\Delta_f) = \begin{bmatrix} H_{x_x f_x}(n\Delta_f) & H_{x_x f_y}(n\Delta_f) \\ H_{x_y f_x}(n\Delta_f) & H_{x_y f_y}(n\Delta_f) \end{bmatrix} \tag{A.4}$$

$$\mathbf{E_{xz}}(n\Delta_f) = \begin{bmatrix} E_{x_x z_x}(n\Delta_f) & E_{x_x z_y}(n\Delta_f) \\ E_{x_y z_x}(n\Delta_f) & E_{x_y z_y}(n\Delta_f) \end{bmatrix} \tag{A.5}$$

The closed loop response $\mathbf{X}(n\Delta_f)$ corresponding to figure 2.6 is given by

$$\begin{aligned}
\mathbf{X} &= \mathbf{M} + \mathbf{E_{xz}}[\mathbf{D} + \mathbf{N} + \mathbf{H_{xf}}^{-1}(\mathbf{X} - \mathbf{M})] \\
&= \mathbf{M} + \mathbf{SE_{xz}}\mathbf{D} + \mathbf{SE_{xz}}\mathbf{N},
\end{aligned} \tag{A.6}$$

where $\mathbf{S} = (\mathbf{I} - \mathbf{E_{xz}}\mathbf{H_{xf}^{-1}})^{-1}$, $\mathbf{I}$ denotes the identity matrix and the arguments are omitted for convenience. Likewise, the reaction force yields

$$\begin{aligned}\mathbf{F} &= \mathbf{N} + [\mathbf{H_{xf}^{-1}}\mathbf{E_{xz}}(\mathbf{D} + \mathbf{F})] \\ &= (\mathbf{I} - \mathbf{H_{xz}^{-1}}\mathbf{E_{xz}})^{-1}\mathbf{N} + (\mathbf{I} - \mathbf{H_{xz}^{-1}}\mathbf{E_{xz}})^{-1}\mathbf{H_{xz}^{-1}}\mathbf{E_{xz}}\mathbf{D} \\ &= \mathbf{H_{xf}^{-1}}(\mathbf{I} - \mathbf{E_{xz}}\mathbf{H_{xz}^{-1}})^{-1}\mathbf{H_{xf}}\mathbf{N} + \mathbf{H_{xz}^{-1}}(\mathbf{I} - \mathbf{E_{xz}}\mathbf{H_{xz}^{-1}})^{-1} \\ &= \mathbf{H_{xf}^{-1}}\mathbf{S}\mathbf{H_{xf}}\mathbf{N} + \mathbf{H_{xz}^{-1}}\mathbf{S}\mathbf{E_{xz}}\mathbf{D}, \end{aligned} \tag{A.7}$$

where the push-through rule is used $(\mathbf{I} - \mathbf{H_{xz}^{-1}}\mathbf{E_{xz}})^{-1}\mathbf{H_{xz}^{-1}} = \mathbf{H_{xz}^{-1}}(\mathbf{I} - \mathbf{E_{xz}}\mathbf{H_{xz}^{-1}})^{-1}$

Next, pre-multiplying the transposed of equation A.6 and A.7 by $\frac{1}{N}\mathbf{D}^*$, where the superscript * denotes the complex conjugate, we obtain

$$\mathbf{\Phi_{dx}} = \mathbf{\Phi_{dm}} + \mathbf{\Phi_{dd}}\mathbf{E_{xz}}^T\mathbf{S}^T + \mathbf{\Phi_{dn}}\mathbf{E_{xz}}^T\mathbf{S}^T \tag{A.8}$$

$$\mathbf{\Phi_{df}} = \mathbf{\Phi_{dn}}\mathbf{H_{xf}}^T\mathbf{S}^T{\mathbf{H_{xf}^{-1}}}^T - \mathbf{\Phi_{dd}}{\mathbf{E_{xz}}}^T\mathbf{S}^T{\mathbf{H_{xf}^{-1}}}^T \tag{A.9}$$

where the estimated spectral densities are defined as

$$\mathbf{\Phi_{dx}} = \begin{bmatrix}\Phi_{d_x x_x} & \Phi_{d_x x_y} \\ \Phi_{d_y x_x} & \Phi_{d_y x_y}\end{bmatrix}, \quad \mathbf{\Phi_{dd}} = \begin{bmatrix}\Phi_{d_x d_x} & \Phi_{d_x d_y} \\ \Phi_{d_y d_x} & \Phi_{d_y d_y}\end{bmatrix},$$

$$\mathbf{\Phi_{dn}} = \begin{bmatrix}\Phi_{d_x n_x} & \Phi_{d_x n_y} \\ \Phi_{d_y n_x} & \Phi_{d_y n_y}\end{bmatrix}, \quad \mathbf{\Phi_{dm}} = \begin{bmatrix}\Phi_{d_x m_x} & \Phi_{d_x m_y} \\ \Phi_{d_y m_x} & \Phi_{d_y m_y}\end{bmatrix},$$

with

$$\begin{aligned}\Phi_{d_i x_j} &= \frac{1}{N}\mathbf{D}_i^*\mathbf{X}_j^T \\ \Phi_{d_i d_j} &= \frac{1}{N}\mathbf{D}_i^*\mathbf{D}_j^T \\ \Phi_{d_i n_j} &= \frac{1}{N}\mathbf{D}_i^*\mathbf{N}_j^T \\ \Phi_{d_i m_j} &= \frac{1}{N}\mathbf{D}_i^*\mathbf{M}_j^T \end{aligned} \qquad i, j \in [x, y],$$

The disturbance signals are uncorrelated with the noise signals. Thus,

$$\mathbf{\Phi_{dn}} = \mathbf{\Phi_{dm}} = \mathbf{0}, \tag{A.10}$$

where $\mathbf{0}$ is the nullmatrix. Hence, we end up with the following spectral estimators

$$\mathbf{\Phi_{dx}} = \mathbf{\Phi_{dd}}\mathbf{E_{xz}}^T\mathbf{S}^T \tag{A.11}$$

$$\mathbf{\Phi_{df}} = \mathbf{\Phi_{dd}}\mathbf{E_{xz}}^T\mathbf{S}^T{\mathbf{H_{xf}^{-1}}}^T \tag{A.12}$$

A.1 Estimated arm admittance

The arm admittance can be obtained from equation A.11 and A.12 according to

$$\begin{aligned}\mathbf{\Phi_{df}^{-1}}\mathbf{\Phi_{dx}} &= \mathbf{H_{xf}}^T{\mathbf{S}^{-1}}^T{\mathbf{E_{xz}^{-1}}}^T\mathbf{\Phi_{dd}^{-1}}\mathbf{\Phi_{dd}}\mathbf{E_{xz}}^T\mathbf{S}^T \\ &= \mathbf{H_{xf}}^T \end{aligned} \tag{A.13}$$

Thus, the estimated arm admittance can be calculated by

$$\hat{\mathbf{H}}_{\mathbf{xf}} = \hat{\mathbf{\Phi}}_{\mathbf{dx}}^T{\hat{\mathbf{\Phi}}_{\mathbf{df}}^{-1}}^T \tag{A.14}$$

Gain and phase characteristics are obtained from the estimated arm admittance.

A.2 Estimated environment admittance

Figure 2.6 shows the input to the environment

$$\mathbf{Z} = \mathbf{D} - \mathbf{F} \tag{A.15}$$

The following spectral density can be obtained

$$\begin{aligned} \Phi_{d_i z_j} &= \frac{1}{N}\mathbf{D}_i^* \mathbf{Z}_j^T \\ &= \frac{1}{N}\mathbf{D}_i^* (\mathbf{D}_j - \mathbf{F}_j)^T \\ &= \Phi_{d_i d_j} - \Phi_{d_i f_j} \qquad\qquad i,j \in [x,y] \end{aligned} \tag{A.16}$$

From equation A.12 follows

$$\mathbf{H_{xf}}^{-1^T} = \mathbf{S}^{-1^T}\mathbf{E_{xz}}^{-1^T}\mathbf{\Phi_{dd}}^{-1}\mathbf{\Phi_{df}} \tag{A.17}$$

The environment impedance can be calculated according to

$$\begin{aligned} \mathbf{\Phi_{dx}}^{-1}\mathbf{\Phi_{dz}} &= \mathbf{S}^{-1^T}\mathbf{E_{xz}}^{-1^T}\mathbf{\Phi_{dd}}^{-1}(\mathbf{\Phi_{dd}} - \mathbf{\Phi_{df}}) \\ &= \mathbf{S}^{-1^T}\mathbf{E_{xz}}^{-1^T} - \mathbf{S}^{-1^T}\mathbf{E_{xz}}^{-1^T}\mathbf{\Phi_{dd}}^{-1}\mathbf{\Phi_{df}} \\ &= \mathbf{S}^{-1^T}\mathbf{E_{xz}}^{-1^T} - \mathbf{H_{xf}}^{-1^T} \\ &= (\mathbf{E_{xz}}^{-1}\mathbf{S}^{-1} - \mathbf{H_{xf}}^{-1})^T \\ &= \mathbf{E_{xz}}^{-1^T} \end{aligned} \tag{A.18}$$

Finally, the estimated environment admittance is given by

$$\hat{\mathbf{E}}_{\mathbf{xz}} = \hat{\mathbf{\Phi}}_{\mathbf{dx}}^T \hat{\mathbf{\Phi}}_{\mathbf{dz}}^{-1^T} \tag{A.19}$$

The estimated environment admittance is used to estimate the parameters of the virtual environment dynamics.

A.3 Estimated total system admittance

The total system $\mathbf{P_{dx}}$ from the input $\mathbf{D}$ to output $\mathbf{X}$ with zero noise is given by

$$\begin{aligned} \mathbf{P_{dx}} &= \mathbf{E_{xz}}(\mathbf{I} - \mathbf{H_{xf}}^{-1}\mathbf{E_{xz}})^{-1} \\ &= \mathbf{S}\mathbf{E_{xz}}, \end{aligned} \tag{A.20}$$

where the push-through rule is used. Equation A.11 can be rewritten in

$$\begin{aligned} \mathbf{\Phi_{dd}}^{-1}\mathbf{\Phi_{dx}} &= (\mathbf{S}\mathbf{E_{xz}})^T \\ &= \mathbf{P_{dx}}^T \end{aligned} \tag{A.21}$$

The resulting estimated admittance of the total system can be obtained by

$$\hat{\mathbf{P}}_{\mathbf{dx}} = \hat{\mathbf{\Phi}}_{\mathbf{dx}}^T \hat{\mathbf{\Phi}}_{\mathbf{dd}}^{-1^T} \tag{A.22}$$

The estimated admittance of the total system is used for calculating the multiple coherence.

APPENDIX B

Arm-environment model

The linear arm-environment model expressed in three DOF joint coordinates from De Vlugt et al. (2006) is reduced to two DOF joint coordinates. Subsequently, this reduced model is extended by adding nonlinearities from inertial, muscular and reflexive properties. This appendix gives a full description of the linear arm-environment model expressed in two DOF joint coordinates.

The arm-environment model describes the dynamic relation between an endpoint force disturbance and the resulting endpoint handle position. The model consists of the environment, grip dynamics and the NMS system. The latter includes the intrinsic musculoskeleton, sensors, neural time delay and activation dynamics. The environment and grip dynamics are expressed in a two DOF cartesian coordinate frame $[x\ y]^T$, whereas the NMS system is expressed in two DOF joint coordinates $[\theta_s\ \theta_e]^T$, where s and e denote respectively the shoulder and elbow joint.

The model variables are

$\mathbf{q}$	$= [\theta_s\ \theta_e]^T$	joint angle
$\boldsymbol{\tau_e}$	$= [\tau_{e_s}\ \tau_{e_e}]^T$	joint torque (from external force)
$\boldsymbol{\tau_r}$	$= [\tau_{r_s}\ \tau_{r_e}]^T$	joint torque (from reflexive muscle force)
$\boldsymbol{\tau_i}$	$= [\tau_{i_s}\ \tau_{i_e}]^T$	joint torque (from intrinsic muscle force)
$\boldsymbol{\tau_m}$	$= [\tau_{m_s}\ \tau_{m_e}]^T$	joint torque (from nett muscle force)
$\mathbf{a}$	$= [a_s\ a_e]^T$	muscle activation (active state)
$\mathbf{r}$	$= [r_s\ r_e]^T$	output Pade filter
$\mathbf{u_r}$	$= [u_{r_s}\ u_{e_s}]^T$	reflexive excitation
$\mathbf{u_d}$	$= [u_{d_s}\ u_{d_s}]^T$	delayed relfexive excitation
$\mathbf{x}$	$= [x_x\ x_y]^T$	endpoint handle coordinate
$\mathbf{x_h}$	$= [x_{h_x}\ x_{h_y}]^T$	endpoint hand coordinate
$\mathbf{f}$	$= [f_x\ f_y]^T$	endpoint hand reaction force
$\mathbf{d}$	$= [d_x\ d_y]^T$	endpoint force disturbance

The model parameters of the environment, grip dynamics, intrinsic musculoskeleton, sensors, neural time delay and activation dynamics in matrix notation is

$$\mathbf{M_e} = \begin{bmatrix} m_{env} & 0 \\ 0 & m_{env} \end{bmatrix} \quad \text{environmental mass}$$

$$\mathbf{B_e} = \begin{bmatrix} b_{env} & 0 \\ 0 & b_{env} \end{bmatrix} \quad \text{environmental viscosity}$$

$$\mathbf{K_e} = \begin{bmatrix} k_{env} & 0 \\ 0 & k_{env} \end{bmatrix} \quad \text{environmental elasticity}$$

$$\mathbf{B_h} = \begin{bmatrix} b_h & 0 \\ 0 & b_h \end{bmatrix} \quad \text{hand grip viscosity}$$

$$\mathbf{K_h} = \begin{bmatrix} k_h & 0 \\ 0 & k_h \end{bmatrix} \quad \text{hand grip elasticity}$$

$$\mathbf{M} = \begin{bmatrix} m_h & 0 & 0 & 0 \\ 0 & m_h & 0 & 0 \\ 0 & 0 & m_e & 0 \\ 0 & 0 & 0 & m_e \end{bmatrix} \quad \text{segmental \& handle mass}$$

$$\mathbf{B} = \begin{bmatrix} b_s & b_{se} \\ b_{se} & b_e \end{bmatrix} \quad \text{Intrinsic joint damping}$$

$$\mathbf{K} = \begin{bmatrix} k_s & k_{se} \\ k_{se} & k_e \end{bmatrix} \quad \text{Intrinsic joint stiffness}$$

$$\mathbf{K_v} = \begin{bmatrix} kv_s & kv_{se} \\ kv_{se} & kv_e \end{bmatrix} \quad \text{velocity feedback gain}$$

$$\mathbf{K_p} = \begin{bmatrix} kp_s & kp_{se} \\ kp_{se} & kp_e \end{bmatrix} \quad \text{position feedback gain}$$

$$\mathbf{T_d} = \begin{bmatrix} T_{ds} \\ T_{de} \end{bmatrix} \quad \text{time delay}$$

$$\mathbf{f_{act}} = \begin{bmatrix} f_{act_s} \\ f_{act_e} \end{bmatrix} \quad \text{cutt-off frequency}$$

Since the environmental parameters are taken constant, the resulting parameter vector to be estimated is

$$\boldsymbol{\theta} = [m_h\ m_f\ b_s\ b_{se}\ b_e\ k_s\ k_{se}\ k_e\ b_h\ k_h\ k_{vs}\ k_{vse}\ k_{ve} \ldots \\ k_{p_s}\ k_{p_{se}}\ k_{p_e}\ T_{ds}\ T_{de}\ f_{act_s}\ f_{act_e}]^T$$

B.1 Linear model

The following sections describe the environment, grip dynamics, intrinsic musculoskeleton, sensors, neural delay and the activation dynamics.

Intrinsic musculoskeleton

The equations of motion of the intrinsic musculoskeleton are derived by using the TMT method; a combination of Newton-Euler and Lagrange (Linde and Schwab, 1997). The equations of motion are expressed in terms of the independent generalized coordinates, given as

$$q_j = \begin{bmatrix} \theta_s \\ \theta_e \end{bmatrix} \tag{B.1}$$

The center of mass of the humerus and forearm can be expressed by a kinematic transformation as function of independent generalized coordinates.

$$x_{com_i} = T_i(q_j) \rightarrow \begin{bmatrix} x_{com_h} \\ y_{com_h} \\ x_{com_f} \\ y_{com_f} \end{bmatrix} = \begin{bmatrix} l_{com_h}\, cos(\theta_s) \\ l_{com_h}\, sin(\theta_s) \\ l_{com_f}\, cos(\theta_e + \theta_s) + l_h\, cos(\theta_s) \\ l_{com_f}\, sin(\theta_e + \theta_s) + l_h\, sin(\theta_s) \end{bmatrix}, \tag{B.2}$$

with

x_{com_h}	x coordinate center of mass humerus
y_{com_h}	y coordinate center of mass humerus
x_{com_f}	x coordinate center of mass forearm
y_{com_f}	y coordinate center of mass forearm
l_h	length humerus
l_f	length forearm
l_{com_h}	distance center of mass humerus with respect to the shoulder
l_{com_f}	distance center of mass forearm with respect to the elbow

Differentiating B.2 gives

$$\dot{x}_{com_i} = \frac{\partial T_i}{\partial q_k}\dot{q}_k = T_{i,k}\dot{q}_k \tag{B.3a}$$

$$\delta\dot{x}_{com_i} = T_{i,k}\delta\dot{q}_k \tag{B.3b}$$

$$\ddot{x}_{com_j} = \frac{\partial T_j}{\partial q_l}\ddot{q}_l + \frac{\partial}{\partial q_q}\frac{\partial T_j}{\partial q_p}\dot{q}_p\dot{q}_q = T_{j,l}\ddot{q}_l + g_j, \tag{B.3c}$$

with the convective acceleration term $g_j = T_{j,pq}\dot{q}_p\dot{q}_q$.

The virtual power equation is given as:

$$\delta\dot{x}_{com_i}\left\{\sum F_i - M_{ij}\ddot{x}_{com_j}\right\} = 0 \tag{B.4}$$

The virtual power of the intrinsic stiffness and damping can be added to the virtual power equation, which gives

$$\delta\dot{x}_{com_i}\left\{\sum F_i - M_{ij}\ddot{x}_{com_j}\right\} = \delta\dot{x}_{com_i}\sum Q_i, \tag{B.5}$$

with $\sum Q_i$ the sum of the intrinsic stiffness and damping forces in the center of mass of the humerus and forearm.

Substituting B.3b and B.3c into equation B.5 results in

$$T_{i,k}\left\{\sum F_i - M_{ij}(T_{j,l}\ddot{q}_l + g_j)\right\} = T_{i,k}\sum Q_i \tag{B.6}$$

Rearranging equation B.6 gives

$$\ddot{q}_l = (T_{i,k}M_{ij}T_{j,l})^{-1}\left\{T_{i,k}\sum F_i - T_{i,k}\sum Q_i - T_{i,k}M_{ij}g_j\right\}, \tag{B.7}$$

where

$$T_{i,k}\sum F_i = \tau_e - \tau_r \tag{B.8}$$

$$T_{i,k}\sum Q_i = \tau_i = B\dot{q} + Kq \tag{B.9}$$

Finally, substitution of B.8 and B.9 into equation B.7 yields

$$\ddot{q}_l = (T_{i,k}M_{ij}T_{j,l})^{-1}\left\{-B\dot{q} - Kq - T_{i,k}M_{ij}g_j + \tau_e - \tau_r\right\}, \tag{B.10}$$

The model is linearized by neglecting the nonlinear term g_j and taken $T_{i,k}$ at a constant value. Hence, the linearized equations of motion for the intrinsic musculoskeleton is given by

$$\ddot{q}_l = (T_{i,k} M_{ij} T_{j,l})^{-1} \{-B\dot{q} - Kq + \tau_e - \tau_r\}, \tag{B.11}$$

The linear equations of the intrinsic musculoskeleton in state-space is given by

$$\begin{bmatrix} \ddot{\mathbf{q}} \\ \dot{\mathbf{q}} \end{bmatrix} = \mathbf{A_i} \begin{bmatrix} \dot{\mathbf{q}} \\ \mathbf{q} \end{bmatrix} + \mathbf{B_i}(\boldsymbol{\tau_e} - \boldsymbol{\tau_r})$$
$$\begin{bmatrix} \dot{\mathbf{q}} \\ \mathbf{q} \end{bmatrix} = \mathbf{C_i} \begin{bmatrix} \dot{\mathbf{q}} \\ \mathbf{q} \end{bmatrix} + \mathbf{D_i}(\boldsymbol{\tau_e} - \boldsymbol{\tau_r}),$$

with

$$\mathbf{A_i} = \begin{bmatrix} -(\mathbf{T_q}^T \mathbf{M} \mathbf{T_q})^{-1} \mathbf{B} & -(\mathbf{T_q}^\mathbf{T} M \mathbf{T_q})^{-1} \mathbf{K} \\ \mathbf{I} & \mathbf{O} \end{bmatrix}$$
$$\mathbf{B_i} = \begin{bmatrix} (\mathbf{T_q}^\mathbf{T} M \mathbf{T_q})^{-1} \\ \mathbf{O} \end{bmatrix}$$
$$\mathbf{C_i} = \begin{bmatrix} \mathbf{I} & \mathbf{O} \\ \mathbf{O} & \mathbf{I} \end{bmatrix}$$
$$\mathbf{D_i} = \begin{bmatrix} \mathbf{O} \\ \mathbf{O} \end{bmatrix},$$

where $\mathbf{T_q} = \frac{\partial \mathbf{T(q)}}{\partial \mathbf{q}}$ and

$$\mathbf{I} = \begin{bmatrix} 1 & 0 \\ 0 & 1 \end{bmatrix}, \qquad \mathbf{O} = \begin{bmatrix} 0 & 0 \\ 0 & 0 \end{bmatrix}$$

Reflexive feedback

Sensors

The sensors are the muscle spindles and the golgi tendon organs. The reflexive excitation of the sensors is given as

$$\mathbf{u_r} = \mathbf{K_v}\dot{\mathbf{q}} + \mathbf{K_p}\mathbf{q}$$

Neural delay

The neural delay is modeled by two third-order Pade approximations; one time delay for the muscles of the shoulder and the bi-articular muscles from shoulder to elbow joint (T_{ds}) and one delay for the muscles of the elbow and the bi-articular muscles from elbow to shoulder joints (T_{de}). The Pade approximations yields

$$\frac{u_{d_i}}{u_{r_i}} = \frac{120 - 60\,T_{di}s + 12\,T_{di}^2 s^2 - T_{di}^3 s^3}{120 + 60\,T_{di}s + 12\,T_{di}^2 s^2 + T_{di}^3 s^3} \qquad i \in [s, e] \tag{B.12}$$

The corresponding state-space matrices can be written as

$$\mathbf{A} = \begin{bmatrix} 0 & 1 & 0 \\ 0 & 0 & 1 \\ -120\,T_{di}{}^{-3} & -60\,T_{di}{}^{-2} & -12\,T_{di}{}^{-1} \end{bmatrix} \tag{B.13}$$

$$\mathbf{B} = \begin{bmatrix} 0 \\ 0 \\ 1 \end{bmatrix} \tag{B.14}$$

$$\mathbf{C} = \begin{bmatrix} 240\,T_{di}{}^{-3} & 0 & 24\,T_{di}{}^{-1} \end{bmatrix} \qquad i \in [s, e] \tag{B.15}$$

$$\mathbf{D} = 1 \tag{B.16}$$

Combining the Pade approximations for the shoulder and the elbow joint results in the following state-space equations

$$\begin{bmatrix} \dddot{\mathbf{r}} \\ \ddot{\mathbf{r}} \\ \dot{\mathbf{r}} \end{bmatrix} = \mathbf{A_{del}} \begin{bmatrix} \ddot{\mathbf{r}} \\ \dot{\mathbf{r}} \\ \mathbf{r} \end{bmatrix} + \mathbf{B_{del}} \mathbf{u_r} \tag{B.17}$$

$$\mathbf{u_d} = \mathbf{C_{del}} \begin{bmatrix} \ddot{\mathbf{r}} \\ \dot{\mathbf{r}} \\ \mathbf{r} \end{bmatrix} + \mathbf{D_{del}} \mathbf{u_r} \tag{B.18}$$

Activation dynamics

The activation dynamics is described by a critically damped second order Butterworth filter consisting of the cut-off frequency for the shoulder, the elbow and the bi-articular joint similar as the delay parameters, ($f_{act,s}$ and $f_{act,e}$). The transfer function for a second order Butterworth filter is given by

$$\frac{\tau_{r_i}}{u_{d_i}} = \frac{\omega_c^2}{s^2 + 2\zeta\omega_c s + \omega_c^2} \qquad i \in [s, e] \tag{B.19}$$

The corresponding state-space matrices can be written as

$$\mathbf{A} = \begin{bmatrix} -2\zeta\omega_c & -\omega_c \\ 1 & 0 \end{bmatrix} \tag{B.20}$$

$$\mathbf{B} = \begin{bmatrix} \omega_c^2 \\ 0 \end{bmatrix} \tag{B.21}$$

$$\mathbf{C} = \begin{bmatrix} 0 & 1 \end{bmatrix} \qquad i \in [s, e] \tag{B.22}$$

$$\mathbf{D} = 0 \tag{B.23}$$

Combining the two Butterworth filters for the shoulder and the elbow joint results in the following state-space equations

$$\begin{bmatrix} \ddot{\mathbf{a}} \\ \dot{\mathbf{a}} \end{bmatrix} = \mathbf{A_{act}} \begin{bmatrix} \dot{\mathbf{a}} \\ \mathbf{a} \end{bmatrix} + \mathbf{B_{act}} \boldsymbol{\tau_r} \tag{B.24}$$

$$\mathbf{u_d} = \mathbf{C_{act}} \begin{bmatrix} \dot{\mathbf{a}} \\ \mathbf{a} \end{bmatrix} + \mathbf{D_{act}} \mathbf{u_d} \tag{B.25}$$

Environment

The equations of motion for the environment are

$$\ddot{\mathbf{x}} = \mathbf{M_e}^{-1} \left(-\mathbf{B_e}\dot{\mathbf{x}} - \mathbf{K_e}\mathbf{x} + \mathbf{d} - \mathbf{f} \right) \tag{B.26}$$

Written in state-space format, we get

$$\begin{bmatrix} \ddot{\mathbf{x}} \\ \dot{\mathbf{x}} \end{bmatrix} = \mathbf{A_{env}} \begin{bmatrix} \dot{\mathbf{x}} \\ \mathbf{x} \end{bmatrix} + \mathbf{B_{env}}(\mathbf{d} - \mathbf{f})$$

$$\mathbf{y} = \mathbf{C_{env}} \begin{bmatrix} \dot{\mathbf{x}} \\ \mathbf{x} \end{bmatrix} + \mathbf{D_{env}}(\mathbf{d} - \mathbf{f}),$$

with

$$\mathbf{A_{env}} = \begin{bmatrix} -\mathbf{M}_e^{-1}\mathbf{B_e} & -\mathbf{M}_e^{-1}\mathbf{K_e} \\ \mathbf{I} & \mathbf{O} \end{bmatrix}$$
$$\mathbf{B_{env}} = \begin{bmatrix} \mathbf{M}_e^{-1} \\ \mathbf{O} \end{bmatrix}$$
$$\mathbf{C_{env}} = \begin{bmatrix} \mathbf{I} & \mathbf{O} \\ \mathbf{O} & \mathbf{I} \end{bmatrix}$$
$$\mathbf{D_{env}} = \begin{bmatrix} \mathbf{O} \\ \mathbf{O} \end{bmatrix},$$

Grip dynamics

The hand reaction force is calculated as

$$\begin{aligned} \mathbf{f} &= \mathbf{B_h}(\dot{\mathbf{x}} - \dot{\mathbf{x}}_\mathbf{h}) + \mathbf{K_h}(\mathbf{x} - \mathbf{x_h}) \\ &= \mathbf{B_h}(\dot{\mathbf{x}} - \dot{\mathbf{q}}\mathbf{J}) + \mathbf{K_h}(\mathbf{x} - \mathbf{q}\mathbf{J}), \end{aligned}$$

where the Jacobian $\mathbf{J}$ is the mapping from generalized coordinates to the cartesian coordinate frame according to

$$\mathbf{J} = \begin{bmatrix} \frac{\partial}{\partial \mathbf{q}} x_h(\mathbf{q}) \\ \frac{\partial}{\partial \mathbf{q}} y_h(\mathbf{q}) \end{bmatrix} = \begin{bmatrix} \frac{\partial}{\partial \mathbf{q}} \{l_f\, cos(\theta_e + \theta_s) + l_h\, cos(\theta_s)\} \\ \frac{\partial}{\partial \mathbf{q}} \{l_f\, sin(\theta_e + \theta_s) + l_h\, sin(\theta_s)\} \end{bmatrix} \tag{B.27}$$

$$= \begin{bmatrix} -l_f \sin(\theta_e + \theta_s) - l_h \sin(\theta_s) & -l_f \sin(\theta_e + \theta_s) \\ l_f \cos(\theta_e + \theta_s) + l_h \cos(\theta_s) & l_f \cos(\theta_e + \theta_s) \end{bmatrix} \tag{B.28}$$

with x_h and y_h respectively the x- and y-coordinate of the hand.

In vector notation the equation becomes

$$\mathbf{f} = \begin{bmatrix} \mathbf{B_h} & \mathbf{K_h} \end{bmatrix} \begin{bmatrix} \dot{\mathbf{x}} \\ \mathbf{x} \end{bmatrix} + \begin{bmatrix} -\mathbf{B_h}\mathbf{J} & -\mathbf{K_h}\mathbf{J} \end{bmatrix} \begin{bmatrix} \dot{\mathbf{q}} \\ \mathbf{q} \end{bmatrix},$$

APPENDIX C

Parameter estimation, stability analysis & model structure

C.1 Introduction

One of the main goals of this graduation project was to estimate the parameters of a model of the human arm. The parameter estimation approach consists of three parts. In this appendix, the parameter estimation of different model structures was evaluated and the stability problem was resolved. The best model structure was chosen for further analysis in appendix D, were optimization was performed with different initial parameter vectors. We will see that the existence of local minima is a problem in the parameter estimation. Therefore, the model structure was simplified in appendix E by reducing the number of parameters to be estimated.
These appendices provides merely the approach for the parameter estimation. For specific details about the experiment, spectral analysis, the parametric model and the optimization I refer to chapter 2.

Three main problems were observed during the first attempts of estimating the model parameters

1. A large part of estimated parameter sets resulted in unstable systems.
2. Even for the stable systems, a large part of the VAFs were negative. Inspection of the model simulation showed oscillatory behavior.
3. The estimated parameter set depended on the initial parameter vector indicating the existence of local minima.

These problems were tackled by the following corresponding optimization settings

1. A penalty function was imposed to the optimization.
2. By tighten the penalty function, the system response was more damped.
3. The optimization was performed with small boundary ranges for some parameters. These boundaries were set at feasible values obtained from the literature. Secondly, the averaged estimated parameter set resulting from an optimization was used as initial condition in a subsequent optimization.

These optimization settings are described in more detail in the next section. The results of the optimizations are presented in tables C.3-C.22.

C.2 Methods

The criterion, VAFs and the SEMs were evaluated for the six different model structures shown in table C.1. The most simple model consisted of intrinsic muscle properties and hand grip dynamics without reflexive feedback. This model was extended by adding reflexive feedback including force, acceleration, velocity and position feedback gains. By doing this, we can see if the dominant parameters (intrinsic damping and stiffness) change when reflexes are added to the model.

Table C.1 – Six different model structures.

Model nr.	Model structure
1	Intrinsic + grip
2	Intrinsic + reflexive (velocity feedback) + grip
3	Intrinsic + reflexive (velocity & position feedback) + grip
4	Intrinsic + reflexive (force & velocity & position feedback) + grip
5	Intrinsic + reflexive (acceleration & velocity & position feedback) + grip
6	Intrinsic + reflexive (force & acceleration & velocity & position feedback) + grip

To evaluate the different model structures, the following two-step procedure was used:

Step 1 Model optimizations without a penalty function.

Step 2 Model optimizations with a penalty function (initial parameter vector obtained from step 1).

These steps are described in the next two subsections.

Step 1: Optimization without penalty function

The parameters of the six different model structures were estimated without a penalty function. This means that the optimized parameter set could lead to an unstable total system (arm + environment). The optimizations in step 1 occurred separately in each trial for condition $PT_{7.5}$ and $RT_{7.5}$. Step 1 was only done for these two conditions because we want to obtain one initial parameter vector for the optimization of all three different amplitude levels of the continuous perturbations.

The following optimization settings were used

- The optimization occurred by the Matlab function `lsqnonlin.m`.
- The optimization options were set at

```
options = optimset('Display', 'iter',...
    'TolX',1e-6,...
    'TolFun',1e-5,...
    'DiffMinChange',1e-4,...
    'MaxIter',1000,...
    'MaxFunEvals',6000);
```

- The initial parameter vector consisted of realistic values obtained from the literature (De Vlugt et al., 2006).

- The lower and upper boundaries for the estimated parameters are given in table C.2. The boundaries for the upper arm mass, neural delays and activation cut-off frequencies were set at small realistic ranges according to (De Vlugt et al., 2006).
- The initial parameter vector and the boundaries were normalized during the optimization.

Simulations of the total system (arm+environment) were performed for the calculation of the VAFs. The parameters of the environment were optimized onto the estimated environment admittance calculated by equation A.16. This resulted in the following estimated parameters

$$m_{env} = 3.27 \text{ kg} \quad \text{(manipulator setting } m_{env} = 3 \text{ kg)} \tag{C.1}$$
$$b_{env} = 0.55 \text{ Ns/m} \quad \text{(manipulator setting } b_{env} = 0 \text{ Ns/m)} \tag{C.2}$$
$$k_{env} = 22.03 \text{ N/m} \quad \text{(manipulator setting } k_{env} = 20 \text{ N/m)} \tag{C.3}$$

These estimated parameters correspond well with the manipulator dynamics settings. The estimated parameters of the environment were used for the simulations and for the calculation of the eigenvalues of the state-space matrix A in step 2.

Table C.2 – Lower and upper boundaries used for optimization.

Parameter	LB / UB	Unit	Parameter	LB / UB	Unit
Segmental mass			*Acceleration feedback*		
m_h	1 / 3	kg	$k_{a\,s}$	-5 / 5	Nms^2/rad
m_f	0.5 / 4	kg	$k_{a\,se}$	-5 / 5	Nms^2/rad
Joint damping			$k_{a\,e}$	-5 / 5	Nms^2/rad
b_s	0 / 1e2	Nms/rad	*Velocity feedback*		
b_{se}	0 / 1e2	Nms/rad	$k_{v\,s}$	-1e2 / 1e2	Nms/rad
b_e	0 / 1e2	Nms/rad	$k_{v\,se}$	-1e2 / 1e2	Nms/rad
Joint stiffness			$k_{v\,e}$	-1e2 / 1e2	Nms/rad
k_s	0 / 1e3	Nm/rad	*Position feedback*		
k_{se}	0 / 1e3	Nm/rad	$k_{p\,s}$	-1e3 / 1e3	Nm/rad
k_e	0 / 1e3	Nm/rad	$k_{p\,se}$	-1e3 / 1e3	Nm/rad
Hand grip damping and stiffness			$k_{p\,e}$	-1e3 / 1e3	Nm/rad
b_h	0 / 5e3	Ns/m	*Neural time delay*		
k_h	2e3 / 3e4	N/m	$T_{d\,s}$	25 / 35	ms
Force feedback			$T_{d\,e}$	35 / 45	ms
$k_{f\,s}$	-1e2 / 1e2	-	*Activation cut-off frequency*		
$k_{f\,se}$	-1e2 / 1e2	-	$f_{act\,s}$	1.7 / 3	Hz
$k_{f\,e}$	-1e2 / 1e2	-	$f_{act\,e}$	1.7 / 3	Hz

Step 2: Optimization with penalty function

The parameters of the six different model structures were estimated with a penalty function function. The optimizations occurred separately in each trial for all conditions ($PT_{2.5}$, $PT_{7.5}$, $PT_{22.5}$, $RT_{2.5}$, $RT_{7.5}$ and $RT_{22.5}$). The following optimization settings were used:

- For each model structure, averaged estimated parameter sets were obtained for condition $PT_{7.5}$ in step 1. Corresponding to each model structure, these group averaged parameter sets were used as initial condition for the optimization in step 2 for the conditions conditions $PT_{2.5}$, $PT_{7.5}$ and $PT_{22.5}$. Likewise, the group averaged estimated parameter sets of the condition $RT_{7.5}$ were used as initial parameter set for the conditions $RT_{2.5}$, $RT_{7.5}$ and $RT_{22.5}$.

- Matlab's function `fmincon.m` has a nice build-in constraint function. However, the SEMs were blown up dramatically (the SEMs were calculated by using the Hessian and the residuals between the estimated MFRF and the model fit). Therefore, the Matlab function `lsqnonlin.m` was used.

  The function `lsqnonlin.m` does not has a build-in constraint function. This was circumvented by using the following a penalty function. The error function is given as

$$\begin{aligned} \epsilon_{xi}(f_k) &= \gamma_{xd_{xy}}(f_k) \left| \ln \left(\frac{\hat{\hat{H}}_{x_x f_i}(f_k)}{\hat{H}_{x_x f_i}(f_k)} \right) \right| \\ \epsilon_{yi}(f_k) &= \gamma_{yd_{xy}}(f_k) \left| \ln \left(\frac{\hat{\hat{H}}_{x_y f_i}(f_k)}{\hat{H}_{x_y f_i}(f_k)} \right) \right| \end{aligned} \qquad i \in [x, y],\ k = 1 \dots n_f, \tag{C.4}$$

  where $\hat{H}_{xf}$ denotes the four elements of the estimated MFRF, $\hat{\hat{H}}_{xf}$ the four elements of the MFRF of the model, n_f the number of frequency points of the frequency vector f_k. The error function was weighted by the square root of the multiple coherence functions (equation 2.4). The quadratic criterion function to be minimized becomes

$$V = \frac{1}{N} \sum_{k=1}^{N} \Big(\boldsymbol{\epsilon}(k) \cdot p(\mathrm{Re}[\sigma_{max}]) \Big)^2 \qquad N = 4 \cdot n_f \tag{C.5}$$

  with n_f the number of frequency points the error vector contains four error vectors for each element of the MFRF, given as

$$\boldsymbol{\epsilon} = [\boldsymbol{\epsilon_{xx}}\ \boldsymbol{\epsilon_{xy}}\ \boldsymbol{\epsilon_{yx}}\ \boldsymbol{\epsilon_{yy}}]^T \tag{C.6}$$

  The penalty function yields

$$p(\mathrm{Re}[\sigma_{max}]) = 10 \cdot (1e10^{\mathrm{Re}[\sigma_{max}]+0.5}) + 1, \tag{C.7}$$

  where $\mathrm{Re}[\sigma_{max}]$ denotes the maximum eigenvalue (real part) of the state-space matrix A of the total system (arm + environment) and a represents the shift operator. When the shift operator was chosen at the value $a = 0.1$, the oscillatory behavior of the model simulation was still present. With a value $a = 0.5$, the model simulations showed nice results with almost only positive VAFs values. The used penalty function is shown in figure C.1.

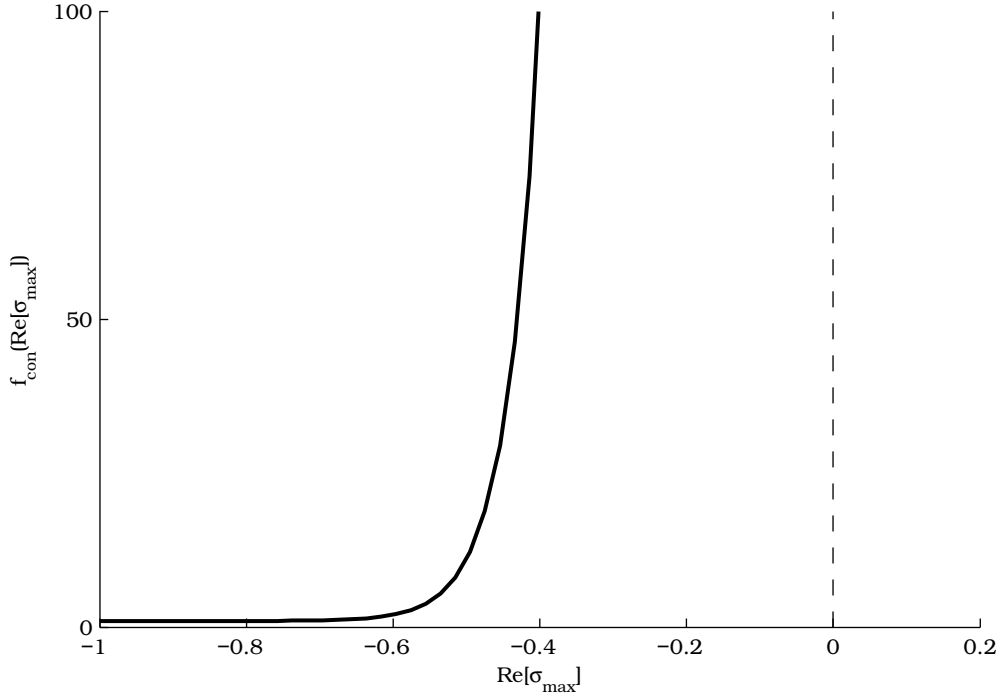

Figure C.1 – Penalty function $p(\mathrm{Re}[\sigma_{max}]) = 10 \cdot (1e10^{\mathrm{Re}[\sigma_{max}]+0.5}) + 1$, which is 1 for $\mathrm{Re}[\sigma_{max}]$ values lower than approximately -0.8.

C.3 Results: overview tables

An overview of all the tables are given below.

Optimization without penalty function

$\mathbf{PT}_{7.5}$	Parameters, table C.3, SEMs, table C.4
$\mathbf{PT}_{7.5}$	Criterion and VAF values, table C.5

Optimization with penalty function

$\mathbf{PT}_{2.5}$	Parameters, table C.6, SEMs, table C.7
$\mathbf{PT}_{7.5}$	Parameters, table C.8, SEMs, table C.9
$\mathbf{PT}_{22.5}$	Parameters, table C.10, SEMs, table C.11
$\mathbf{PT}_{2.5}$, $\mathbf{PT}_{7.5}$ and $\mathbf{PT}_{22.5}$	Criterion and VAFs values, table C.12

Optimization without penalty function

$\mathbf{RT}_{7.5}$	Parameters, table C.13, SEMs, table C.14
$\mathbf{RT}_{7.5}$	Criterion and VAF values, table C.15

Optimization with penalty function

$\mathbf{RT}_{2.5}$	Parameters, table C.16, SEMs, table C.17
$\mathbf{RT}_{7.5}$	Parameters, table C.18, SEMs, table C.19
$\mathbf{RT}_{22.5}$	Parameters, table C.20, SEMs, table C.21
$\mathbf{RT}_{2.5}$, $\mathbf{RT}_{7.5}$ and $\mathbf{RT}_{22.5}$	Criterion and VAFs values, table C.22

C.4 Results: without penalty function ($PT_{7.5}$)

Table C.3 – Mean (SD) parameters over subjects for six different model structures. *Condition: $PT_{7.5}$, without penalty function* Go to overview.

Parameter	Model 1	Model 2	Model 3	Model 4	Model 5	Model 6	Unit
Segmental mass							
m_h	1.49 (0.33)	1.52 (0.35)	1.79 (0.21)	1.60 (0.27)	1.96 (0.29)	1.87 (0.27)	kg
m_f	2.89 (0.46)	2.30 (0.43)	2.68 (0.50)	2.60 (0.51)	2.24 (0.38)	2.23 (0.45)	kg
Joint damping							
b_s	8.13 (1.70)	4.91 (1.72)	2.10 (1.39)	2.36 (1.42)	2.99 (1.84)	2.96 (0.89)	Nms/rad
b_{se}	6.97 (1.78)	5.04 (2.81)	4.78 (1.64)	3.62 (1.69)	2.18 (0.75)	1.83 (0.58)	Nms/rad
b_e	7.14 (4.97)	9.62 (7.55)	8.42 (4.62)	7.17 (3.91)	7.71 (1.94)	6.83 (2.17)	Nms/rad
Joint stiffness							
k_s	176.36 (38.49)	112.71 (45.90)	181.40 (49.57)	145.31 (50.31)	78.83 (17.85)	131.31 (30.76)	Nm/rad
k_{se}	65.14 (24.64)	60.76 (42.32)	60.82 (44.89)	57.03 (45.29)	46.05 (22.73)	39.53 (15.70)	Nm/rad
k_e	167.94 (61.96)	190.29 (76.94)	158.46 (77.94)	135.82 (63.12)	32.36 (25.98)	31.96 (29.85)	Nm/rad
Hand grip damping and stiffness							
b_h	55.19 (17.67)	60.83 (25.93)	66.73 (17.84)	64.28 (14.80)	66.80 (19.23)	63.61 (21.85)	Ns/m
k_h	22.11 (2.18)	23.74 (3.34)	24.88 (2.49)	24.97 (1.94)	26.97 (2.13)	26.49 (2.11)	kN/m
Force feedback							
k_{f_s}	-	-	-	−0.69 (0.52)	-	−1.57 (0.21)	-
$k_{f_{se}}$	-	-	-	−0.28 (0.64)	-	−0.02 (0.23)	-
k_{f_e}	-	-	-	−0.43 (0.94)	-	−1.06 (0.23)	-
Acceleration feedback							
k_{a_s}	-	-	-	-	0.46 (0.32)	−0.31 (0.38)	Nms^2/rad
$k_{a_{se}}$	-	-	-	-	0.29 (0.23)	0.10 (0.29)	Nms^2/rad
k_{a_e}	-	-	-	-	1.09 (0.43)	0.96 (0.49)	Nms^2/rad
Velocity feedback							
k_{v_s}	-	18.81 (2.74)	13.30 (5.27)	17.86 (5.29)	18.58 (1.20)	19.20 (2.83)	Nms/rad
$k_{v_{se}}$	-	17.61 (3.72)	16.84 (7.09)	15.99 (5.22)	12.92 (3.16)	13.44 (2.76)	Nms/rad
k_{v_e}	-	29.22 (10.41)	21.64 (9.93)	20.51 (5.72)	23.34 (3.61)	22.37 (3.86)	Nms/rad
Position feedback							
k_{p_s}	-	-	−57.59 (33.17)	64.96 (75.95)	60.87 (38.72)	177.57 (60.46)	Nm/rad
$k_{p_{se}}$	-	-	36.59 (23.97)	59.01 (83.52)	95.69 (50.03)	99.94 (25.44)	Nm/rad
k_{p_e}	-	-	71.73 (97.01)	52.81 (129)	370.04 (150.51)	412.18 (104)	Nm/rad
Neural time delay							
T_{d_s}	-	27.18 (1.57)	31.23 (0.96)	30.05 (1.44)	31.36 (1.32)	29.47 (1.35)	ms
T_{d_e}	-	32.41 (2.62)	31.37 (1.30)	31.81 (1.30)	32.98 (2.30)	32.60 (1.67)	ms
Activation cut-off frequency							
f_{act_s}	-	2.93 (0.09)	2.80 (0.08)	2.55 (0.13)	2.78 (0.11)	2.50 (0.15)	Hz
f_{act_e}	-	2.57 (0.14)	2.74 (0.13)	2.69 (0.16)	2.75 (0.12)	2.66 (0.12)	Hz

Table C.4 – Mean (SD) SEMs over subjects for six different model structures (values are not normalized). *Condition: $PT_{7.5}$, without penalty function.* Go to overview

Parameter	Model 1	Model 2	Model 3	Model 4	Model 5	Model 6
Segmental mass						
m_h	9.84 (2.31)	10.90 (3.74)	11.99 (2.63)	10.51 (2.24)	12.99 (1.77)	13.35 (1.84)
m_f	1.73 (0.44)	1.89 (0.79)	2.00 (0.48)	1.73 (0.40)	1.59 (0.21)	1.49 (0.15)
Joint damping						
b_s	6.74 (1.33)	6.40 (1.29)	11.34 (3.85)	11.39 (2.91)	26.33 (7.00)	30.31 (9.29)
b_{se}	5.08 (2.11)	6.00 (2.89)	7.27 (1.69)	6.37 (1.48)	8.06 (1.04)	7.81 (1.41)
b_e	4.62 (4.44)	8.31 (9.39)	6.89 (3.77)	5.18 (2.73)	5.46 (1.26)	5.05 (1.35)
Joint stiffness						
k_s	69.11 (16.20)	118.75 (43.98)	301.82 (101.43)	312.62 (60.29)	1050.10 (270.79)	1244.00 (340.24)
k_{se}	90.24 (35.93)	169.00 (80.78)	270.35 (75.87)	207.34 (45.76)	312.76 (44.32)	301.91 (52.93)
k_e	131.37 (90.09)	303.91 (218.17)	358.03 (236.99)	251.91 (155.24)	277.31 (80.46)	246.92 (76.63)
Hand grip damping and stiffness						
b_h	89.71 (19.56)	94.65 (21.90)	93.43 (13.27)	90.34 (15.20)	104.28 (13.59)	103.16 (19.12)
k_h	15820 (2571)	17412 (3479)	18191 (3138)	17748 (2944)	17722 (1452)	18929 (4124)
Force feedback						
k_{f_s}	-	-	-	4.40 (1.51)	-	3.20 (0.73)
$k_{f_{se}}$	-	-	-	2.44 (0.99)	-	1.30 (0.15)
k_{f_e}	-	-	-	5.11 (1.61)	-	2.70 (0.50)
Acceleration feedback						
k_{a_s}	-	-	-	-	4.78 (1.05)	7.17 (2.46)
$k_{a_{se}}$	-	-	-	-	1.87 (0.19)	1.88 (0.42)
k_{a_e}	-	-	-	-	2.37 (0.48)	2.04 (0.64)
Velocity feedback						
k_{v_s}	-	19.45 (6.40)	29.83 (8.84)	57.94 (12.54)	92.64 (24.04)	111.60 (36.39)
$k_{v_{se}}$	-	27.37 (13.05)	33.79 (10.00)	47.28 (15.39)	31.77 (5.53)	31.60 (5.92)
k_{v_e}	-	59.17 (41.64)	57.96 (35.47)	67.04 (48.31)	39.46 (7.90)	38.26 (9.50)
Position feedback						
k_{p_s}	-	-	368.82 (104.50)	844.42 (318.64)	1058.05 (263.87)	1199.57 (312.51)
$k_{p_{se}}$	-	-	391.20 (125.17)	642.16 (271.27)	395.75 (54.84)	430.00 (77.45)
k_{p_e}	-	-	631.64 (367.15)	1082.93 (568.85)	578.78 (171.17)	700.71 (199.46)
Neural time delay						
T_{d_s}	-	0.051 (0.011)	0.092 (0.049)	0.100 (0.042)	0.041 (0.010)	0.035 (0.006)
T_{d_e}	-	0.052 (0.022)	0.066 (0.026)	0.089 (0.039)	0.023 (0.010)	0.026 (0.010)
Activation cut-off frequency						
f_{act_s}	-	1.88 (0.39)	2.74 (0.62)	4.00 (1.47)	2.60 (0.24)	2.07 (0.30)
f_{act_e}	-	2.22 (0.70)	2.70 (0.71)	4.04 (1.17)	2.58 (0.25)	2.25 (0.33)

Table C.5 – Total mean (SD) of the criterion and VAF values for six different model structures. Only trials with a positive VAF value were used to calculate the VAF. N_{pos} represents the number of stable models with a positive VAF and N_{stab} indicates the number of stable systems. *Condition: $PT_{7.5}$, without penalty function.* Go to overview

	Model 1	Model 2	Model 3	Model 4	Model 5	Model 6
Criterion	117.97 (24.06)	85.92 (17.69)	81.43 (18.98)	77.67 (19.23)	64.71 (17.97)	63.47 (19.84)
VAF_x (%)	61.87 (10.25)	63.95 (13.86)	61.26 (11.95)	64.85 (11.58)	67.48 (14.78)	69.67 (8.31)
VAF_y (%)	44.57 (14.51)	56.35 (13.63)	56.03 (14.05)	57.07 (12.89)	59.18 (21.20)	64.57 (8.75)
$N_{pos}(\leq 80)$	35	6	6	18	21	28
$N_{stab}(\leq 80)$	54	18	23	38	41	44

C.5 Results: with penalty function ($PT_{2.5}$, $PT_{7.5}$ and $PT_{22.5}$)

Table C.6 – Mean (SD) parameters over subjects for six different model structures. The optimization was performed with a penalty function. *Condition: $PT_{2.5}$, with penalty function.* Go to overview

Parameter	Model 1	Model 2	Model 3	Model 4	Model 5	Model 6	Unit
Segmental mass							
m_h	2.04 (0.40)	1.78 (0.33)	1.81 (0.17)	1.70 (0.30)	1.94 (0.22)	1.91 (0.22)	kg
m_f	2.08 (0.76)	1.85 (0.51)	2.22 (0.51)	2.19 (0.43)	1.96 (0.31)	2.09 (0.17)	kg
Joint damping							
b_s	7.04 (1.43)	4.72 (1.43)	2.43 (0.69)	2.54 (0.52)	2.92 (1.15)	2.84 (0.74)	Nms/rad
b_{se}	7.21 (2.88)	5.65 (1.75)	5.41 (0.43)	3.75 (0.60)	2.94 (0.86)	2.18 (0.41)	Nms/rad
b_e	8.89 (4.54)	11.60 (6.03)	11.01 (4.88)	8.78 (3.83)	8.66 (2.18)	7.40 (1.17)	Nms/rad
Joint stiffness							
k_s	141.6 (43.3)	114.2 (43.2)	157.1 (38.0)	132.9 (26.5)	68.2 (16.8)	121.5 (15.2)	Nm/rad
k_{se}	69.2 (38.5)	96.0 (46.7)	83.6 (26.8)	83.6 (26.1)	51.9 (12.8)	44.0 (11.5)	Nm/rad
k_e	168.3 (89.3)	232.0 (172.4)	166.6 (37.3)	149.6 (49.8)	34.7 (9.0)	36.7 (11.6)	Nm/rad
Hand grip damping and stiffness							
b_h	55.9 (56.8)	77.3 (59.2)	85.2 (37.1)	72.6 (19.7)	79.0 (38.2)	76.4 (43.3)	Ns/m
k_h	21.2 (3.94)	23.8 (4.08)	24.7 (2.29)	25.4 (1.83)	26.4 (2.21)	26.4 (1.21)	kN/m
Force feedback							
k_{f_s}	-	-	-	−0.77 (0.37)	-	−1.53 (0.23)	-
$k_{f_{se}}$	-	-	-	−0.20 (0.29)	-	0.02 (0.17)	-
k_{f_e}	-	-	-	−0.44 (0.33)	-	−1.32 (0.35)	-
Acceleration feedback							
k_{a_s}	-	-	-	-	0.39 (0.10)	−0.31 (0.14)	Nms^2/rad
$k_{a_{se}}$	-	-	-	-	0.33 (0.11)	0.11 (0.09)	Nms^2/rad
k_{a_e}	-	-	-	-	1.02 (0.32)	0.82 (0.16)	Nms^2/rad
Velocity feedback							
k_{v_s}	-	16.40 (3.98)	13.71 (3.39)	18.08 (4.52)	17.77 (2.70)	18.30 (1.72)	Nms/rad
$k_{v_{se}}$	-	16.45 (6.65)	15.84 (5.42)	15.22 (4.14)	11.83 (3.00)	14.15 (1.91)	Nms/rad
k_{v_e}	-	26.57 (15.51)	22.49 (7.79)	19.27 (4.30)	20.21 (4.99)	22.26 (2.73)	Nms/rad
Position feedback							
k_{p_s}	-	-	−35.0 (36.9)	79.3 (44.3)	60.9 (16.5)	148.7 (24.7)	Nm/rad
$k_{p_{se}}$	-	-	32.2 (40.9)	58.6 (35.9)	93.8 (32.0)	103.8 (25.7)	Nm/rad
k_{p_e}	-	-	64.3 (34.8)	65.0 (47)	332.0 (106.4)	404.2 (63)	Nm/rad
Neural time delay							
T_{d_s}	-	27.3 (1.37)	31.2 (0.48)	30.3 (1.37)	31.3 (0.70)	29.1 (0.86)	ms
T_{d_e}	-	33.7 (2.27)	32.3 (1.46)	32.8 (1.43)	34.3 (2.59)	33.4 (1.06)	ms
Activation cut-off frequency							
f_{act_s}	-	2.80 (0.13)	2.74 (0.17)	2.44 (0.11)	2.8 (0.06)	2.49 (0.06)	Hz
f_{act_e}	-	2.55 (0.21)	2.74 (0.09)	2.70 (0.10)	2.7 (0.06)	2.65 (0.06)	Hz

Table C.7 – Mean (SD) SEMs over subjects for six different model structures (values are not normalized). The optimization was performed with a penalty function. *Condition: $PT_{2.5}$, with penalty function.* Go to overview

Parameter	Model 1	Model 2	Model 3	Model 4	Model 5	Model 6
Segmental mass						
m_h	9.78 (4.51)	12.71 (4.83)	14.52 (4.50)	12.80 (2.49)	17.62 (4.54)	19.07 (3.62)
m_f	1.94 (0.96)	2.36 (1.01)	2.62 (0.80)	2.18 (0.51)	2.16 (0.61)	1.98 (0.28)
Joint damping						
b_s	6.05 (1.90)	5.69 (1.25)	11.36 (2.99)	11.21 (3.13)	32.87 (10.39)	44.85 (11.33)
b_{se}	5.87 (3.53)	4.87 (2.33)	8.31 (2.58)	6.82 (1.37)	9.67 (2.40)	10.03 (1.85)
b_e	6.70 (6.89)	9.77 (9.38)	9.67 (7.52)	7.18 (4.79)	7.92 (2.61)	7.26 (1.75)
Joint stiffness						
k_s	69.26 (17.57)	161.33 (64.23)	324.40 (96.08)	358.17 (103.68)	1240.68 (375.46)	1845.03 (457.97)
k_{se}	99.07 (41.03)	234.51 (91.34)	303.35 (77.78)	253.15 (49.79)	361.66 (95.48)	385.88 (76.10)
k_e	158.93 (104.40)	413.23 (338.40)	432.77 (278.85)	340.20 (211.12)	361.90 (123.71)	333.38 (67.63)
Hand grip damping and stiffness						
b_h	101.95 (47.45)	118.98 (44.26)	121.83 (26.90)	111.37 (16.69)	144.99 (33.54)	145.87 (34.05)
k_h	19351 (12852)	23920 (12489)	24502 (6348)	24076 (5433)	30181 (13194)	33838 (20442)
Force feedback						
k_{f_s}	-	-	-	4.09 (2.60)	-	3.90 (0.80)
$k_{f_{se}}$	-	-	-	2.12 (0.72)	-	1.57 (0.29)
k_{f_e}	-	-	-	4.25 (3.06)	-	3.80 (0.74)
Acceleration feedback						
k_{a_s}	-	-	-	-	5.62 (1.65)	10.02 (2.25)
$k_{a_{se}}$	-	-	-	-	2.23 (0.49)	2.32 (0.47)
k_{a_e}	-	-	-	-	2.80 (0.78)	2.62 (0.56)
Velocity feedback						
k_{v_s}	-	22.94 (6.51)	32.01 (7.08)	71.03 (32.03)	107.83 (33.64)	159.13 (41.30)
$k_{v_{se}}$	-	34.17 (17.84)	38.03 (9.93)	58.61 (23.26)	36.34 (10.43)	40.24 (6.71)
k_{v_e}	-	69.66 (62.15)	67.94 (40.36)	87.89 (55.06)	42.76 (13.23)	55.29 (12.43)
Position feedback						
k_{p_s}	-	-	476.63 (108.30)	826.92 (302.16)	1235.07 (366.46)	1714.67 (450.91)
$k_{p_{se}}$	-	-	539.72 (164.24)	666.11 (222.90)	466.17 (112.53)	536.73 (99.44)
k_{p_e}	-	-	906.13 (419.98)	923.60 (574.34)	623.84 (214.72)	922.07 (142.80)
Neural time delay						
T_{d_s}	-	0.063 (0.016)	0.126 (0.084)	0.126 (0.052)	0.048 (0.013)	0.050 (0.011)
T_{d_e}	-	0.068 (0.021)	0.085 (0.019)	0.115 (0.049)	0.029 (0.007)	0.037 (0.008)
Activation cut-off frequency						
f_{act_s}	-	2.21 (0.39)	3.36 (0.86)	4.09 (1.35)	3.29 (0.53)	2.65 (0.46)
f_{act_e}	-	2.54 (0.45)	3.68 (0.55)	5.27 (2.35)	3.22 (0.38)	2.96 (0.51)

Table C.8 – Mean (SD) parameters over subjects for six different model structures. The optimization was performed with a penalty function. *Condition: $PT_{7.5}$, with penalty function.* Go to overview

Parameter	Model 1	Model 2	Model 3	Model 4	Model 5	Model 6	Unit
Segmental mass							
m_h	1.54 (0.31)	1.49 (0.26)	1.73 (0.12)	1.49 (0.10)	2.06 (0.21)	1.91 (0.14)	kg
m_f	2.32 (0.23)	1.98 (0.26)	2.41 (0.28)	2.46 (0.24)	2.21 (0.12)	2.15 (0.14)	kg
Joint damping							
b_s	9.08 (1.57)	6.40 (1.05)	2.62 (0.81)	2.60 (0.71)	3.72 (1.24)	3.44 (1.12)	Nms/rad
b_{se}	10.71 (2.42)	7.58 (2.42)	6.06 (1.10)	4.31 (0.98)	2.95 (0.82)	2.14 (0.39)	Nms/rad
b_e	12.84 (5.37)	14.11 (4.96)	11.07 (3.55)	8.88 (2.99)	9.04 (1.44)	7.84 (1.30)	Nms/rad
Joint stiffness							
k_s	168.8 (40.0)	125.4 (25.6)	203.0 (25.6)	175.7 (28.0)	72.0 (19.8)	134.7 (22.1)	Nm/rad
k_{se}	68.3 (27.2)	85.8 (27.5)	76.4 (26.1)	80.8 (22.2)	49.3 (10.4)	43.6 (5.7)	Nm/rad
k_e	193.6 (46.0)	242.4 (68.0)	182.1 (58.2)	162.5 (45.3)	36.3 (21.9)	35.9 (20.4)	Nm/rad
Hand grip damping and stiffness							
b_h	34.9 (12.4)	58.3 (15.7)	73.8 (11.9)	70.8 (12.7)	70.1 (11.1)	65.8 (14.3)	Ns/m
k_h	24.5 (2.00)	26.1 (1.35)	26.1 (0.84)	26.1 (1.00)	27.8 (0.82)	27.1 (1.14)	kN/m
Force feedback							
k_{fs}	-	-	-	−0.65 (0.07)	-	−1.37 (0.18)	-
k_{fse}	-	-	-	−0.26 (0.15)	-	0.00 (0.05)	-
k_{fe}	-	-	-	−0.48 (0.15)	-	−1.13 (0.31)	-
Acceleration feedback							
k_{as}	-	-	-	-	0.64 (0.18)	−0.15 (0.16)	Nms^2/rad
k_{ase}	-	-	-	-	0.42 (0.18)	0.21 (0.14)	Nms^2/rad
k_{ae}	-	-	-	-	1.21 (0.33)	1.08 (0.33)	Nms^2/rad
Velocity feedback							
k_{vs}	-	20.52 (2.22)	13.58 (1.90)	16.47 (2.30)	20.10 (1.43)	20.14 (1.91)	Nms/rad
k_{vse}	-	21.07 (3.59)	19.73 (2.45)	16.48 (2.28)	13.60 (1.75)	15.13 (1.16)	Nms/rad
k_{ve}	-	29.08 (8.12)	24.92 (4.00)	21.07 (2.62)	23.89 (2.45)	25.03 (1.55)	Nms/rad
Position feedback							
k_{ps}	-	-	−63.4 (16.6)	52.5 (21.8)	76.4 (26.3)	164.6 (29.6)	Nm/rad
k_{pse}	-	-	38.4 (24.1)	69.4 (25.5)	108.3 (28.4)	110.7 (22.8)	Nm/rad
k_{pe}	-	-	65.9 (40.9)	69.6 (44)	390.2 (111.4)	451.5 (47)	Nm/rad
Neural time delay							
T_{ds}	-	27.4 (0.64)	31.6 (0.45)	30.2 (0.71)	32.2 (0.80)	28.9 (0.62)	ms
T_{de}	-	33.0 (1.91)	31.7 (1.05)	31.4 (0.97)	32.8 (1.45)	32.3 (0.90)	ms
Activation cut-off frequency							
f_{acts}	-	2.96 (0.04)	2.77 (0.07)	2.61 (0.07)	2.8 (0.06)	2.59 (0.09)	Hz
f_{acte}	-	2.60 (0.09)	2.79 (0.04)	2.77 (0.05)	2.8 (0.07)	2.73 (0.06)	Hz

Table C.9 – Mean (SD) SEMs over subjects for six different model structures (values are not normalized). The optimization was performed with a penalty function. *Condition: $PT_{7.5}$, with penalty function.* Go to overview

Parameter	Model 1	Model 2	Model 3	Model 4	Model 5	Model 6
Segmental mass						
m_h	10.08 (2.86)	12.16 (3.20)	11.99 (1.88)	11.26 (1.37)	14.93 (2.79)	15.02 (2.98)
m_f	2.08 (0.66)	2.31 (0.68)	2.20 (0.37)	1.94 (0.26)	1.80 (0.32)	1.66 (0.27)
Joint damping						
b_s	8.33 (2.33)	7.26 (2.69)	9.68 (2.23)	10.91 (2.18)	29.17 (9.00)	33.71 (9.00)
b_{se}	8.17 (4.42)	6.54 (4.05)	7.62 (1.60)	6.79 (1.14)	9.95 (2.63)	9.19 (1.87)
b_e	10.01 (9.25)	16.04 (14.12)	8.18 (3.56)	6.56 (2.74)	6.93 (1.86)	6.07 (1.50)
Joint stiffness						
k_s	82.65 (16.25)	185.82 (56.83)	260.66 (57.32)	320.94 (50.32)	1102.95 (349.42)	1401.12 (370.21)
k_{se}	123.75 (32.15)	286.27 (131.08)	296.00 (66.06)	245.41 (29.12)	360.41 (79.44)	356.90 (73.45)
k_e	205.02 (102.10)	513.93 (303.62)	403.39 (173.43)	303.68 (96.66)	318.06 (65.47)	311.11 (77.85)
Hand grip damping and stiffness						
b_h	87.68 (17.88)	106.70 (22.03)	105.15 (14.66)	101.70 (16.18)	114.34 (17.99)	112.82 (19.03)
k_h	17781 (3357)	20663 (2575)	20698 (2318)	20482 (2573)	19609 (3256)	20081 (3727)
Force feedback						
k_{f_s}	-	-	-	2.94 (0.89)	-	3.06 (0.78)
$k_{f_{se}}$	-	-	-	1.81 (0.44)	-	1.34 (0.23)
k_{f_e}	-	-	-	3.07 (0.91)	-	3.04 (0.79)
Acceleration feedback						
k_{a_s}	-	-	-	-	5.10 (1.50)	7.22 (2.22)
$k_{a_{se}}$	-	-	-	-	2.20 (0.45)	2.01 (0.42)
k_{a_e}	-	-	-	-	2.87 (0.62)	2.48 (0.50)
Velocity feedback						
k_{v_s}	-	25.93 (4.25)	29.90 (5.32)	60.77 (13.68)	96.09 (31.89)	116.47 (34.52)
$k_{v_{se}}$	-	37.50 (8.36)	43.24 (6.78)	54.50 (11.56)	35.22 (8.65)	35.63 (7.75)
k_{v_e}	-	67.87 (23.46)	65.47 (19.49)	73.77 (24.66)	40.59 (7.22)	48.63 (10.93)
Position feedback						
k_{p_s}	-	-	418.65 (78.77)	726.56 (176.16)	1105.10 (348.81)	1303.00 (327.12)
$k_{p_{se}}$	-	-	540.93 (78.26)	620.65 (120.50)	462.54 (84.02)	501.14 (69.55)
k_{p_e}	-	-	845.48 (206.72)	804.55 (292.70)	601.55 (148.88)	901.58 (112.59)
Neural time delay						
T_{d_s}	-	0.050 (0.010)	0.085 (0.018)	0.107 (0.029)	0.039 (0.013)	0.038 (0.009)
T_{d_e}	-	0.062 (0.028)	0.069 (0.016)	0.089 (0.021)	0.022 (0.010)	0.026 (0.010)
Activation cut-off frequency						
f_{act_s}	-	2.18 (0.34)	3.11 (0.31)	3.85 (0.97)	3.05 (0.50)	2.22 (0.33)
f_{act_e}	-	2.30 (0.37)	3.31 (0.38)	4.35 (0.94)	3.05 (0.59)	2.49 (0.43)

Table C.10 – Mean (SD) parameters over subjects for six different model structures. The optimization was performed with a penalty function. *Condition: $PT_{22.5}$, with penalty function.* Go to overview

Parameter	Model 1	Model 2	Model 3	Model 4	Model 5	Model 6	Unit
Segmental mass							
m_h	1.61 (0.52)	1.66 (0.57)	1.84 (0.23)	1.51 (0.09)	1.97 (0.20)	1.88 (0.18)	kg
m_f	2.31 (0.58)	1.73 (0.55)	2.22 (0.51)	2.27 (0.47)	2.13 (0.19)	2.10 (0.22)	kg
Joint damping							
b_s	8.37 (2.81)	5.69 (1.84)	2.47 (0.98)	2.36 (0.77)	3.61 (1.09)	3.22 (0.95)	Nms/rad
b_{se}	10.83 (4.62)	6.56 (3.85)	5.95 (1.86)	3.74 (1.32)	2.65 (0.57)	2.08 (0.70)	Nms/rad
b_e	13.95 (10.92)	13.19 (8.43)	10.02 (3.61)	7.89 (2.43)	8.67 (0.93)	7.84 (0.84)	Nms/rad
Joint stiffness							
k_s	185.8 (27.8)	132.4 (33.3)	227.6 (46.3)	200.6 (39.3)	81.6 (19.7)	144.8 (36.2)	Nm/rad
k_{se}	68.9 (26.2)	67.8 (36.3)	71.3 (28.2)	73.8 (27.9)	45.7 (12.5)	42.2 (18.2)	Nm/rad
k_e	232.4 (85.1)	256.5 (128.0)	218.2 (75.7)	179.7 (42.3)	31.0 (14.9)	26.8 (14.2)	Nm/rad
Hand grip damping and stiffness							
b_h	47.6 (23.0)	45.3 (19.4)	54.4 (16.8)	63.4 (14.3)	61.4 (14.1)	65.1 (17.7)	Ns/m
k_h	23.5 (3.11)	26.0 (1.90)	25.7 (1.79)	26.0 (1.78)	27.1 (1.70)	26.8 (1.48)	kN/m
Force feedback							
k_{fs}	-	-	-	−0.56 (0.17)	-	−1.16 (0.51)	-
k_{fse}	-	-	-	−0.22 (0.21)	-	−0.12 (0.22)	-
k_{fe}	-	-	-	−0.39 (0.28)	-	−0.89 (0.41)	-
Acceleration feedback							
k_{as}	-	-	-	-	0.68 (0.19)	−0.05 (0.28)	Nms^2/rad
k_{ase}	-	-	-	-	0.35 (0.14)	0.14 (0.17)	Nms^2/rad
k_{ae}	-	-	-	-	1.18 (0.17)	1.12 (0.17)	Nms^2/rad
Velocity feedback							
k_{vs}	-	22.35 (5.21)	13.26 (3.42)	16.17 (3.69)	20.47 (2.48)	19.77 (2.54)	Nms/rad
k_{vse}	-	26.25 (8.69)	23.91 (5.35)	20.00 (5.28)	15.30 (1.72)	16.16 (3.01)	Nms/rad
k_{ve}	-	34.63 (13.09)	30.31 (10.26)	25.01 (6.29)	26.09 (3.50)	26.21 (3.00)	Nms/rad
Position feedback							
k_{ps}	-	-	−80.5 (45.5)	42.6 (26.6)	72.6 (26.3)	163.9 (39.9)	Nm/rad
k_{pse}	-	-	35.7 (58.9)	67.7 (51.5)	90.5 (31.2)	111.8 (33.9)	Nm/rad
k_{pe}	-	-	37.1 (136.7)	44.5 (82)	375.1 (45.7)	446.5 (49)	Nm/rad
Neural time delay							
T_{ds}	-	27.4 (2.07)	31.7 (1.28)	30.3 (1.07)	31.4 (1.79)	28.8 (0.68)	ms
T_{de}	-	33.3 (3.16)	31.9 (1.73)	31.4 (1.29)	33.6 (1.39)	33.0 (1.70)	ms
Activation cut-off frequency							
f_{act_s}	-	2.96 (0.04)	2.76 (0.13)	2.59 (0.08)	2.8 (0.07)	2.61 (0.08)	Hz
f_{act_e}	-	2.70 (0.12)	2.86 (0.08)	2.78 (0.08)	2.8 (0.08)	2.71 (0.07)	Hz

Table C.11 – Mean (SD) SEMs over subjects for six different model structures (values are not normalized). The optimization was performed with a penalty function. *Condition: $PT_{22.5}$, with penalty function.* Go to overview

Parameter	Model 1	Model 2	Model 3	Model 4	Model 5	Model 6
Segmental mass						
m_h	11.44 (6.26)	11.72 (4.89)	10.72 (2.21)	11.50 (1.88)	13.61 (3.45)	13.97 (3.59)
m_f	2.39 (1.33)	2.20 (1.08)	2.05 (0.37)	1.96 (0.27)	1.70 (0.26)	1.60 (0.18)
Joint damping						
b_s	8.93 (3.39)	6.07 (1.98)	8.06 (2.66)	9.57 (3.73)	27.31 (8.57)	31.66 (9.04)
b_{se}	9.32 (7.63)	7.74 (5.11)	6.65 (1.09)	6.33 (1.28)	8.42 (2.30)	8.22 (1.72)
b_e	13.09 (21.01)	11.89 (14.13)	6.83 (2.53)	5.53 (2.17)	5.90 (1.88)	5.64 (1.54)
Joint stiffness						
k_s	87.37 (14.44)	172.79 (60.76)	216.72 (45.63)	281.03 (72.78)	1031.19 (309.13)	1309.65 (385.35)
k_{se}	142.82 (52.39)	255.69 (110.57)	270.04 (44.67)	252.45 (50.03)	310.86 (69.84)	322.44 (62.50)
k_e	269.79 (246.32)	478.97 (345.12)	355.91 (145.55)	299.08 (102.63)	276.12 (62.15)	284.77 (62.77)
Hand grip damping and stiffness						
b_h	97.42 (30.26)	103.82 (30.47)	98.95 (26.96)	103.06 (36.98)	105.56 (28.88)	115.10 (44.47)
k_h	16480 (5044)	20799 (5710)	18646 (4650)	22473 (3480)	17228 (3670)	19344 (4907)
Force feedback						
k_{f_s}	-	-	-	2.49 (0.57)	-	2.61 (0.86)
$k_{f_{se}}$	-	-	-	1.61 (0.38)	-	1.20 (0.23)
k_{f_e}	-	-	-	2.71 (0.62)	-	2.51 (0.60)
Acceleration feedback						
k_{a_s}	-	-	-	-	4.58 (1.30)	6.44 (1.98)
$k_{a_{se}}$	-	-	-	-	1.93 (0.39)	1.85 (0.46)
k_{a_e}	-	-	-	-	2.47 (0.30)	2.38 (0.39)
Velocity feedback						
k_{v_s}	-	30.59 (8.47)	26.98 (3.60)	49.77 (8.79)	88.68 (27.52)	106.53 (32.85)
$k_{v_{se}}$	-	46.52 (19.18)	45.04 (12.06)	54.85 (18.39)	32.02 (10.00)	29.80 (8.58)
k_{v_e}	-	78.24 (41.39)	69.53 (30.36)	76.94 (29.80)	36.93 (9.17)	42.92 (8.74)
Position feedback						
k_{p_s}	-	-	370.72 (106.79)	689.02 (98.03)	1028.59 (296.84)	1231.93 (343.77)
$k_{p_{se}}$	-	-	521.35 (171.37)	642.50 (172.37)	392.36 (73.91)	455.61 (82.04)
k_{p_e}	-	-	829.63 (365.77)	816.40 (277.42)	539.31 (101.40)	825.25 (95.09)
Neural time delay						
T_{d_s}	-	0.044 (0.010)	0.066 (0.010)	0.087 (0.011)	0.035 (0.010)	0.035 (0.007)
T_{d_e}	-	0.047 (0.019)	0.052 (0.010)	0.071 (0.011)	0.019 (0.007)	0.023 (0.009)
Activation cut-off frequency						
f_{act_s}	-	2.46 (0.41)	2.90 (0.54)	3.57 (0.65)	2.73 (0.64)	2.09 (0.28)
f_{act_e}	-	2.42 (0.38)	3.09 (0.64)	4.05 (0.66)	2.62 (0.58)	2.24 (0.26)

Table C.12 – Total mean (SD) of the criterion and VAF values for six different model structures. The optimization was performed with a penalty function. Only trials with a positive VAF value were used to calculate the VAF. N_{pos} represents the number of trials with a positive VAF. The optimization resulted in stable systems for all trials. *Conditions: $PT_{2.5}$, $PT_{7.5}$ and $PT_{22.5}$, with penalty function.* Go to overview

		Model 1	Model 2	Model 3	Model 4	Model 5	Model 6
$PT_{2.5}$	Criterion	110.25 (19.95)	97.61 (23.09)	99.05 (23.11)	94.49 (22.71)	90.09 (22.71)	88.53 (23.02)
	VAF_x (%)	50.19 (10.90)	44.48 (13.05)	43.74 (12.84)	48.68 (10.60)	46.53 (12.53)	53.77 (9.83)
	VAF_y (%)	33.94 (15.30)	37.88 (16.97)	34.82 (18.75)	38.68 (13.78)	36.77 (17.45)	39.61 (14.11)
	$N_{pos}(\leq 20)$	18	20	20	20	19	20
$PT_{7.5}$	Criterion	112.65 (18.77)	95.89 (18.50)	92.40 (19.38)	88.17 (18.36)	71.95 (22.72)	70.71 (22.16)
	VAF_x (%)	63.63 (8.70)	58.47 (11.59)	60.37 (10.89)	63.59 (11.08)	62.43 (12.77)	68.26 (8.77)
	VAF_y (%)	41.30 (13.51)	49.39 (15.63)	49.79 (17.51)	53.32 (14.16)	51.50 (19.21)	57.14 (15.68)
	$N_{pos}(\leq 80)$	77	80	79	80	79	80
$PT_{22.5}$	Criterion	115.61 (23.41)	96.18 (20.49)	89.83 (19.79)	92.02 (19.46)	70.38 (23.96)	70.35 (23.03)
	VAF_x (%)	67.61 (9.61)	58.85 (10.70)	59.75 (11.23)	65.48 (9.29)	60.32 (12.97)	67.21 (10.94)
	VAF_y (%)	48.20 (11.95)	52.41 (11.26)	50.55 (15.73)	58.00 (14.15)	52.26 (20.41)	60.42 (15.12)
	$N_{pos}(\leq 20)$	17	19	20	19	20	20

C.6 Results: without penalty function ($RT_{7.5}$)

Table C.13 – Mean (SD) parameters over subjects for six different model structures. The optimization was performed with a penalty function. *Condition: $RT_{7.5}$, without penalty function.* Go to overview

Parameter	Model 1	Model 2	Model 3	Model 4	Model 5	Model 6	Unit
Segmental mass							
m_h	2.04 (0.45)	2.20 (0.38)	2.05 (0.46)	2.09 (0.36)	1.98 (0.28)	1.98 (0.38)	kg
m_f	1.92 (0.45)	1.92 (0.48)	1.81 (0.36)	1.81 (0.40)	1.65 (0.46)	1.71 (0.36)	kg
Joint damping							
b_s	1.91 (0.23)	1.90 (0.54)	1.76 (0.66)	1.84 (0.52)	2.84 (0.72)	2.89 (0.85)	Nms/rad
b_{se}	1.25 (0.24)	1.29 (0.29)	0.85 (0.32)	0.85 (0.19)	1.02 (0.34)	1.12 (0.37)	Nms/rad
b_e	1.47 (0.27)	1.63 (0.33)	1.57 (0.46)	1.47 (0.23)	1.56 (0.40)	1.60 (0.29)	Nms/rad
Joint stiffness							
k_s	7.7 (2.6)	7.0 (2.5)	8.3 (5.2)	6.8 (3.1)	8.7 (5.5)	8.6 (2.8)	Nm/rad
k_{se}	1.8 (1.0)	1.5 (1.0)	7.7 (5.4)	8.5 (3.9)	16.8 (7.3)	13.6 (6.5)	Nm/rad
k_e	5.5 (2.3)	3.4 (1.6)	2.9 (3.2)	6.6 (3.8)	5.1 (2.4)	3.9 (2.0)	Nm/rad
Hand grip damping and stiffness							
b_h	32.8 (19.6)	36.9 (19.6)	38.6 (20.3)	34.9 (17.4)	33.1 (18.0)	38.3 (19.4)	Ns/m
k_h	8.4 (1.84)	8.6 (1.71)	8.6 (1.14)	8.7 (1.54)	8.8 (1.79)	8.7 (1.80)	kN/m
Force feedback							
k_{f_s}	-	-	-	−0.77 (0.82)	-	−0.34 (0.50)	-
$k_{f_{se}}$	-	-	-	−0.54 (0.31)	-	−0.33 (0.47)	-
k_{f_e}	-	-	-	−1.04 (0.71)	-	−0.17 (0.76)	-
Acceleration feedback							
k_{a_s}	-	-	-	-	−0.18 (0.09)	−0.19 (0.07)	Nms^2/rad
$k_{a_{se}}$	-	-	-	-	−0.14 (0.07)	−0.11 (0.06)	Nms^2/rad
k_{a_e}	-	-	-	-	−0.08 (0.05)	−0.06 (0.05)	Nms^2/rad
Velocity feedback							
k_{v_s}	-	0.44 (0.47)	0.66 (0.39)	2.55 (1.76)	−0.81 (0.92)	0.17 (1.45)	Nms/rad
$k_{v_{se}}$	-	0.48 (0.22)	0.39 (0.71)	1.94 (1.28)	−1.39 (1.03)	−0.15 (1.23)	Nms/rad
k_{v_e}	-	0.79 (0.34)	1.48 (0.73)	2.93 (1.50)	0.24 (0.51)	1.18 (0.77)	Nms/rad
Position feedback							
k_{p_s}	-	-	−0.8 (6.5)	9.1 (7.3)	−4.9 (5.8)	−1.7 (4.0)	Nm/rad
$k_{p_{se}}$	-	-	−4.6 (6.9)	2.9 (6.0)	−20.6 (7.4)	−11.9 (7.6)	Nm/rad
k_{p_e}	-	-	5.0 (14.0)	15.1 (13)	−14.5 (11.5)	−4.0 (9)	Nm/rad
Neural time delay							
T_{d_s}	-	30.2 (1.85)	30.3 (1.47)	30.5 (2.04)	30.0 (1.54)	30.2 (0.90)	ms
T_{d_e}	-	40.0 (2.73)	39.7 (1.78)	38.9 (2.21)	34.5 (2.62)	35.1 (2.24)	ms
Activation cut-off frequency							
f_{act_s}	-	2.17 (0.22)	2.20 (0.22)	2.02 (0.13)	2.2 (0.15)	2.06 (0.15)	Hz
f_{act_e}	-	2.45 (0.22)	2.44 (0.17)	2.07 (0.16)	2.5 (0.17)	2.34 (0.13)	Hz

Table C.14 – Mean (SD) SEMs over subjects for six different model structures (values are not normalized). The optimization was performed with a penalty function. *Condition: $RT_{7.5}$, without penalty function.* Go to overview

Parameter	Model 1	Model 2	Model 3	Model 4	Model 5	Model 6
Segmental mass						
m_h	4.79 (0.74)	6.05 (1.11)	7.79 (1.32)	7.26 (1.43)	13.75 (2.35)	13.56 (4.08)
m_f	0.65 (0.11)	0.74 (0.12)	0.89 (0.15)	0.81 (0.18)	0.94 (0.21)	0.99 (0.18)
Joint damping						
b_s	1.27 (0.24)	2.56 (0.49)	6.54 (2.02)	5.34 (2.15)	31.81 (12.56)	28.82 (6.47)
b_{se}	0.87 (0.15)	1.31 (0.17)	2.40 (0.74)	2.20 (0.69)	4.16 (0.84)	4.62 (1.47)
b_e	0.57 (0.09)	0.84 (0.14)	1.60 (0.43)	1.37 (0.42)	2.50 (0.53)	2.71 (0.86)
Joint stiffness						
k_s	5.67 (0.89)	8.52 (1.41)	121.96 (63.42)	104.60 (55.68)	1178.65 (489.58)	1062.61 (262.18)
k_{se}	6.13 (1.30)	8.76 (1.95)	47.72 (16.73)	38.75 (14.73)	151.00 (33.53)	165.04 (48.26)
k_e	6.20 (1.59)	11.16 (4.11)	44.67 (13.78)	31.76 (12.71)	106.68 (25.85)	106.98 (31.74)
Hand grip damping and stiffness						
b_h	36.09 (18.53)	38.40 (12.82)	42.52 (12.92)	38.64 (13.32)	42.23 (17.84)	44.54 (17.47)
k_h	5154 (1923)	5505 (1888)	6148 (2201)	5853 (1896)	6843 (3113)	7626 (3992)
Force feedback						
k_{f_s}	-	-	-	5.60 (2.19)	-	4.32 (1.02)
$k_{f_{se}}$	-	-	-	2.82 (0.83)	-	3.09 (1.52)
k_{f_e}	-	-	-	6.83 (1.66)	-	5.52 (2.03)
Acceleration feedback						
k_{a_s}	-	-	-	-	7.27 (3.89)	7.00 (1.90)
$k_{a_{se}}$	-	-	-	-	0.89 (0.25)	1.28 (0.32)
k_{a_e}	-	-	-	-	0.70 (0.18)	0.79 (0.28)
Velocity feedback						
k_{v_s}	-	2.93 (0.46)	10.53 (4.89)	15.42 (5.33)	129.91 (60.85)	120.03 (30.78)
$k_{v_{se}}$	-	1.99 (0.43)	6.38 (5.02)	11.44 (3.81)	15.82 (3.54)	19.19 (6.10)
k_{v_e}	-	2.20 (0.81)	10.55 (14.59)	16.21 (6.32)	10.84 (2.62)	13.05 (4.21)
Position feedback						
k_{p_s}	-	-	121.90 (64.98)	110.97 (50.99)	1179.12 (489.13)	1063.17 (263.80)
$k_{p_{se}}$	-	-	51.73 (22.97)	58.37 (28.76)	154.08 (32.64)	172.00 (54.55)
k_{p_e}	-	-	61.69 (37.90)	91.91 (50.48)	114.37 (28.36)	118.21 (45.23)
Neural time delay						
T_{d_s}	-	0.475 (0.189)	0.453 (0.115)	0.349 (0.200)	0.257 (0.203)	0.217 (0.088)
T_{d_e}	-	0.249 (0.152)	0.317 (0.162)	0.216 (0.071)	0.142 (0.069)	0.148 (0.042)
Activation cut-off frequency						
f_{act_s}	-	7.67 (3.25)	5.42 (1.33)	6.27 (1.64)	4.08 (1.88)	4.83 (1.02)
f_{act_e}	-	5.37 (3.49)	3.20 (0.82)	5.14 (1.51)	3.45 (1.49)	5.39 (1.13)

Table C.15 – Total mean (SD) of the criterion and VAF values for six different model structures. Only trials with a positive VAF value were used to calculate the VAF. N_{pos} represents the number of stable models with a positive VAF and N_{stab} indicates the number of stable systems. *Condition: $RT_{7.5}$, without penalty function.* Go to overview

	Model 1	Model 2	Model 3	Model 4	Model 5	Model 6
Criterion	82.08 (18.90)	81.42 (20.56)	85.39 (24.69)	79.92 (20.99)	75.86 (18.36)	75.46 (17.28)
VAF_x (%)	77.13 (8.07)	79.29 (8.07)	74.29 (13.59)	73.21 (10.89)	80.25 (7.31)	78.91 (9.90)
VAF_y (%)	67.11 (16.97)	69.49 (19.82)	66.44 (19.17)	73.17 (13.83)	75.11 (11.63)	70.76 (17.56)
$N_{pos}(\leq 40)$	37	32	32	11	22	26
$Nstab(\leq 40)$	40	36	35	23	29	31

C.7 Results: with penalty function ($RT_{2.5}$, $RT_{7.5}$ and $RT_{22.5}$)

Table C.16 – Mean (SD) parameters over subjects for six different model structures. The optimization was performed with a penalty function. *Condition: $RT_{2.5}$, with penalty function.* Go to overview

Parameter	Model 1	Model 2	Model 3	Model 4	Model 5	Model 6	Unit
Segmental mass							
m_h	2.24 (0.38)	2.13 (0.38)	1.95 (0.51)	1.85 (0.49)	1.69 (0.42)	1.91 (0.45)	kg
m_f	1.88 (0.62)	1.82 (0.57)	1.83 (0.57)	1.82 (0.51)	1.63 (0.55)	1.64 (0.49)	kg
Joint damping							
b_s	2.75 (0.41)	3.08 (0.60)	2.94 (0.88)	3.07 (1.10)	4.16 (1.49)	4.13 (0.97)	Nms/rad
b_{se}	1.83 (0.43)	2.02 (0.28)	1.60 (0.35)	1.54 (0.32)	1.59 (0.36)	1.61 (0.29)	Nms/rad
b_e	1.92 (0.34)	2.24 (0.41)	2.13 (0.35)	2.02 (0.30)	2.38 (0.57)	2.33 (0.50)	Nms/rad
Joint stiffness							
k_s	14.7 (7.5)	11.0 (3.9)	13.1 (7.2)	16.4 (4.0)	17.5 (4.8)	16.1 (5.5)	Nm/rad
k_{se}	6.9 (3.4)	2.7 (1.5)	10.0 (3.8)	12.7 (4.3)	30.6 (8.8)	26.0 (7.6)	Nm/rad
k_e	14.0 (7.0)	6.8 (2.4)	8.0 (5.6)	10.3 (4.1)	6.6 (6.8)	5.1 (3.6)	Nm/rad
Hand grip damping and stiffness							
b_h	52.3 (106.4)	40.3 (63.2)	39.3 (54.5)	67.1 (148.0)	44.7 (78.6)	51.1 (52.6)	Ns/m
k_h	8.3 (2.49)	9.0 (2.14)	9.2 (1.91)	8.7 (2.18)	9.1 (2.08)	9.4 (1.92)	kN/m
Force feedback							
$k_{f\,s}$	-	-	-	−1.04 (0.65)	-	−0.58 (0.39)	-
$k_{f\,se}$	-	-	-	−0.32 (0.43)	-	0.09 (0.34)	-
$k_{f\,e}$	-	-	-	−0.97 (0.70)	-	−0.50 (0.62)	-
Acceleration feedback							
$k_{a\,s}$	-	-	-	-	−0.24 (0.15)	−0.19 (0.18)	Nms^2/rad
$k_{a\,se}$	-	-	-	-	−0.18 (0.10)	−0.18 (0.10)	Nms^2/rad
$k_{a\,e}$	-	-	-	-	−0.02 (0.06)	−0.01 (0.06)	Nms^2/rad
Velocity feedback							
$k_{v\,s}$	-	1.13 (1.55)	0.72 (1.13)	2.90 (2.32)	−0.90 (1.74)	0.69 (1.66)	Nms/rad
$k_{v\,se}$	-	1.47 (0.87)	0.71 (0.64)	2.27 (1.48)	−1.74 (1.03)	−0.74 (1.16)	Nms/rad
$k_{v\,e}$	-	1.88 (0.95)	1.72 (0.52)	3.54 (1.16)	1.52 (1.08)	2.46 (1.10)	Nms/rad
Position feedback							
k_{p_s}	-	-	−2.6 (8.2)	12.2 (6.4)	−7.6 (7.1)	−0.2 (7.7)	Nm/rad
$k_{p_{se}}$	-	-	−7.8 (3.8)	2.0 (6.8)	−28.2 (9.7)	−23.8 (8.1)	Nm/rad
k_{p_e}	-	-	−1.9 (5.3)	11.0 (7)	0.2 (8.6)	5.9 (7)	Nm/rad
Neural time delay							
T_{d_s}	-	31.1 (2.07)	30.6 (2.21)	30.3 (2.29)	29.3 (2.72)	29.1 (1.65)	ms
T_{d_e}	-	37.5 (3.08)	39.1 (3.04)	36.9 (2.81)	35.3 (2.89)	36.4 (1.92)	ms
Activation cut-off frequency							
f_{act_s}	-	2.44 (0.38)	2.29 (0.28)	2.10 (0.21)	2.4 (0.20)	2.15 (0.13)	Hz
f_{act_e}	-	2.60 (0.22)	2.67 (0.18)	2.24 (0.23)	2.6 (0.18)	2.42 (0.19)	Hz

Table C.17 – Mean (SD) SEMs over subjects for six different model structures (values are not normalized). The optimization was performed with a penalty function. *Condition: $RT_{2.5}$, with penalty function.* Go to overview

Parameter	Model 1	Model 2	Model 3	Model 4	Model 5	Model 6
Segmental mass						
m_h	4.91 (0.76)	5.90 (0.94)	7.13 (1.61)	6.28 (1.15)	10.67 (2.95)	13.47 (5.46)
m_f	0.67 (0.10)	0.75 (0.15)	0.86 (0.16)	0.78 (0.14)	1.01 (0.27)	0.96 (0.16)
Joint damping						
b_s	1.41 (0.18)	2.81 (0.54)	5.81 (1.37)	5.92 (2.18)	22.94 (7.50)	30.93 (16.84)
b_{se}	1.02 (0.12)	1.48 (0.17)	2.50 (0.48)	2.51 (0.79)	4.78 (1.66)	5.26 (1.47)
b_e	0.71 (0.11)	1.03 (0.22)	1.69 (0.37)	1.49 (0.48)	2.76 (0.78)	2.86 (0.64)
Joint stiffness						
k_s	9.05 (1.73)	16.23 (12.14)	96.15 (26.86)	112.85 (54.01)	846.59 (266.83)	1140.80 (648.77)
k_{se}	9.79 (1.99)	16.56 (14.14)	45.73 (17.70)	46.16 (23.55)	188.44 (93.48)	195.68 (81.51)
k_e	10.29 (2.31)	19.18 (16.15)	49.15 (13.66)	38.02 (18.47)	102.85 (28.21)	97.33 (20.97)
Hand grip damping and stiffness						
b_h	93.00 (199.51)	101.12 (211.20)	77.44 (128.98)	89.69 (181.94)	205.55 (520.30)	109.85 (137.39)
k_h	25662 (64850)	26911 (66815)	16431 (33176)	21388 (49926)	25849 (62020)	18184 (25222)
Force feedback						
k_{fs}	-	-	-	6.88 (3.65)	-	3.58 (1.05)
k_{fse}	-	-	-	2.61 (0.96)	-	1.78 (0.64)
k_{fe}	-	-	-	6.89 (4.33)	-	3.34 (1.46)
Acceleration feedback						
k_{as}	-	-	-	-	4.36 (1.54)	6.92 (4.15)
k_{ase}	-	-	-	-	0.96 (0.47)	1.26 (0.54)
k_{ae}	-	-	-	-	0.60 (0.18)	0.68 (0.16)
Velocity feedback						
k_{vs}	-	3.82 (1.19)	9.09 (2.30)	23.79 (12.34)	85.96 (28.24)	123.18 (74.02)
k_{vse}	-	2.87 (1.37)	4.91 (1.50)	17.85 (8.43)	18.24 (9.25)	20.34 (8.15)
k_{ve}	-	3.18 (1.64)	5.28 (1.39)	21.05 (9.37)	10.36 (3.15)	13.44 (3.10)
Position feedback						
k_{ps}	-	-	96.25 (25.40)	147.95 (68.25)	846.65 (267.10)	1139.99 (651.70)
k_{pse}	-	-	46.05 (17.65)	87.29 (44.74)	189.40 (93.19)	198.80 (83.00)
k_{pe}	-	-	50.63 (14.44)	110.66 (49.19)	104.45 (29.37)	108.45 (23.32)
Neural time delay						
T_{ds}	-	0.279 (0.153)	0.375 (0.169)	0.261 (0.125)	0.116 (0.041)	0.140 (0.064)
T_{de}	-	0.131 (0.087)	0.202 (0.075)	0.193 (0.073)	0.098 (0.044)	0.106 (0.054)
Activation cut-off frequency						
f_{act_s}	-	4.89 (1.79)	5.52 (2.40)	5.91 (1.42)	3.12 (0.93)	3.65 (0.85)
f_{act_e}	-	3.47 (2.15)	2.92 (0.98)	5.34 (1.41)	2.81 (0.82)	3.83 (0.70)

Table C.18 – Mean (SD) parameters over subjects for six different model structures. The optimization was performed with a penalty function. *Condition: $RT_{7.5}$, with penalty function.* Go to overview

Parameter	Model 1	Model 2	Model 3	Model 4	Model 5	Model 6	Unit
Segmental mass							
m_h	2.06 (0.39)	2.05 (0.38)	1.96 (0.32)	2.03 (0.19)	1.89 (0.18)	1.99 (0.26)	kg
m_f	1.86 (0.42)	1.91 (0.47)	1.85 (0.41)	1.74 (0.42)	1.58 (0.43)	1.64 (0.30)	kg
Joint damping							
b_s	2.15 (0.25)	2.20 (0.39)	2.20 (0.33)	2.96 (0.67)	3.81 (0.69)	3.43 (0.33)	Nms/rad
b_{se}	1.40 (0.19)	1.43 (0.18)	1.07 (0.15)	1.23 (0.21)	1.19 (0.31)	1.18 (0.24)	Nms/rad
b_e	1.55 (0.23)	1.64 (0.24)	1.68 (0.21)	1.68 (0.16)	1.92 (0.29)	1.82 (0.24)	Nms/rad
Joint stiffness							
k_s	7.3 (2.6)	6.6 (2.0)	8.7 (3.0)	9.0 (4.0)	13.4 (6.2)	12.9 (4.1)	Nm/rad
k_{se}	1.8 (0.9)	1.1 (0.7)	7.2 (1.8)	9.2 (3.3)	28.2 (8.5)	20.9 (4.4)	Nm/rad
k_e	5.4 (2.0)	3.6 (1.4)	2.7 (1.4)	4.4 (1.9)	4.0 (2.7)	3.9 (2.1)	Nm/rad
Hand grip damping and stiffness							
b_h	22.3 (16.6)	27.0 (16.5)	32.6 (14.0)	28.1 (17.3)	28.9 (14.2)	34.9 (11.6)	Ns/m
k_h	8.2 (1.77)	8.9 (1.55)	9.0 (1.14)	8.8 (1.23)	8.9 (1.24)	8.8 (0.80)	kN/m
Force feedback							
k_{fs}	-	-	-	−1.25 (0.30)	-	−0.66 (0.31)	-
k_{fse}	-	-	-	−0.35 (0.25)	-	−0.26 (0.25)	-
k_{fe}	-	-	-	−1.19 (0.28)	-	−0.46 (0.19)	-
Acceleration feedback							
k_{as}	-	-	-	-	−0.28 (0.08)	−0.21 (0.04)	Nms^2/rad
k_{ase}	-	-	-	-	−0.22 (0.06)	−0.16 (0.04)	Nms^2/rad
k_{ae}	-	-	-	-	−0.06 (0.03)	−0.05 (0.02)	Nms^2/rad
Velocity feedback							
k_{vs}	-	0.36 (0.41)	0.04 (0.39)	2.32 (1.12)	−1.92 (0.96)	0.05 (0.53)	Nms/rad
k_{vse}	-	0.47 (0.30)	0.01 (0.29)	1.64 (0.82)	−2.52 (0.78)	−0.67 (0.51)	Nms/rad
k_{ve}	-	0.67 (0.35)	0.89 (0.22)	2.90 (0.72)	0.42 (0.38)	1.54 (0.66)	Nms/rad
Position feedback							
k_{ps}	-	-	−2.5 (3.0)	8.1 (7.2)	−8.1 (5.8)	−3.3 (3.2)	Nm/rad
k_{pse}	-	-	−7.0 (1.9)	−2.8 (4.2)	−28.2 (8.6)	−19.4 (4.5)	Nm/rad
k_{pe}	-	-	0.5 (1.7)	6.6 (3)	−0.8 (2.5)	1.1 (3)	Nm/rad
Neural time delay							
T_{ds}	-	30.9 (1.61)	30.4 (1.65)	29.7 (1.44)	29.9 (1.20)	29.7 (1.23)	ms
T_{de}	-	41.0 (2.24)	39.0 (2.02)	39.2 (1.75)	33.9 (1.03)	34.6 (1.11)	ms
Activation cut-off frequency							
f_{act_s}	-	2.20 (0.26)	2.16 (0.23)	2.09 (0.10)	2.4 (0.16)	2.22 (0.13)	Hz
f_{act_e}	-	2.52 (0.19)	2.58 (0.10)	2.13 (0.10)	2.6 (0.12)	2.36 (0.09)	Hz

Table C.19 – Mean (SD) SEMs over subjects for six different model structures (values are not normalized). The optimization was performed with a penalty function. *Condition: $RT_{7.5}$, with penalty function.* Go to overview

Parameter	Model 1	Model 2	Model 3	Model 4	Model 5	Model 6
Segmental mass						
m_h	4.73 (0.84)	5.95 (1.06)	7.54 (0.99)	6.56 (0.92)	11.68 (1.32)	14.09 (1.63)
m_f	0.64 (0.10)	0.71 (0.11)	0.88 (0.16)	0.72 (0.11)	0.93 (0.12)	0.94 (0.12)
Joint damping						
b_s	1.31 (0.26)	2.70 (0.53)	5.87 (1.39)	5.94 (1.83)	23.48 (6.64)	30.68 (6.80)
b_{se}	0.95 (0.20)	1.38 (0.26)	2.47 (0.50)	2.38 (0.47)	5.36 (1.12)	5.64 (1.28)
b_e	0.62 (0.10)	0.84 (0.14)	1.58 (0.38)	1.23 (0.20)	2.63 (0.46)	2.66 (0.58)
Joint stiffness						
k_s	5.86 (1.19)	8.80 (2.02)	88.45 (32.46)	120.61 (42.77)	826.09 (273.24)	1116.70 (293.78)
k_{se}	5.94 (1.31)	8.82 (2.44)	39.69 (8.99)	42.54 (11.13)	254.25 (76.09)	254.19 (66.59)
k_e	6.13 (1.88)	9.78 (2.97)	42.59 (12.83)	23.66 (8.19)	113.42 (25.40)	104.25 (29.25)
Hand grip damping and stiffness						
b_h	28.25 (11.13)	32.39 (12.65)	38.37 (12.53)	33.69 (13.52)	39.48 (14.62)	42.89 (13.59)
k_h	4401 (1331)	4906 (937)	5733 (966)	5273 (1183)	6596 (1055)	7293 (1966)
Force feedback						
k_{f_s}	-	-	-	8.99 (1.91)	-	4.95 (1.80)
$k_{f_{se}}$	-	-	-	2.92 (0.76)	-	2.37 (0.47)
k_{f_e}	-	-	-	9.11 (2.62)	-	4.45 (1.29)
Acceleration feedback						
k_{a_s}	-	-	-	-	3.98 (1.34)	6.52 (2.30)
$k_{a_{se}}$	-	-	-	-	1.30 (0.40)	1.67 (0.38)
k_{a_e}	-	-	-	-	0.66 (0.15)	0.73 (0.21)
Velocity feedback						
k_{v_s}	-	2.91 (0.59)	7.78 (2.49)	18.44 (4.72)	80.96 (27.33)	118.93 (35.84)
$k_{v_{se}}$	-	1.82 (0.35)	3.98 (1.01)	15.31 (4.33)	24.73 (7.59)	24.67 (6.18)
k_{v_e}	-	1.82 (0.44)	4.43 (1.14)	20.06 (6.75)	11.42 (2.75)	13.07 (2.92)
Position feedback						
k_{p_s}	-	-	88.65 (32.69)	112.72 (25.34)	826.16 (272.66)	1116.83 (292.70)
$k_{p_{se}}$	-	-	40.75 (9.34)	51.58 (10.24)	255.18 (76.25)	253.00 (65.31)
k_{p_e}	-	-	43.03 (13.01)	58.93 (24.54)	113.68 (25.90)	105.37 (27.42)
Neural time delay						
T_{d_s}	-	0.518 (0.192)	0.546 (0.126)	0.301 (0.075)	0.139 (0.039)	0.179 (0.052)
T_{d_e}	-	0.245 (0.133)	0.331 (0.094)	0.227 (0.048)	0.142 (0.039)	0.182 (0.053)
Activation cut-off frequency						
f_{act_s}	-	8.09 (3.03)	7.15 (2.54)	6.61 (1.84)	3.55 (0.92)	4.79 (1.18)
f_{act_e}	-	5.78 (3.07)	4.22 (1.20)	6.47 (1.39)	3.35 (1.16)	5.26 (1.31)

Table C.20 – Mean (SD) parameters over subjects for six different model structures. The optimization was performed with a penalty function. *Condition: $RT_{22.5}$, with penalty function.* Go to overview

Parameter	Model 1	Model 2	Model 3	Model 4	Model 5	Model 6	Unit
Segmental mass							
m_h	2.11 (0.25)	2.21 (0.07)	2.06 (0.17)	2.06 (0.20)	2.00 (0.15)	1.99 (0.04)	kg
m_f	2.08 (0.28)	2.03 (0.16)	1.80 (0.17)	1.86 (0.15)	1.66 (0.12)	1.70 (0.12)	kg
Joint damping							
b_s	2.67 (0.72)	2.67 (0.30)	2.40 (0.39)	2.51 (0.66)	3.26 (0.58)	3.26 (0.30)	Nms/rad
b_{se}	1.75 (0.38)	1.88 (0.23)	1.27 (0.09)	1.43 (0.17)	1.05 (0.16)	1.01 (0.24)	Nms/rad
b_e	1.42 (0.13)	1.56 (0.08)	1.67 (0.17)	1.61 (0.21)	1.53 (0.11)	1.57 (0.06)	Nms/rad
Joint stiffness							
k_s	6.9 (1.5)	7.3 (1.0)	9.5 (2.5)	8.7 (2.5)	9.1 (0.9)	9.9 (1.3)	Nm/rad
k_{se}	3.4 (1.3)	3.8 (0.7)	10.7 (1.4)	11.4 (1.5)	20.3 (6.3)	17.5 (2.8)	Nm/rad
k_e	4.6 (1.2)	4.6 (1.0)	2.9 (0.6)	5.6 (0.9)	4.9 (1.4)	4.4 (0.7)	Nm/rad
Hand grip damping and stiffness							
b_h	32.9 (7.6)	40.0 (9.3)	37.2 (6.6)	34.8 (9.2)	33.8 (5.9)	38.2 (4.0)	Ns/m
k_h	7.9 (1.30)	8.4 (0.59)	8.2 (0.89)	8.4 (0.85)	8.4 (0.70)	8.5 (0.59)	kN/m
Force feedback							
k_{fs}	-	-	-	−1.40 (0.31)	-	−0.69 (0.21)	-
k_{fse}	-	-	-	−0.69 (0.28)	-	−0.46 (0.24)	-
k_{fe}	-	-	-	−1.18 (0.31)	-	−0.36 (0.22)	-
Acceleration feedback							
k_{as}	-	-	-	-	−0.21 (0.07)	−0.19 (0.03)	Nms^2/rad
k_{ase}	-	-	-	-	−0.15 (0.06)	−0.11 (0.02)	Nms^2/rad
k_{ae}	-	-	-	-	−0.08 (0.02)	−0.06 (0.02)	Nms^2/rad
Velocity feedback							
k_{vs}	-	−0.16 (0.41)	−0.01 (0.74)	2.52 (0.94)	−1.50 (0.63)	0.09 (0.22)	Nms/rad
k_{vse}	-	−0.26 (0.30)	−0.28 (0.47)	1.32 (0.55)	−1.92 (1.01)	−0.36 (0.30)	Nms/rad
k_{ve}	-	−0.14 (0.25)	0.30 (0.28)	1.98 (0.29)	−0.30 (0.26)	0.78 (0.16)	Nms/rad
Position feedback							
k_{ps}	-	-	−3.0 (3.0)	7.9 (3.8)	−5.1 (0.7)	−2.8 (0.8)	Nm/rad
k_{pse}	-	-	−6.4 (0.9)	0.1 (2.8)	−19.2 (6.6)	−14.8 (2.2)	Nm/rad
k_{pe}	-	-	3.7 (2.3)	5.9 (2)	−2.6 (1.3)	−0.9 (1)	Nm/rad
Neural time delay							
T_{ds}	-	30.2 (0.48)	30.1 (0.57)	30.2 (0.51)	30.1 (0.70)	30.1 (0.18)	ms
T_{de}	-	40.0 (0.41)	40.0 (1.00)	39.1 (1.57)	34.2 (0.86)	34.8 (0.33)	ms
Activation cut-off frequency							
f_{act_s}	-	2.18 (0.06)	2.22 (0.08)	2.04 (0.06)	2.2 (0.06)	2.09 (0.04)	Hz
f_{act_e}	-	2.45 (0.05)	2.42 (0.06)	2.04 (0.05)	2.4 (0.05)	2.34 (0.01)	Hz

Table C.21 – Mean (SD) SEMs over subjects for six different model structures (values are not normalized). The optimization was performed with a penalty function. *Condition: $RT_{22.5}$, with penalty function.* Go to overview

Parameter	Model 1	Model 2	Model 3	Model 4	Model 5	Model 6
Segmental mass						
m_h	6.35 (1.01)	7.67 (0.81)	9.51 (0.68)	7.91 (0.99)	15.74 (3.05)	15.46 (3.78)
m_f	0.82 (0.14)	0.93 (0.17)	1.09 (0.22)	0.96 (0.16)	1.08 (0.17)	1.09 (0.16)
Joint damping						
b_s	1.82 (0.64)	3.30 (0.61)	8.05 (1.53)	5.96 (2.34)	34.07 (8.91)	32.95 (10.48)
b_{se}	1.16 (0.30)	1.87 (0.37)	3.66 (0.69)	3.20 (0.77)	5.65 (0.86)	5.72 (1.55)
b_e	0.73 (0.15)	1.03 (0.12)	2.09 (0.29)	1.70 (0.33)	2.92 (0.56)	2.79 (0.61)
Joint stiffness						
k_s	6.92 (2.47)	8.56 (1.63)	128.08 (32.49)	92.92 (39.16)	1153.63 (350.96)	1147.45 (384.25)
k_{se}	5.08 (1.41)	7.21 (1.21)	59.48 (25.41)	52.11 (10.83)	223.20 (69.97)	186.20 (91.93)
k_e	4.09 (0.82)	7.44 (1.61)	47.41 (10.72)	30.15 (8.51)	129.63 (34.67)	103.69 (21.19)
Hand grip damping and stiffness						
b_h	39.14 (10.82)	46.93 (11.09)	49.22 (12.67)	44.21 (13.44)	48.99 (11.87)	52.01 (10.39)
k_h	6142 (1611)	6842 (1457)	7272 (1515)	6884 (1826)	8013 (1942)	8466 (1028)
Force feedback						
k_{f_s}	-	-	-	10.65 (3.46)	-	5.15 (1.84)
$k_{f_{se}}$	-	-	-	3.95 (1.63)	-	3.08 (0.80)
k_{f_e}	-	-	-	9.73 (3.68)	-	4.63 (1.17)
Acceleration feedback						
k_{a_s}	-	-	-	-	6.21 (1.93)	7.17 (2.43)
$k_{a_{se}}$	-	-	-	-	1.21 (0.36)	1.31 (0.55)
k_{a_e}	-	-	-	-	0.75 (0.16)	0.74 (0.13)
Velocity feedback						
k_{v_s}	-	3.50 (0.58)	11.51 (3.58)	21.50 (5.54)	120.68 (37.88)	125.53 (41.54)
$k_{v_{se}}$	-	2.09 (0.33)	6.75 (1.52)	14.96 (4.14)	22.50 (7.20)	19.47 (7.13)
k_{v_e}	-	1.49 (0.21)	4.25 (0.74)	15.49 (5.87)	13.62 (3.52)	11.36 (2.21)
Position feedback						
k_{p_s}	-	-	129.59 (32.59)	97.24 (33.10)	1151.86 (349.58)	1143.47 (379.36)
$k_{p_{se}}$	-	-	61.87 (24.04)	57.50 (19.30)	224.41 (70.47)	185.18 (89.20)
k_{p_e}	-	-	48.65 (11.10)	42.53 (20.92)	131.13 (34.90)	102.38 (21.28)
Neural time delay						
T_{d_s}	-	1.135 (0.601)	0.694 (0.132)	0.219 (0.084)	0.194 (0.046)	0.218 (0.045)
T_{d_e}	-	0.720 (0.443)	0.619 (0.113)	0.227 (0.079)	0.169 (0.047)	0.187 (0.046)
Activation cut-off frequency						
f_{act_s}	-	17.97 (9.63)	9.05 (2.32)	6.36 (1.98)	4.20 (1.06)	4.38 (0.92)
f_{act_e}	-	15.02 (8.84)	8.57 (2.13)	6.87 (2.24)	3.30 (1.51)	5.77 (1.35)

Table C.22 – Total mean (SD) of the criterion and VAF values for six different model structures. The optimization was performed with a penalty function. Only trials with a positive VAF value were used to calculate the VAF. N_{pos} represents the number of trials with a positive VAF. The optimization resulted in stable systems for all trials. *Conditions: $RT_{2.5}$, $RT_{7.5}$ and $RT_{22.5}$, with penalty function.* Go to overview

		Model 1	Model 2	Model 3	Model 4	Model 5	Model 6
$RT_{2.5}$	Criterion	75.86 (24.45)	70.99 (24.32)	71.41 (25.22)	67.06 (23.15)	68.80 (24.02)	67.53 (24.13)
	VAF_x (%)	63.69 (12.62)	69.94 (10.92)	70.01 (10.51)	66.75 (12.46)	69.63 (11.12)	68.87 (15.12)
	VAF_y (%)	57.19 (22.53)	63.91 (18.02)	64.96 (20.02)	65.71 (19.07)	65.07 (19.53)	65.39 (18.36)
	$N_{pos}(\leq 20)$	20	20	20	20	20	20
$RT_{7.5}$	Criterion	82.88 (18.04)	80.27 (20.38)	80.99 (20.98)	77.48 (17.90)	78.28 (20.86)	78.12 (19.66)
	VAF_x (%)	76.70 (8.50)	78.84 (8.46)	79.04 (8.27)	75.29 (14.97)	80.28 (6.84)	79.25 (12.86)
	VAF_y (%)	66.71 (18.11)	70.88 (17.32)	74.39 (13.07)	70.39 (15.74)	72.24 (15.87)	72.96 (11.06)
	$N_{pos}(\leq 40)$	37	39	39	39	40	39
$RT_{22.5}$	Criterion	114.73 (21.42)	114.17 (20.34)	116.98 (19.21)	110.05 (20.74)	105.74 (19.43)	106.59 (20.58)
	VAF_x (%)	53.37 (20.68)	56.83 (13.61)	51.80 (21.71)	60.81 (16.89)	65.54 (18.12)	70.54 (13.31)
	VAF_y (%)	60.26 (19.78)	61.97 (19.45)	55.83 (19.71)	54.90 (28.18)	62.53 (14.51)	66.78 (19.51)
	$N_{pos}(\leq 20)$	20	19	20	16	19	20

C.8 Discussion

The means and standard deviations over subjects of the estimated parameters, the SEMs and the criterion & VAF values are presented in tables C.3-C.12 for the position task and in tables C.13-C.22 for the relax task.

The main findings for the optimizations for the position task are listed below.

- The optimization without penalty function resulted in unstable systems (table C.5). This was solved by performing optimization with a penalty function (table C.12).
- Overall, the SEMs exceeded the corresponding parameter value. The SEMs were very high for position, force and acceleration feedback parameters of model 4-6 (tables C.7, C.9 and C.11).
- In general, the more complex the model, the better the accuracy of the model fits in time and frequency domain (table C.12). The accuracy of the conditions $PT_{7.5}$ and $PT_{22.5}$ is much better than the accuracy of model $PT_{2.5}$.
- The parameter values and SEMs of the dominant parameters (intrinsic damping and stiffness) were estimated quite consistent, except for the parameter k_e. This parameter value drops enormously when acceleration feedback was added to the model C.6-C.11).

The main findings for the optimizations for the relax task are given below.

- The optimization without penalty function resulted in stable systems for model 1 (table C.15) and unstable systems for the other five models.
- The SEMs were high for all reflexive feedback parameters for model 2-6 (tables C.17, C.19 and C.21). The lowest SEMs were obtained for model 1.
- In general, the more complex the model, the better the accuracy of the model fits in time and frequency domain (table C.12). The accuracy of the conditions $RT_{2.5}$ and $RT_{7.5}$ is much better than the accuracy of model $RT_{22.5}$.

Finally, model structures for the position and relax task can be chosen for further analysis. A trade-off has to be made between the SEMs and the accuracy in time and frequency domain. Let's consider the position task first. Although the accuracy in time and frequency domain for the complex model structures (model 4-6) is better than for the simpler model structures (model 1-3), the force and acceleration feedback parameters were not estimated accurate. Position feedback parameters were also estimated inaccurate, but we want to choose a model structure with at least position and velocity feedback. Therefore, model 3 is chosen for further analysis in the next appendix where optimization was performed with different initial parameter vectors.
We choose an other model structure for the relax task. Given the bad estimated reflexive parameters, model 1 is considered the best model for the relax task. Moreover, a penalty function was not necessary for this model to obtain stable systems. The relax task will not be analyzed further.

APPENDIX D

Parameter estimation variation of initial parameters

D.1 Introduction

The parameters of six different model structures were estimated in the previous appendix. Optimization with a penalty function was necessary to obtain stable systems for the position task. The optimization boundaries for the upper arm mass, neural delays and activation dynamics were set at small ranges to simplify the optimization. For the position task, we choose model 3 as the best model structure for further analysis.

Subsequently, we are going to optimize model 3 with different initial parameter vectors. By doing this, the optimization is tested for local minima. The optimization boundaries of the upper arm mass, neural delays and activation dynamics were set at larger ranges. Since we still want to obtain a stable system, the same penalty function as in the previous appendix was used in the optimization. Because we want to get a general notion of the presence of local minima, only the main condition with 8 trials per subject ($PT_{7.5}$) was investigated in this appendix.

D.2 Methods

The criterion, VAFs and the SEMs were evaluated for optimization of model 3 for six different initial parameter vectors.

The following optimization settings were used

- The six different initial parameter vectors are given in table D.1.
- The lower and upper boundaries for the estimated parameters are given in table D.2.
- The optimization occurred by the Matlab function `lsqnonlin.m`.
- The optimization options were set at

```
options = optimset('Display', 'iter',...
    'TolX',1e-6,...
    'TolFun',1e-5,...
    'DiffMinChange',1e-4,...
    'MaxIter',1000,...
    'MaxFunEvals',6000);
```

- The criterion with penalty function was used (see section C.2).
- The initial parameter vector and the boundaries were normalized during the optimization.

Table D.1 – Six different initial parameter vectors. These initial parameter vectors were used for the parameter estimation of model 3.

Initial parameter vector nr.	Initial parameter vector structure
$\boldsymbol{\theta_{i1}}$	$\hat{\boldsymbol{\theta}}_{\mathbf{mod3}}$[1].
$\boldsymbol{\theta_{i2}}$	$\hat{\boldsymbol{\theta}}_{\mathbf{mod3}}$, where the value of the reflexive parameters is added to the intrinsic parameters corresponding to each joint. The reflexive parameters are set at very small values.
$\boldsymbol{\theta_{i3}}$	$\hat{\boldsymbol{\theta}}_{\mathbf{mod3}}$, where both time delays are set at 50 ms.
$\boldsymbol{\theta_{i4}}$	$\hat{\boldsymbol{\theta}}_{\mathbf{mod3}}$, where both activation dynamics parameters are set at 5 Hz.
$\boldsymbol{\theta_{i5}}$	$\hat{\boldsymbol{\theta}}_{\mathbf{mod3}}$, where the bi-articular parameters are set at very small values.
$\boldsymbol{\theta_{i6}}$	$\hat{\boldsymbol{\theta}}_{\mathbf{mod3}}$, where each parameter is changed randomly with ±25% of the parameter value. Model optimization occurred for each trial of every subject with the same randomized initial parameter vector.

[1] *The estimated parameter vector of model 3 as presented in table C.8 was the starting point for all six initial parameter vectors.*

Table D.2 – Lower and upper boundaries used for optimization.

Parameter	LB / UB	Unit	Parameter	LB / UB	Unit
Segmental mass			*Velocity feedback*		
m_h	0.5 / 4	kg	k_{v_s}	-1e-2 / 1e2	Nms/rad
m_f	0.5 / 4	kg	$k_{v_{se}}$	-1e-2 / 1e2	Nms/rad
Joint damping			k_{v_e}	-1e-2 / 1e2	Nms/rad
b_s	0 / 1e2	Nms/rad	*Position feedback*		
b_{se}	0 / 1e2	Nms/rad	k_{p_s}	-1e3 / 1e3	Nm/rad
b_e	0 / 1e2	Nms/rad	$k_{p_{se}}$	-1e3 / 1e3	Nm/rad
Joint stiffness			k_{p_e}	-1e3 / 1e3	Nm/rad
k_s	0 / 1e3	Nm/rad	*Neural time delay*		
k_{se}	0 / 1e3	Nm/rad	T_{d_s}	25 / 75	ms
k_e	0 / 1e3	Nm/rad	T_{d_e}	25 / 75	ms
Hand grip damping and stiffness			*Activation cut-off frequency*		
b_h	0 / 5e3	Ns/m	f_{act_s}	1.7 / 6	Hz
k_h	2e3 / 3e4	N/m	f_{act_e}	1.7 / 6	Hz

D.3 Results: with penalty function ($PT_{7.5}$)

Table D.3 – Mean (SD) parameters over subjects for six different initial parameter vectors. *Condition: $PT_{7.5}$, with penalty function.*

Parameter	$\boldsymbol{\theta_{i1}}$-Model 3	$\boldsymbol{\theta_{i2}}$-Model 3	$\boldsymbol{\theta_{i3}}$-Model 3	$\boldsymbol{\theta_{i4}}$-Model 3	$\boldsymbol{\theta_{i5}}$-Model 3	$\boldsymbol{\theta_{i6}}$-Model 3s	Unit
Segmental mass							
m_h	*1.7*: 1.8 (0.4)	*1.7*: 1.2 (0.3)	*1.7*: 1.9 (0.2)	*1.7*: 2.0 (0.4)	*1.7*: 1.7 (0.2)	*1.3*: 1.2 (0.2)	kg
m_f	*2.4*: 2.2 (0.2)	*2.4*: 1.8 (0.1)	*2.4*: 2.2 (0.2)	*2.4*: 2.3 (0.1)	*2.4*: 2.0 (0.2)	*3.0*: 2.5 (0.3)	kg
Joint damping							
b_s	*2.6*: 3.5 (1.0)	*16.2*: 10.0 (2.5)	*2.6*: 3.6 (0.8)	*2.6*: 4.4 (1.1)	*2.6*: 2.8 (0.9)	*3.3*: 4.0 (0.8)	Nms/rad
b_{se}	*6.1*: 7.9 (1.5)	*23.2*: 17.8 (3.5)	*6.1*: 8.1 (2.0)	*6.1*: 6.8 (1.1)	*0.1*: 2.7 (1.3)	*4.5*: 6.4 (1.3)	Nms/rad
b_e	*11.1*: 14.0 (2.7)	*36.0*: 34.8 (6.6)	*11.1*: 15.0 (4.5)	*11.1*: 13.2 (1.8)	*11.1*: 13.4 (2.9)	*8.3*: 10.7 (2.8)	Nms/rad
Joint stiffness							
k_s	*202.9*: 212.3 (30.0)	*139.6*: 186.6 (28.8)	*202.9*: 206.3 (33.2)	*202.9*: 173.1 (33.0)	*202.9*: 146.7 (35.6)	*152.2*: 197.6 (37.3)	Nm/rad
k_{se}	*76.4*: 99.7 (39.7)	*103.3*: 122.8 (40.9)	*76.4*: 98.4 (38.3)	*76.4*: 87.5 (17.0)	*0.8*: 41.1 (28.0)	*95.5*: 109.5 (33.9)	Nm/rad
k_e	*182.1*: 180.7 (49.9)	*248.1*: 284.9 (61.0)	*182.1*: 213.9 (79.2)	*182.1*: 168.8 (28.3)	*182.1*: 152.1 (52.7)	*227.7*: 175.4 (53.0)	Nm/rad
Hand grip damping and stiffness							
b_h	*73.8*: 84.5 (16.0)	*73.8*: 39.7 (24.8)	*73.8*: 87.1 (14.0)	*73.8*: 108.6 (17.0)	*73.8*: 101.8 (31.3)	*55.4*: 56.6 (17.4)	Ns/m
k_h	*26.1*: 27.3 (1.0)	*26.1*: 27.9 (1.7)	*26.1*: 27.5 (1.0)	*26.1*: 27.1 (1.0)	*26.1*: 27.1 (1.1)	*32.6*: 22.4 (1.0)	kN/m
Velocity feedback							
k_{vs}	*13.6*: 13.5 (2.0)	*0.1*: 3.7 (3.3)	*13.6*: 12.2 (2.9)	*13.6*: 15.5 (1.8)	*13.6*: 8.0 (2.0)	*10.2*: 12.9 (2.4)	Nms/rad
k_{vse}	*19.7*: 18.0 (2.7)	*0.2*: 3.1 (5.2)	*19.7*: 18.2 (4.4)	*19.7*: 15.9 (1.2)	*0.2*: 3.6 (2.2)	*14.8*: 13.6 (3.2)	Nms/rad
k_{ve}	*24.9*: 23.0 (4.3)	*0.2*: 3.8 (4.6)	*24.9*: 23.0 (4.1)	*24.9*: 20.8 (2.0)	*24.9*: 19.5 (3.8)	*18.7*: 19.7 (3.0)	Nms/rad
Position feedback							
k_{ps}	*−63.4*: −64.3 (14.9)	*−0.6*: −37.2 (15.9)	*−63.4*: −62.8 (17.4)	*−63.4*: −25.3 (29.8)	*−63.4*: −41.8 (18.0)	*−47.5*: −47.5 (23.5)	Nm/rad
k_{pse}	*38.4*: 34.3 (32.4)	*0.4*: 21.3 (31.1)	*38.4*: 37.8 (42.1)	*38.4*: 25.8 (18.8)	*0.4*: −9.2 (24.7)	*28.8*: 10.8 (40.3)	Nm/rad
k_{pe}	*65.9*: 81.5 (46.8)	*0.7*: 61.5 (50.8)	*65.9*: 97.1 (58.7)	*65.9*: 64.8 (16.7)	*65.9*: 61.4 (37.1)	*49.4*: 37.8 (49.5)	Nm/rad
Neural time delay							
T_{ds}	*31.6*: 34.0 (2.1)	*31.6*: 40.6 (4.0)	*50.0*: 49.2 (4.1)	*31.6*: 33.1 (1.7)	*31.6*: 37.1 (4.2)	*25.3*: 31.9 (3.3)	ms
T_{de}	*31.7*: 32.4 (5.2)	*31.7*: 42.0 (5.1)	*50.0*: 43.3 (5.8)	*31.7*: 30.6 (1.9)	*31.7*: 32.3 (4.0)	*25.3*: 27.3 (2.5)	ms
Activation cut-off frequency							
f_{act_s}	*2.8*: 3.2 (0.4)	*2.8*: 3.4 (0.4)	*2.8*: 3.3 (0.5)	*5.0*: 5.0 (0.1)	*2.8*: 3.7 (0.2)	*3.5*: 3.7 (0.2)	Hz
f_{act_e}	*2.8*: 3.5 (0.4)	*2.8*: 3.8 (0.5)	*2.8*: 3.7 (0.4)	*5.0*: 5.3 (0.2)	*2.8*: 3.8 (0.3)	*2.1*: 3.3 (0.3)	Hz

Table D.4 – Mean (SD) SEMs over subjects for six different initial parameter vectors. The initial parameter vector is given in italic. *Condition: $PT_{7.5}$, with penalty function.*

Parameter	$\boldsymbol{\theta_{i1}}$	$\boldsymbol{\theta_{i2}}$	$\boldsymbol{\theta_{i3}}$	$\boldsymbol{\theta_{i4}}$	$\boldsymbol{\theta_{i5}}$	$\boldsymbol{\theta_{i6}}$
Segmental mass						
m_h	12.86 (2.77)	26.85 (6.54)	13.34 (3.04)	14.40 (2.16)	19.73 (3.44)	12.19 (1.45)
m_f	2.42 (0.54)	5.56 (1.42)	2.52 (0.64)	2.44 (0.48)	2.59 (0.47)	2.16 (0.39)
Joint damping						
b_s	10.12 (1.55)	16.33 (4.00)	8.66 (1.39)	15.11 (2.54)	20.10 (6.32)	12.08 (1.44)
b_{se}	8.76 (1.65)	25.05 (7.39)	9.23 (2.62)	9.38 (1.70)	7.03 (1.35)	7.88 (1.72)
b_e	10.39 (3.80)	47.97 (16.04)	12.20 (6.13)	8.93 (2.85)	12.50 (3.36)	8.22 (3.78)
Joint stiffness						
k_s	298.5 (55.9)	509.0 (94.1)	222.6 (40.0)	477.2 (75.6)	676.0 (221.2)	354.4 (35.1)
k_{se}	339.8 (79.5)	715.5 (164.1)	324.5 (91.1)	377.4 (78.2)	191.0 (36.6)	298.3 (51.7)
k_e	481.2 (154.8)	1492.5 (327.9)	555.4 (236.8)	457.9 (130.0)	536.7 (139.9)	415.4 (161.7)
Hand grip damping and stiffness						
b_h	114.4 (18.4)	114.9 (22.2)	119.7 (18.8)	146.2 (31.3)	156.6 (43.2)	95.7 (17.8)
k_h	23.8 (3.06)	22.1 (5.57)	24.6 (3.59)	25.3 (3.40)	30.4 (9.64)	14.6 (1.92)
Velocity feedback						
k_{vs}	27.4 (2.3)	42.4 (10.0)	22.8 (2.4)	26.2 (5.7)	60.2 (19.2)	25.4 (2.4)
k_{vse}	34.6 (4.7)	45.7 (9.1)	33.7 (6.7)	26.4 (7.5)	16.4 (1.9)	26.6 (3.3)
k_{ve}	51.4 (6.2)	99.8 (18.0)	51.8 (13.2)	36.4 (11.0)	69.3 (16.3)	44.5 (12.3)
Position feedback						
k_{ps}	438.0 (84.4)	401.7 (57.6)	384.3 (92.3)	550.1 (95.9)	679.8 (218.8)	445.9 (14.8)
k_{pse}	536.4 (103.6)	435.8 (68.5)	569.7 (157.7)	508.4 (123.2)	192.0 (41.5)	448.2 (62.9)
k_{pe}	786.1 (161.3)	907.2 (191.6)	958.5 (397.5)	707.5 (206.4)	868.3 (238.2)	701.6 (137.9)
Neural time delay						
T_{ds}	81.9 (13.2)	588.3 (329.9)	81.9 (15.1)	60.6 (14.5)	339.0 (200.4)	80.3 (22.2)
T_{de}	60.5 (13.7)	482.7 (224.9)	61.9 (15.8)	42.9 (13.5)	88.3 (27.8)	68.1 (21.1)
Activation cut-off frequency						
f_{acts}	3.3 (0.5)	12.0 (5.5)	3.5 (0.7)	5.4 (1.1)	4.4 (0.8)	3.7 (0.6)
f_{acte}	3.9 (0.7)	15.5 (5.4)	4.2 (0.7)	5.7 (1.4)	7.1 (1.1)	3.2 (0.5)

Table D.5 – Total mean (SD) of the criterion and VAF values for six different initial parameter vectors. Only trials with a positive VAF value were used to calculate the VAF. N_{pos} represents the number of trials with a positive VAF. The optimization resulted in stable systems for all trials. *Condition: $PT_{7.5}$, with penalty function.*

Parameter	$\boldsymbol{\theta_{i1}}$	$\boldsymbol{\theta_{i2}}$	$\boldsymbol{\theta_{i3}}$	$\boldsymbol{\theta_{i4}}$	$\boldsymbol{\theta_{i5}}$	$\boldsymbol{\theta_{i6}}$
Criterion	88.01 (18.58)	96.52 (22.45)	90.21 (20.12)	93.20 (28.34)	96.40 (21.44)	85.01 (19.55)
VAF_x (%)	62.17 (9.37)	65.90 (9.46)	63.30 (10.30)	61.81 (11.22)	68.72 (10.99)	61.09 (10.57)
VAF_y (%)	50.69 (15.64)	52.96 (13.55)	50.60 (16.49)	52.97 (14.59)	54.29 (13.95)	51.77 (16.65)
$N_{pos}(\leq 80)$	77	78	76	80	80	79

D.4 Discussion

The means and standard deviations over subjects of the estimated parameters, the SEMs and the criterion & VAF values are presented in tables D.3-D.5.

The main findings for the optimizations with the different initial parameter vectors are listed below.

- Overall, the SEMs were higher then the corresponding parameter value (tables D.3 and D.4).
- The optimization with initial parameter vector $\boldsymbol{\theta_{i6}}$ has the best accuracy in frequency domain together with reasonable SEM and VAF values compared to the other initial parameter vectors.
- On average, the maximum estimated parameter change is 44% between the results of the different initial parameter vectors, which indicates the presence local minima.

APPENDIX E

Parameter estimation reduced parameter set

E.1 Introduction

Appendix C and D showed that model 3 with initial parameter vector $\boldsymbol{\theta_{i6}}$ resulted in the best parameter estimation. However, the results were still unsatisfactory, because the optimal parameter set depended on the initial parameter vector and the SEMs exceeded the corresponding estimated parameter values. It is reasonable to think that the model structure is too complex for a nice convergence to a global minimum with different initial parameter vectors.

The last step we are going to take is simplifying model 3. Simplification occurred by fixing parameters and the estimated parameters obtained with $\boldsymbol{\theta_{i6}}$ shown in figure D.3 was taken as initial parameter vector. We also going to evaluate optimization results of a model with only positive reflex gains for different initial parameter vectors. As in the previous appendix, only the main condition with 8 trials per subject ($PT_{7.5}$) was investigated in this appendix. The next section describes the simplification in detail.

E.2 Methods

The criterion, VAFs and the SEMs were evaluated for the model optimizations. In this appendix, model 3 is simplified where we distinguish between model 3a and model 3b. Negative feedback gains were allowed in model 3a whereas only feedback gains larger than zero were allowed in model 3b. The simplifications are given below.

- The two mass parameters m_h and m_f were combined to only one parameter to be estimated m_{tot}, where

$$m_h = 0.49 \cdot m_{tot} \tag{E.1}$$
$$m_f = 0.51 \cdot m_{tot} \tag{E.2}$$

  The proportions are determined by average mass values from De Vlugt et al. (2006) where the cuff and handle mass were taken into account.

- At least we want to estimate the intrinsic parameters and the reflex gains. Therefore, the handgrip, neural delay and activation dynamics parameters were fixed. Handgrip parameters were fixed at the estimated parameters obtained with $\boldsymbol{\theta_{i6}}$ shown in figure D.3. Neural delay and activation dynamics parameters were fixed with equal values for each joint respectively at 30 ms and 3.5 Hz.

- For model 3a, the estimated parameters obtained with $\boldsymbol{\theta_{i6}}$ shown in figure D.3 was taken as initial parameter vector for the parameters which were not fixed. The same initial parameter vector is used for model 3b, but k_{p_s} was set to a positive value in order not to exceed the boundaries. In addition, four initial parameter vectors were generated for model 3b where each parameter was changed randomly with $\pm 25\%$ of the parameter value. Model optimization occurred for each trial of every subject with the same randomized initial parameter vector. All different initial parameter vectors are shown in table E.1.

- The boundaries for model 3b are given in table E.2. For model 3a, negative boundaries of the velocity and position feedback parameters were allowed as shown in table D.2.

Other optimization settings were the same as in appendix D; i.e. again the optimization was performed with a penalty function.

Table E.1 – Six different initial parameter vectors. The first initial parameter vector was used for the parameter estimation of model 3a. The other five initial parameter vectors were used for the parameter estimation of model 3b.

Initial parameter vector nr.	Initial parameter vector structure
$\boldsymbol{\vartheta_{i1}}$	$\hat{\boldsymbol{\theta}}_{\boldsymbol{i6}}$[1].
$\boldsymbol{\vartheta_{i2}}$	$\hat{\boldsymbol{\theta}}_{\boldsymbol{i6}}$, where the value of the reflexive parameters k_{p_s} is set at positive value.
$\boldsymbol{\vartheta_{i3}}$, $\boldsymbol{\vartheta_{i4}}$, $\boldsymbol{\vartheta_{i5}}$, $\boldsymbol{\vartheta_{i6}}$	$\boldsymbol{\vartheta_{i2}}$, where each parameter is changed randomly with ±25% of the parameter value. Model optimization occurred for each trial of every subject with the same randomized initial parameter vector.

[1] *The estimated parameter vector of model 3 with initial parameter vector* $\hat{\boldsymbol{\theta}}_{\boldsymbol{i6}}$ *presented in table D.3 was the starting point for the initial parameter vectors.*

Table E.2 – The lower boundaries of the velocity and position feedback parameters were set at 0 for optimization of model 3b. Lower and upper boundaries used for optimization of model 3a are shown in table D.2.

Parameter	LB / UB	Unit	Parameter	LB / UB	Unit
Segmental mass			*Velocity feedback*		
m_{tot}	0.5 / 8	kg	k_{v_s}	0 / 1e2	Nms/rad
			$k_{v_{se}}$	0 / 1e2	Nms/rad
Joint damping			k_{v_e}	0 / 1e2	Nms/rad
b_s	0 / 1e2	Nms/rad	*Position feedback*		
b_{se}	0 / 1e2	Nms/rad	k_{p_s}	0 / 1e3	Nm/rad
b_e	0 / 1e2	Nms/rad	$k_{p_{se}}$	0 / 1e3	Nm/rad
Joint stiffness			k_{p_e}	0 / 1e3	Nm/rad
k_s	0 / 1e3	Nm/rad	*Neural time delay*		
k_{se}	0 / 1e3	Nm/rad	T_{d_s}	-	ms
k_e	0 / 1e3	Nm/rad	T_{d_e}	-	ms
Hand grip damping and stiffness			*Activation cut-off frequency*		
b_h	-	Ns/m	f_{act_s}	-	Hz
k_h	-	N/m	f_{act_e}	-	Hz

E.3 Results: with penalty function ($PT_{7.5}$)

Table E.3 – Mean (SD) parameters over subjects for six different initial parameter vectors. The initial parameter vector is given in italic. Negative feedback gains were allowed in model 3a whereas only feedback gains larger than zero were allowed in model 3b. *Condition: $PT_{7.5}$, with penalty function.*

Parameter	ϑ_{i1}-Model 3a	ϑ_{i2}-Model 3b	ϑ_{i3}-Model 3b	ϑ_{i4}-Model 3b	ϑ_{i5}-Model 3b	ϑ_{i6}-Model 3b	Unit
Segmental mass							
m_{tot}	*3.94*: 3.94 (0.46)	*3.94*: 3.79 (0.29)	*4.93*: 4.10 (0.49)	*2.96*: 3.30 (0.38)	*2.96*: 3.38 (0.53)	*4.93*: 3.94 (0.38)	kg
Joint damping							
b_s	*3.98*: 4.09 (0.97)	*3.98*: 5.67 (0.74)	*4.97*: 5.99 (1.05)	*4.97*: 6.82 (1.68)	*2.98*: 5.78 (1.70)	*4.97*: 6.31 (1.36)	Nms/rad
b_{se}	*6.38*: 7.23 (2.24)	*6.38*: 7.56 (1.65)	*4.78*: 9.25 (2.00)	*4.78*: 9.14 (2.74)	*4.78*: 8.83 (3.14)	*4.78*: 8.66 (2.07)	Nms/rad
b_e	*10.72*: 13.23 (4.06)	*10.72*: 13.66 (3.07)	*13.41*: 16.96 (4.62)	*13.41*: 17.79 (5.08)	*13.41*: 17.53 (6.56)	*13.41*: 15.56 (4.15)	Nms/rad
Joint stiffness							
k_s	*197.6*: 207.8 (39.2)	*197.6*: 188.8 (22.7)	*247.0*: 186.1 (23.4)	*148.2*: 165.8 (35.4)	*148.2*: 161.4 (42.2)	*148.2*: 169.4 (19.3)	Nm/rad
k_{se}	*109.5*: 125.5 (42.5)	*109.5*: 138.3 (43.0)	*82.1*: 110.4 (33.6)	*82.1*: 126.1 (70.6)	*82.1*: 115.4 (61.1)	*82.1*: 112.6 (50.8)	Nm/rad
k_e	*175.4*: 185.7 (83.6)	*175.4*: 210.2 (105.0)	*131.5*: 210.8 (71.4)	*131.5*: 205.2 (132.7)	*131.5*: 206.7 (120.2)	*219.2*: 249.3 (103.6)	Nm/rad
Velocity feedback							
k_{vs}	*12.9*: 12.8 (2.3)	*12.9*: 16.5 (1.6)	*16.1*: 19.8 (2.5)	*9.7*: 15.6 (2.7)	*9.7*: 15.7 (1.8)	*9.7*: 18.3 (1.3)	Nms/rad
k_{vse}	*13.6*: 13.2 (1.9)	*13.6*: 15.8 (1.5)	*16.9*: 21.2 (2.7)	*10.2*: 15.7 (2.4)	*10.2*: 15.6 (2.2)	*16.9*: 19.8 (1.6)	Nms/rad
k_{ve}	*19.7*: 20.6 (5.1)	*19.7*: 23.7 (5.3)	*24.6*: 28.2 (5.1)	*24.6*: 27.8 (8.4)	*14.8*: 24.3 (8.0)	*24.6*: 28.7 (6.2)	Nms/rad
Position feedback							
k_{ps}	*−47.5*: −63.1 (27.0)	*10.0*: 9.7 (1.8)	*7.5*: 13.1 (6.3)	*12.5*: 13.8 (7.7)	*7.5*: 11.5 (11.8)	*12.5*: 19.2 (9.6)	Nm/rad
k_{pse}	*10.8*: −6.1 (51.9)	*10.8*: 44.7 (13.2)	*13.5*: 74.7 (20.8)	*13.5*: 49.1 (21.3)	*8.1*: 56.5 (19.9)	*8.1*: 74.1 (23.5)	Nm/rad
k_{pe}	*37.8*: 22.8 (96.3)	*37.8*: 68.5 (20.2)	*47.2*: 107.5 (56.9)	*28.3*: 97.0 (61.3)	*28.3*: 96.4 (47.7)	*47.2*: 98.8 (33.1)	Nm/rad

Table E.4 – Mean (SD) SEMs over subjects for six different initial parameter vectors. Negative feedback gains were allowed in model 3a whereas only feedback gains larger than zero were allowed in model 3b. *Condition: $PT_{7.5}$, with penalty function.*

Parameter	$\boldsymbol{\vartheta_{i1}}$-Model 3a	$\boldsymbol{\vartheta_{i2}}$-Model 3b	$\boldsymbol{\vartheta_{i3}}$-Model 3b	$\boldsymbol{\vartheta_{i4}}$-Model 3b	$\boldsymbol{\vartheta_{i5}}$-Model 3b	$\boldsymbol{\vartheta_{i6}}$-Model 3b
Segmental mass						
m_{tot}	1.36 (0.16)	1.43 (0.13)	1.51 (0.21)	1.23 (0.12)	1.21 (0.18)	1.50 (0.19)
Joint damping						
b_s	7.65 (3.13)	7.82 (1.44)	9.12 (1.71)	8.20 (1.84)	8.28 (2.59)	8.71 (1.48)
b_{se}	7.70 (5.91)	7.23 (2.11)	9.01 (2.92)	9.13 (3.31)	9.70 (5.35)	8.12 (2.34)
b_e	10.44 (12.10)	8.93 (4.88)	13.18 (7.07)	13.60 (7.35)	15.73 (12.03)	10.54 (4.64)
Joint stiffness						
k_s	202.8 (69.0)	209.5 (42.9)	234.3 (56.5)	227.9 (67.8)	222.2 (73.1)	220.8 (47.7)
k_{se}	213.1 (129.4)	214.8 (89.2)	260.4 (97.7)	296.5 (156.6)	290.4 (162.3)	253.0 (90.5)
k_e	335.3 (269.6)	345.4 (223.5)	473.1 (257.2)	558.5 (395.9)	555.3 (375.4)	472.7 (251.1)
Velocity feedback						
k_{vs}	16.6 (3.4)	18.1 (2.5)	21.9 (4.4)	19.2 (4.1)	18.4 (2.8)	20.2 (2.8)
k_{vse}	18.3 (5.4)	20.1 (6.2)	24.6 (8.2)	25.4 (9.5)	23.8 (7.8)	22.7 (7.0)
k_{ve}	24.4 (10.4)	27.5 (14.4)	37.5 (19.0)	41.7 (22.8)	40.0 (19.6)	34.3 (16.8)
Position feedback						
k_{ps}	270.1 (50.7)	300.0 (55.0)	336.1 (61.4)	300.7 (79.0)	284.9 (53.1)	315.6 (50.3)
k_{pse}	332.5 (81.3)	393.6 (139.7)	453.1 (123.7)	460.4 (225.2)	420.6 (153.9)	468.9 (160.1)
k_{pe}	506.2 (165.6)	621.5 (347.4)	772.7 (317.3)	864.0 (643.7)	767.8 (405.0)	902.0 (469.2)

Table E.5 – Total mean (SD) of the criterion and VAF values for six different initial parameter vectors. Negative feedback gains were allowed in model 3a whereas only feedback gains larger than zero were allowed in model 3b. Only trials with a positive VAF value were used to calculate the VAF. N_{pos} represents the number of trials with a positive VAF. The optimization resulted in stable systems for all trials. *Condition: $PT_{7.5}$, with penalty function.*

Parameter	$\boldsymbol{\vartheta_{i1}}$-Model 3a	$\boldsymbol{\vartheta_{i2}}$-Model 3b	$\boldsymbol{\vartheta_{i3}}$-Model 3b	$\boldsymbol{\vartheta_{i4}}$-Model 3b	$\boldsymbol{\vartheta_{i5}}$-Model 3b	$\boldsymbol{\vartheta_{i6}}$-Model 3b
Criterion	90.14 (17.81)	96.86 (21.01)	96.48 (20.31)	95.03 (18.74)	91.94 (17.87)	94.86 (19.07)
VAF_x (%)	61.53 (10.22)	57.32 (10.47)	55.54 (12.80)	61.39 (10.39)	62.47 (9.16)	58.89 (11.75)
VAF_y (%)	49.15 (16.98)	43.89 (17.94)	44.10 (19.56)	46.76 (17.02)	45.90 (17.55)	48.45 (17.02)
$N_{pos}(\leq 80)$	78	77	74	78	77	77

E.4 Discussion

The means and standard deviations over subjects of the estimated parameters, the SEMs and the criterion & VAF values are presented in tables E.3-E.5.

A few remarks can be made about model 3a

- The SEMs decrease by reducing the number of parameters to be estimated (compare table D.4 and E.4). However, most of the SEMs are still higher then the corresponding parameter value.
- When comparing table D.5 and E.5, we observe that the criterion value increases by reducing the number of parameters to be estimated, whereas the VAFs don't show large differences.

The results of model 3b are evaluated below

- Setting the lower boundaries of the reflexive parameter ≥ 0 does not have a large effect on the velocity feedback gains whereas the position feedback gains increase.
- We still observe local minima, since some optimal parameters change with different initial parameter values.
- For model 3b, optimization with initial parameter vector $\boldsymbol{\vartheta_{i5}}$ resulted in a low criterion value and high VAFs compared to the other initial parameter vectors. On average, The SEMs are high for all initial parameter vectors.

E.5 Conclusion

As already described in appendix C, the best model for the relax task was model structure 1. A penalty function was not necessary.

In appendix C, D, and E we observed that the model parameters were estimated rather inaccurate for the position task:

- For most of the parameters, the SEMs were higher then the corresponding parameter value.
- A penalty function function was necessary to get stable systems.
- The optimal parameter set depended on the initial parameter vector.

We can bring up two hypotheses from the above mentioned problems.

- The experimental data might contain insufficient information to estimate the intrinsic and reflexive parameters of the human arm model.
- We did not found the global minimum and there is an unknown optimal parameter set with better accuracy in time and frequency domain and low SEMs compared to the values we found.

The problem is that we do not know if we have found the global minimum. This is hard to verify with a gradient search. A next step to find the global minimum would be a grid search, but this gives a high computational burden. Due to time limitations in this master thesis project, a grid search was not performed.

From the results in appendix appendices C, D, and E we can conclude that we are left with some uncertainty in the parameter estimation. Our most reliable result is model 3b with feedback gains ≥ 0 and initial parameter vector $\boldsymbol{\vartheta_{i5}}$. We are going to use this model structure for predicting the pulse response in this master thesis.

APPENDIX F

Elastic Limit & Joint Rotations

In this appendix, the elastic limit for the shoulder and elbow joint are estimated. Subsequently, it is evaluated wether the elastic limit is exceeded for the continuous and pulse perturbations.

F.1 Elastic limit

A bi-phasic pattern is observed when a muscle is stretching. The force linearly increases with lengthening of the muscle up to a certain point, the elastic limit. Further muscle stretch results in a less than proportional increase in force. For joint velocities between 74.5-186.2 deg/s, the elastic limit for the wrist has been found to increase linearly between 1.4-3.8 degrees (de Vlugt et al., 2011; van Eesbeek et al., 2010).
We can make a rather rough estimate of what the elastic limit would be in the shoulder and elbow. The elastic limit in joint rotation (x_e) can be expressed in the elastic limit in sarcomere lengthening (ΔL_s), according to

$$\Delta L_s = x_e \cdot r \cdot \frac{L_s}{L_m}, \tag{F.1}$$

where r is the muscle moment arm, L_s the sarcomere length and L_m the muscle length. Now we can estimate the elastic limit in joint rotation of the shoulder and elbow joint. For simplicity, we consider the elastic limit in sarcomere lengthening, the sarcomere and muscle length equal for the wrist, shoulder and elbow joint. Table F.1 shows muscle moment arms r for different muscles of the wrist, shoulder and elbow joint. In the last row, the averaged muscle moments are presented. It can be seen that the averaged muscle moment arm of the shoulder and elbow are respectively a factor 2.2 and 2.5 larger than the averaged muscle moment arm for the wrist.

> Then, by equation F.1 and the simplification we made, the elastic limit for the shoulder and elbow in joint rotation would be somewhere between 0.6-1.7 degrees.

There are some remarks to mention. First, ramp-and-hold perturbations were applied at the wrist in the study of de Vlugt et al. (2011) and van Eesbeek et al. (2010). Thus, we cannot be sure wether the results can be extrapolated to continuous and pulse perturbations in the shoulder and elbow. Secondly, they were able to demonstrated the elastic limit in active muscles, but the elastic limit in the relaxed muscle was less accurate (van Eesbeek et al., 2010). So we don't know if we can use these results for the relax task.
Suppose that we can extrapolate the results found for the wrist to our experiment on the shoulder and elbow. Then we have to take joint velocity into consideration. Table F.2 shows the mean (SD) RMS and maximum joint velocities during the continuous perturbations. Except for the maximum continuous perturbation levels, the RMS and maximum joint velocities are low compared to the velocities applied in the experiment of de Vlugt et al. (2011). This might imply a very low elastic limit. Table F.3 shows the mean (SD) peak joint velocities during the pulse perturbations. Averaged velocities for the minimum and maximum pulse level corresponds well with the applied velocities in de Vlugt et al. (2011). Hence, the elastic limit might vary between 0.6-1.7 degrees depending on the joint velocity of the pulse response.

Table F.1 – Muscle moment arms r for different muscles of the wrist shoulder and elbow joint. ECRB: Extensor Carpi Radialis Brevis, ECRL: Extensor Carpi Radialis Longus, ECU: Extensor Carpi Ulnaris, EDC: Extensor Digitorum Communis, FCR: Flexor Carpi Radialis, FCU: Flexor Carpi Ulnaris, FDS: Flexor Digitorum Superficialis, LATDOR: Latissimus Dorsi, DELTANT: Deltoideus Anterior, DELTPOS: Deltoideus Posterior, PECTMAJ: Pectoralis Major, TRI: Triceps, BRA: Brachialis, BIC: Biceps, BRD: Brachioradialis.

Muscle	r wrist[a] [mm]	Muscle	r shoulder[b] [mm]	Muscle	r elbow[c] [mm]
ECRB	13.43	LATDOR	1.00	TRI	22.19
ECRL	11.72	DELTANT	37.00	BRA	26.87
ECU	8.52	DELTANT	37.00	BIC	41.58
EDC	14.13	DELPOST	22.00	BRD	52.96
FCR	13.20	PECTMAJ	43.00	ECRB	11.60
FCU	11.21			ECRL	20.72
FDS	10.35				
Mean	11.79	Mean	25.75	Mean	29.32

[a] van Eesbeek et al. (2010)
[b] Kuechle et al. (1997)
[c] Ramsay et al. (2009)

Table F.2 – Mean (SD) RMS and maximum joint velocities during the continuous perturbations. The shoulder and elbow joint are respectively denoted by s and e.

Condition	Joint	Mean (SD[a]) RMS joint velocities [deg/s]	Mean (SD) maximum joint velocities [deg/s]
$PT_{2.5}$	s	4.5 (0.7)	15.1 (2.4)
	e	5.2 (1.2)	19.4 (6.3)
$PT_{7.5}$	s	16.3 (2.9)	50.6 (9.8)
	e	17.1 (3.2)	57.3 (11.1)
$PT_{22.5}$	s	44.7 (10.0)	137.7 (29.6)
	e	43.7 (11.5)	151.0 (44.7)
$RT_{2.5}$	s	4.0 (1.3)	11.4 (3.8)
	e	4.3 (1.4)	13.7 (4.7)
$RT_{7.5}$	s	6.6 (1.5)	18.0 (3.8)
	e	7.9 (2.5)	23.9 (6.8)
$RT_{22.5}$	s	17.3 (4.7)	46.9 (13.4)
	e	28.0 (8.5)	78.4 (24.9)

[a] Standard deviation over subjects

Table F.3 – Mean (SD) peak joint velocities in response to the minimum and maximum pulse level. The shoulder and elbow joint are respectively denoted by s and e.

Condition	Joint	Mean (SD[a]) peak joint velocities (pulse amplitude: minimum) [deg/s]	Mean (SD) peak joint velocities (pulse amplitude: maximum) [deg/s]
PT_0	s	49.7 (16.0)	103.7 (34.0)
	e	103.1 (35.3)	197.3 (44.1)
$PT_{2.5}$	s	-	95.2 (30.5)
	e	-	175.0 (36.4)
$PT_{7.5}$	s	57.9 (17.8)	104.0 (27.9)
	e	93.6 (18.5)	162.0 (30.8)
$PT_{22.5}$	s	-	118.0 (29.3)
	e	-	156.2 (37.7)
RT_0	s	38.7 (17.7)	-
	e	114.8 (31.6)	-
$RT_{2.5}$	s	38.4 (19.4)	-
	e	117.1 (32.4)	-
$RT_{7.5}$	s	40.3 (19.1)	-
	e	118.0 (32.3)	-
$RT_{22.5}$	s	69.2 (67.3)	-
	e	158.9 (131.7)	-

[a] Standard deviation over subjects

F.2 Joint rotations: continuous perturbations

The left column of table F.4 shows the RMS (SD) joint rotations during the continuous perturbations. The right column of the table shows the mean (SD) maximum joint rotation that occurred during the continuous perturbations. Overall, the joint rotations for the shoulder joint were much larger with respect to the elbow joint. The previous section showed that the elastic limit might be between 0.6 and 1.7 degrees. Then only the averaged RMS joint rotations for the conditions $PT_{2.5}$ and $RT_{2.5}$ could be below the elastic limit. However, some peak joint displacements might exceed the elastic limit as can be seen in the right column.

F.3 Joint rotations: pulse perturbations

Table F.5 shows the mean (SD) peak joint rotations in response to the minimum and maximum pulse level. The joint rotations for the elbow joint were much larger with respect to the shoulder joint. It is interesting to see that the joint rotations of the elbow and shoulder joint during pulse perturbations occurred in succession (figure F.1). Clearly, all pulse responses showed much larger joint displacements than the estimated elastic limit (0.6-1.7 degrees). Furthermore, the peak joint rotations for the maximum amplitude are on average approximately two times the peak joint rotations of the minimum pulse amplitude. For conclusions about linearity, the input to the system (hand reaction force) should be taken into account as in figure 3.16.
Table F.6 shows the mean (SD) peak joint rotations in response to pulse perturbations in left and right direction. The results in this table show that there are no large difference between the pulses responses in left and right direction, except for the elbow joint for the relax task.

Table F.4 – Mean (SD) RMS and maximum joint rotations during the continuous perturbations. The shoulder and elbow joint are respectively denoted by s and e.

Condition	Joint	Mean (SD[a]) RMS joint rotations [deg]	Mean (SD) maximum joint rotations [deg]
$PT_{2.5}$	s	0.6 (0.1)	1.7 (0.3)
	e	0.4 (0.1)	1.5 (0.5)
$PT_{7.5}$	s	1.7 (0.2)	5.0 (0.7)
	e	1.1 (0.2)	3.7 (0.7)
$PT_{22.5}$	s	4.5 (0.6)	13.5 (1.5)
	e	2.7 (0.5)	9.5 (2.1)
$RT_{2.5}$	s	1.1 (0.4)	3.0 (1.4)
	e	1.0 (0.5)	3.1 (2.0)
$RT_{7.5}$	s	1.8 (0.4)	4.9 (1.1)
	e	2.0 (0.9)	5.8 (2.6)
$RT_{22.5}$	s	5.2 (1.5)	14.5 (4.5)
	e	8.1 (2.8)	21.7 (7.5)

[a] Standard deviation over subjects

Table F.5 – Mean (SD) peak joint rotations in response to the minimum and maximum pulse level. The shoulder and elbow joint are respectively denoted by s and e.

Condition	Joint	Mean (SD[a]) peak joint rotations (pulse amplitude: minimum) [deg]	Mean (SD) peak joint rotations (pulse amplitude: maximum) [deg]
PT_0	s	5.6 (1.7)	11.7 (3.3)
	e	7.7 (2.9)	17.2 (5.0)
$PT_{2.5}$	s	-	10.3 (2.3)
	e	-	12.7 (2.5)
$PT_{7.5}$	s	5.8 (1.5)	10.4 (1.8)
	e	5.6 (0.6)	9.7 (1.5)
$PT_{22.5}$	s	-	10.5 (3.4)
	e	-	9.6 (2.0)
RT_0	s	12.0 (5.5)	-
	e	26.0 (6.5)	-
$RT_{2.5}$	s	11.5 (5.9)	-
	e	28.5 (7.4)	-
$RT_{7.5}$	s	12.5 (5.5)	-
	e	28.9 (7.2)	-
$RT_{22.5}$	s	18.0 (7.0)	-
	e	34.9 (11.3)	-

[a] Standard deviation over subjects

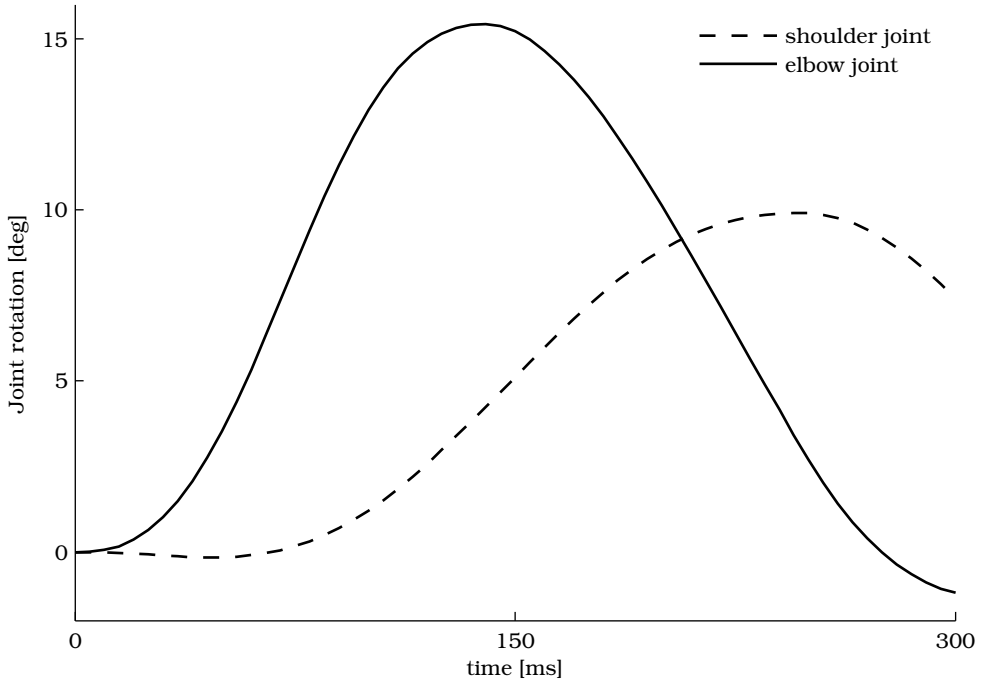

Figure F.1 – Typical example of the shoulder and elbow joint rotations in response to a maximum pulse level (condition PT_0). This figure shows that the elbow joint rotated first, followed by the shoulder joint. Consequently the end-point displacements are lower than if the rotations would occur simultaneously. The relax task show similar characteristics.

Table F.6 – Mean (SD) peak joint rotations in response to pulse perturbations applied to the left and to the right. The shoulder and elbow joint are respectively denoted by s and e.

Condition	Joint	Mean (SD[a]) peak joint rotations (pulse direction: left) [deg]	Mean (SD) peak joint rotations pulse direction: right) [deg]
PT_0	s	8.8 (2.8)	8.5 (2.4)
	e	11.5 (3.8)	13.5 (4.1)
$PT_{7.5}$	s	8.0 (1.4)	8.2 (1.7)
	e	7.7 (1.3)	7.7 (1.1)
RT_0	s	11.6 (5.3)	12.4 (5.9)
	e	22.5 (4.2)	29.4 (9.1)
$RT_{7.5}$	s	11.9 (6.0)	13.1 (5.5)
	e	25.3 (5.0)	32.4 (10.3)

[a] Standard deviation over subjects

F.4 Conclusions

We can conclude that it is difficult to estimate the elastic limit for the shoulder and elbow joint from perturbation experiments at the wrist. Nevertheless, the elastic limit for the shoulder and elbow joint might be between 0.6-1.7 degrees depending on joint velocity. For the joint displacements during the continuous perturbations, only the conditions with the lowest amplitude level ($PT_{2.5}$ and $RT_{2.5}$) might be below the elastic limit. For the pulse perturbations, most likely all pulse responses exceeded the elastic limit. Furthermore, the largest rotations are observed

in the shoulder joint during the continuous perturbations, whereas the elbow joint showed the largest rotations in response to the pulses.

Bibliography

Abbink, D.A. (2007). Task instruction: The largest influence on human operator motion control dynamics. In *EuroHaptics Conference, 2007 and Symposium on Haptic Interfaces for Virtual Environment and Teleoperator Systems. World Haptics 2007. Second Joint*, pages 206–211. IEEE.

Abbink, D.A. and van der Helm, F.C.T. and Boer, E.R. (2004). Admittance measurements of the foot during 'maintain position' and 'relax' tasks on a gas pedal. In *Systems, man and cybernetics, 2004 IEEE international conference on*, volume 3, pages 2519–2524. IEEE.

Axelson, HW and Hagbarth, KE (2001). Human motor control consequences of thixotropic changes in muscular short-range stiffness. *The Journal of physiology*, 535(1):279–288.

Cathers, I. and ODwyer, N. and Neilson, P. (1999). Dependence of stretch reflexes on amplitude and bandwidth of stretch in human wrist muscle. *Experimental Brain Research*, 129(2):278–287.

de Vlugt, E. and de Groot, J.H. and Schenkeveld, K.E. and Arendzen, J.H. and van der Helm, F.C.T. and Meskers, C.G.M. (2010). The relation between neuromechanical parameters and Ashworth score in stroke patients. *Journal of NeuroEngineering and Rehabilitation*, 7:35.

de Vlugt, E. and Schouten, A.C. and van der Helm, F.C.T. (2002). Adaptation of reflexive feedback during arm posture to different environments. *Biological cybernetics*, 87(1):10–26.

de Vlugt, E. and Schouten, A.C. and van der Helm, F.C.T. (2003). Closed-loop multivariable system identification for the characterization of the dynamic arm compliance using continuous force disturbances: a model study. *Journal of neuroscience methods*, 122(2):123–140.

De Vlugt, E. and Schouten, A.C. and Van Der Helm, F.C.T. (2006). Quantification of intrinsic and reflexive properties during multijoint arm posture. *Journal of neuroscience methods*, 155(2):328–349.

de Vlugt, E. and van Eesbeek, S. and Baines, P. and Hilte, J. and Meskers, CG and de Groot, J.H. (2011). Short range stiffness elastic limit depends on joint velocity. *Journal of biomechanics*.

Diener, HC and Dichgans, J. and Bootz, F. and Bacher, M. (1984). Early stabilization of human posture after a sudden disturbance: influence of rate and amplitude of displacement. *Experimental Brain Research*, 56(1):126–134.

ETSC (2011). Traffic law enforcement across the eu tackling the three main killers on europe's roads. `http://www.etsc.eu/documents/Final_Traffic_Law_Enforcement_in_the_EU.pdf`.

Forbes, P.A. and Happee, R. and van der Helm, F.C.T. and Schouten, A.C. (2011). Emg feedback tasks reduce reflexive stiffness during force and position perturbations. *Experimental brain research*, pages 1–13.

Gollhofer, A. and Sch
"opp, A. and Rapp, W. and Stroinik, V. (1997). Changes in reflex excitability following isometric contraction in humans. *European journal of applied physiology and occupational physiology*, 77(1):89–97.

Happee, R. and van Drunen, P. (2009). Posture maintenance of the human neck. *SAE Technical Paper*, pages 01–2304.

Hogan, N. (1985). The mechanics of multi-joint posture and movement control. *Biological cybernetics*, 52(5):315–331.

N. Kakuda (2000). Response of human muscle spindle afferents to sinusoidal stretching with a wide range of amplitudes. *J Physiol*, 527 Pt 2:397–404.

Kearney, RE and Hunter, IW (1982). Dynamics of human ankle stiffness: variation with displacement amplitude. *Journal of Biomechanics*, 15(10):753–756.

Kearney, RE and Hunter, IW (1983). System identification of human triceps surae stretch reflex dynamics. *Experimental Brain Research*, 51(1):117–127.

Kearney, RE and Hunter, IW (1984). System identification of human stretch reflex dynamics: tibialis anterior. *Experimental Brain Research*, 56(1):40–49.

Kearney, R.E. and Stein, R.B. and Parameswaran, L. (1997). Identification of intrinsic and reflex contributions to human ankle stiffness dynamics. *Biomedical Engineering, IEEE Transactions on*, 44(6):493–504.

Kuechle, D.K. and Newman, S.R. and Itoi, E. and Morrey, B.F. and An, K.N. (1997). Shoulder muscle moment arms during horizontal flexion and elevation. *Journal of Shoulder and Elbow Surgery*, 6(5):429–439.

Lakie, M. and Walsh, EG and Wright, GW (1984). Resonance at the wrist demonstrated by the use of a torque motor: an instrumental analysis of muscle tone in man. *The Journal of Physiology*, 353(1):265.

Linde, R.Q. and Schwab, A.L. (1997). Lecture notes multibody dynamics b,. *Course wb1413, Lab. for Eng. Mech., Delft Univeristy of Technology*.

Loram, I.D. and Maganaris, C.N. and Lakie, M. (2007). The passive, human calf muscles in relation to standing: the non-linear decrease from short range to long range stiffness. *The Journal of physiology*, 584(2):661–675.

MacKay, WA and Crammond, DJ and Kwan, HC and Murphy, JT (1986). Measurements of human forearm viscoelasticity. *Journal of Biomechanics*, 19(3):231–238.

Mileusnic, M.P. and Brown, I.E. and Lan, N. and Loeb, G.E. (2006). Mathematical models of proprioceptors. i. control and transduction in the muscle spindle. *Journal of neurophysiology*, 96(4):1772–1788.

Mirbagheri, MM and Barbeau, H. and Kearney, RE (2000). Intrinsic and reflex contributions to human ankle stiffness: variation with activation level and position. *Experimental brain research*, 135(4):423–436.

Mugge, W. and Abbink, D.A. and Schouten, A.C. and Dewald, J.P.A. and van der Helm, F.C.T. (2010). A rigorous model of reflex function indicates that position and force feedback are flexibly tuned to position and force tasks. *Experimental brain research*, 200(3):325–340.

Mugge, W. and Abbink, DA and Van der Helm, FCT (2007). Reduced power method: how to evoke low-bandwidth behaviour while estimating full-bandwidth dynamics. In *Rehabilitation Robotics, 2007. ICORR 2007. IEEE 10th International Conference on*, pages 575–581. IEEE.

Mugge, W. and Schuurmans, J. and Schouten, A.C. and van der Helm, F.C.T. (2009). Sensory weighting of force and position feedback in human motor control tasks. *The Journal of Neuroscience*, 29(17):5476–5482.

Neilson, PD and McCaughey, J. (1981). Effect of contraction level and magnitude of stretch on tonic stretch reflex transmission characteristics. *Journal of Neurology, Neurosurgery & Psychiatry*, 44(11):1007.

Nemirovsky, N. and van Rooij, L. (2010). A new methodology for biofidelic head-neck postural control. In *2010 IRCOBI Conference Proceedings*.

Östh, J. and Brolin, K. and Happee, R. (2010). Active muscle response using feedback control of a finite element human arm model.

Ramsay, J.W. and Hunter, B.V. and Gonzalez, R.V. (2009). Muscle moment arm and normalized moment contributions as reference data for musculoskeletal elbow and wrist joint models. *Journal of biomechanics*, 42(4):463–473.

Rooij, L. and Welten , J. and Broos, J. and Camp, O. (2011). Preliminary Study on Effect of Double Lane Change Manoeuvre on Occupant Kinematics. In *First International Symposium on Future Active Safety Technology toward zero-traffic-accident*.

Schouten, A.C. and de Vlugt, E. and Van Hilten, JJB and van der Helm, F.C.T. (2008). Quantifying proprioceptive reflexes during position control of the human arm. *Biomedical Engineering, IEEE Transactions on*, 55(1):311–321.

Schouten, AC and Van de Beek, W.J.T. and Van Hilten, JJ and Van der Helm, F.C.T. (2003). Proprioceptive reflexes in patients with reflex sympathetic dystrophy. *Experimental brain research*, 151(1):1–8.

Stein, RB and Kearney, RE (1995). Nonlinear behavior of muscle reflexes at the human ankle joint. *Journal of neurophysiology*, 73(1):65.

Van der Helm, F.C.T. and Schouten, A.C. and de Vlugt, E. and Brouwn, G.G. (2002). Identification of intrinsic and reflexive components of human arm dynamics during postural control. *Journal of neuroscience methods*, 119(1):1–14.

van der Horst, M.J. (2002). *Human head neck response in frontal, lateral and rear end impact loading: modelling and validation*. Technische Universiteit Eindhoven.

van Eesbeek, S. and de Groot, J.H. and van der Helm, F.C.T. and de Vlugt, E. (2010). In vivo estimation of the short-range stiffness of cross-bridges from joint rotation. *Journal of Biomechanics*, 43(13):2539–2547.

Venrooij, J. and Abbink, D.A. and Mulder, M. and van Paassen, M.M. and Mulder, M. (2010). Biodynamic feedthrough is task dependent. In *Systems Man and Cybernetics (SMC), 2010 IEEE International Conference on*, pages 2571–2578. IEEE.